DOCTORAL THESIS

Alkali Metal Bismuthate and Bismuth Vanadate Microstructure for Visible Light Driven Photocatalytic Activity

2018 March

Author : Arini Nuran Binti Zulkifili

Supervisor : Prof. Shinji Kimijima

A thesis submitted in fulfillment of the requirements

for the degree of Doctor of Philosophy

Shibaura Institute of Technology

TABLE OF CONTENTS

LIST OF TABLES

LIST OF FIGURES

ACKNOWLEDGEMENT

In the name of Allah S.W.T, the Most Gracious and Merciful.

First and foremost, I would like to express my sincere gratitude to my supervisor, Prof. Shinji Kimijima and Prof. Akira Fujiki for their never-ending supports and motivations in guiding me to complete my PhD. Their guidance had helped me to complete my research and the writing of this thesis.

Next, I would like to convey my sincere gratitude to National Institute of Material Science (NIMS), especially to Prof. Jinhua Ye and her group, for providing me an opportunity to joined the team as a research intern, as well as providing me a valuable access to use the laboratory equipment and research facilities in NIMS. Without their support and guidance, it would be impossible for me to complete this research.

I would also like to express my gratitude to the panels, Prof. Naoki Ono, Prof. Akito Takasaki, Prof. Kazuhiko Noda and Prof. Tadashi Shinohara for their kind advices and honest comments during the preliminary and public hearing phase for me to improve the overall composition of this thesis.

Biggest thanks to Yayasan Pelajaran Mara (YPM) and University of Science Malaysia (USM) for entrusting me with the scholarship and opening up the opportunity for me to further my study in Shibaura Institute of Technology, Japan. I will forever be indebted for their support.

Last but not least, my deepest gratitude goes to my beloved parents, Zulkifili Mustaffa and Rohani Abd Hamid, my dearest husband, Shakir Shariff, my parents-in-law, Shariff Othman and Faridah Isa, as well as to all my families and friends for their endless love, prayers, and encouragement.

Thank you very much.

ABSTRACT

The photocatalyst such as titanium dioxide (TiO_2), is known for its effectiveness in treating waste from industrial pollutions such as dyes, pesticides and other emerging contaminants. In decades, TiO_2 has attracted attention from worldwide researchers because it is cheap, abundant and stable. However, TiO_2 is not ideal and performs poorly in processes associated with solar photocatalysis due to its large band gap (3 to 3.2eV) that results in utilizing not more than 5% of the total solar energy ($\lambda < 387$nm). Therefore, in this research, we are trying to find alternative materials that can endeavor better results or at least, identical to TiO_2 in the degradation of organic dye under visible light irradiation ($\lambda < 387$nm) by approaching the simple and low cost synthesize method.

In order to find alternatives materials, we will be focusing on the bismuth-based semiconductor that has a potential for visible light responsive photocatalysts. This is because it has an electronic structure which its valence band consists of hybrid orbitals of O 2p and Bi 6s. The Bi 6s orbitals results in increasing the mobility of its photo-generated charge carriers, besides decreasing the band gaps to less than 3.0 eV. Due to its potential, varieties of bismuth-based semiconductor with various morphologies have been studied for its photocatalytic activity such as $NaBiO_3$, $KBiO_3$, $LiBiO_2$, $Bi_{11}VO_{19}$ and $BiVO_4$. In this study, we have divided the study into two main parts, which are the alkali bismuthate materials such as $NaBiO_3$, $KBiO_3$ and $LiBiO_2$ that are efficient in the decolorization of the dyes and the bismuth vanadate such as $Bi_{11}VO_{19}$ and $BiVO_4$ that can mineralize the dye effectively.

Accordingly, in this study, we have successfully understood the degradation of dyes by $NaBiO_3$ in various pH conditions that provide in a better understanding in developing new photocatalytic materials. Besides, we have successfully synthesized the alkali metal bismuthate of potassium and lithium by a simple solid state reaction, using $NaBiO_3$ as the starting materials. Furthermore, we have achieved various morphologies and microstructures such as $Bi_{11}VO_{19}$ and $BiVO_4$ just by using a simple precipitation method in the synthetization process.

CHAPTER 1

INTRODUCTION

This chapter provides the background of the study, which focusses on the discussion of industrial wastewater contaminants, the problems, the objectives of this study and the significance of this study.

1.1 Background

As global population growth and economic development continue to rise, the worsening environmental pollution and energy shortages have emerged as one of the top issues and challenges over the decades. Among these, wastewater pollution has been one of the critical issues that needs to be tackled and the industrial wastewater is one of the main source of the wastewater pollution. During the last centuries, a huge amount of industrial wastewater was discharged into rivers, lakes and coastal areas which contributes to the negative effects of the eco-system and human's life. Figure 1.1 shows the general cycle of the freshwater and wastewater as what had been reported by WHO. It shows that about 22% of industrial wastewater being discharged, compared to 8% of domestic wastewater discharged.

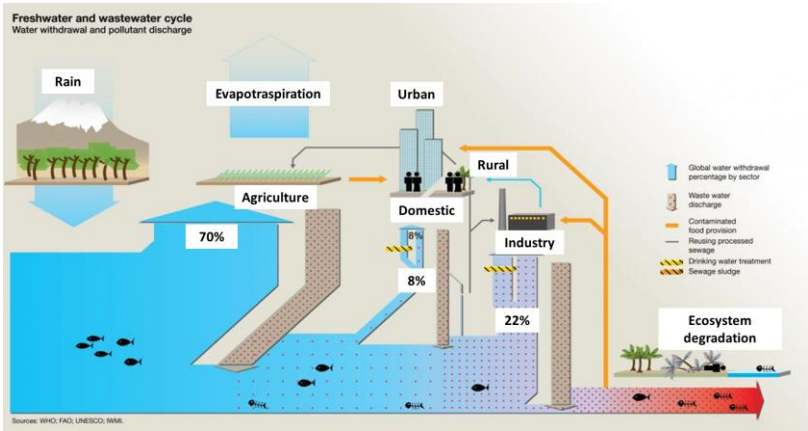

Figure 1.1 Freshwater and wastewater cycle [1-4]

There are various types of industrial wastewater based on different industries which produced its own particular combination of pollutants and contaminants for each sector. For example, depending on the characteristics of industrial wastewater, the treatment method that is specifically for the particular type of effluent produced need to be designed. Based on the United Nation- Water 2009 report, about 70% of the industrial wastewater in developing countries are being disposed untreated into the water where it contaminates the existing water supplies, up to the extends that 40% of the water sources are not suitable for basic uses like fishing or swimming [5].

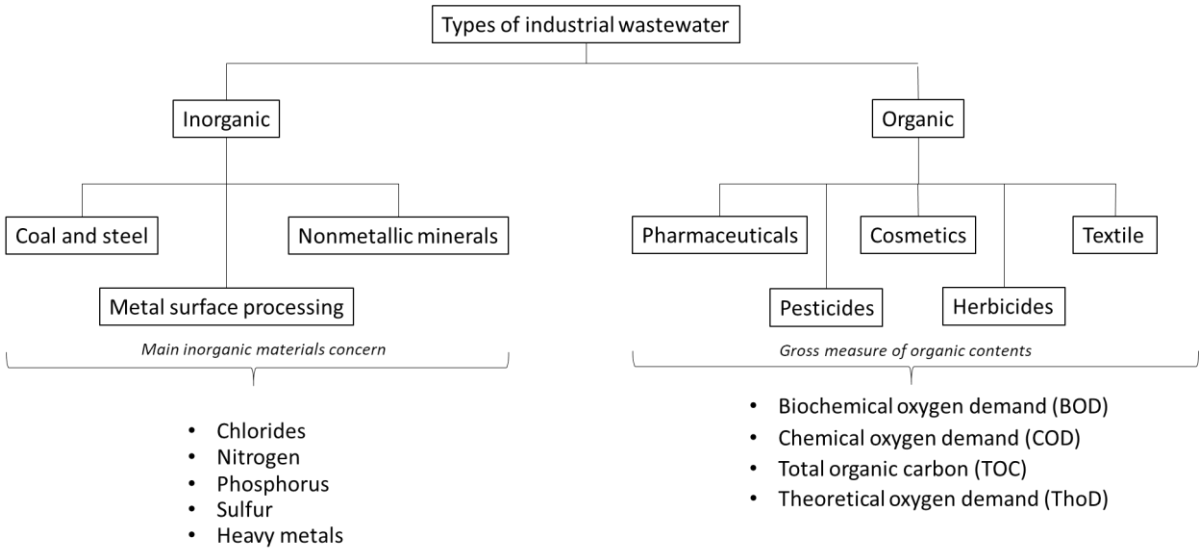

Figure 1.2 Types of industrial wastewater

The types of industrial wastewater can be divided into two groups, which are the inorganic and organic waste, as shown in Figure 1.2. Usually, coal and steel, nonmetallic minerals and metal surface processing industries produced a large amount of inorganic waste, which differs according to the industries. The main chemical tests for the wastewater production and treatment include chlorides, nitrogen, phosphorus, sulfur, heavy metals and a few others. Nitrogen and phosphorus are important because these two nutrients are responsible for the growth of aquatic plants. Other tests such as chloride, sulfate, pH and alkalinity are performed to assess the suitability of reusing the treated

wastewater and in controlling the various treatment processes. Heavy metals which have high toxicity often classified as priority pollutants.

For the organic wastewater, the tests may be divided into four methods in order to measure gross concentrations of organic matter. In laboratory scale method, we usually measure gross amounts of organic matter in wastewater at trace organic greater than 1mg/l by (1) biochemical oxygen demand (BOD), (2) chemical oxygen demand (COD), (3) total organic carbon (TOC) and (4) theoretical oxygen demand (ThoD). However, for trace organics in the larger range of 10-12 to 10-0 mg/l, instrumental methods such as gas chromatography and mass spectroscopy are being used. Specific organic compounds are determined to assess the presence of priority pollutants (Figure 1.3) [6].

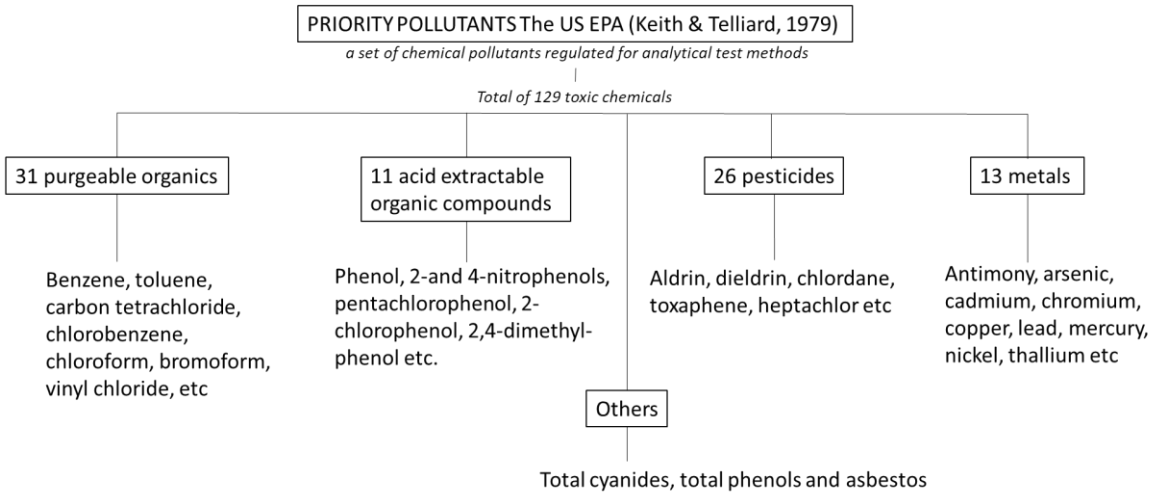

Figure 1.3 The priority pollutants by US EPA [7]

It is estimated that hundreds of billion dollars needed in order to construct and improve the wastewater treatment facilities to improve the water quality of the industrial wastewater discharged, especially in textile industries that uses textile dyes and other industrial dyestuffs which contribute to the largest group of organic pollutants.

Therefore, lots of methods (Figure 1.4) has been studied in order to reduce the implementation cost, besides having high efficiency to remove and treat the industrial wastewater contaminants. Over the past decades, biological methods, physio-chemicals, chemicals and advanced oxidation process(AOPs) have been the subject of research. Among these methods, AOPs by heterogeneous photocatalysis has been pointed out as a good alternative to promote the decolorization and mineralization of organic pollutants, by using light irradiation.

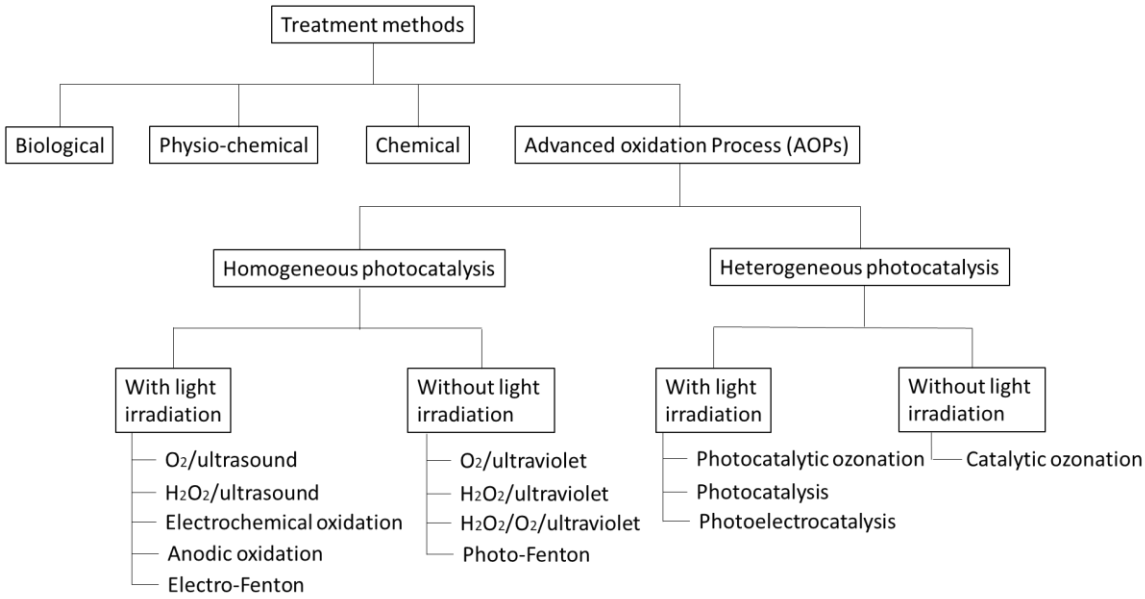

Figure 1.4 The wastewater treatment method

"Photocatalysis" comes from a Greek origin, which composes of two parts; the prefix *"photo"* (phos : light) and the word *"catalysis"* (katalyo : brake apart, decompose). It is a process which light is used to activate a substance, the *photocatalyst*, which modifies or enhance the rate of a chemical reaction without involving itself in the chemical transformation [8]. It is believed to be one of the most promising technologies because it uses an easy way to utilize the energy by natural sunlight or artificial indoor illumination, which is abundantly available.

1.2 Problem Statement

Titanium dioxide, TiO_2 has been the pioneer of the semiconductor photocatalyst and has been the subject of research for decades due to high photo-activity, low cost, low toxicity and good chemical and thermal stability [9-11]. However, TiO_2 is not ideal and performs poorly in processes associated with solar photocatalysis. This is because TiO_2 has a large band gap (3 to 3.2eV) that results in utilizing not more than 5% of the total solar energy, which is in the range of uv light spectrum (λ< 387nm). Nonetheless, visible light (λ = 400–700 nm) accounts for about 50% of solar energy. Therefore, a narrower bandgap such as the bismuth-based semiconductors (Bi_2O_3, $NaBiO_3$, $BiVO_4$ and others) are widely studied in order to have high efficiency in the visible light spectrum region (Figure 1.5).

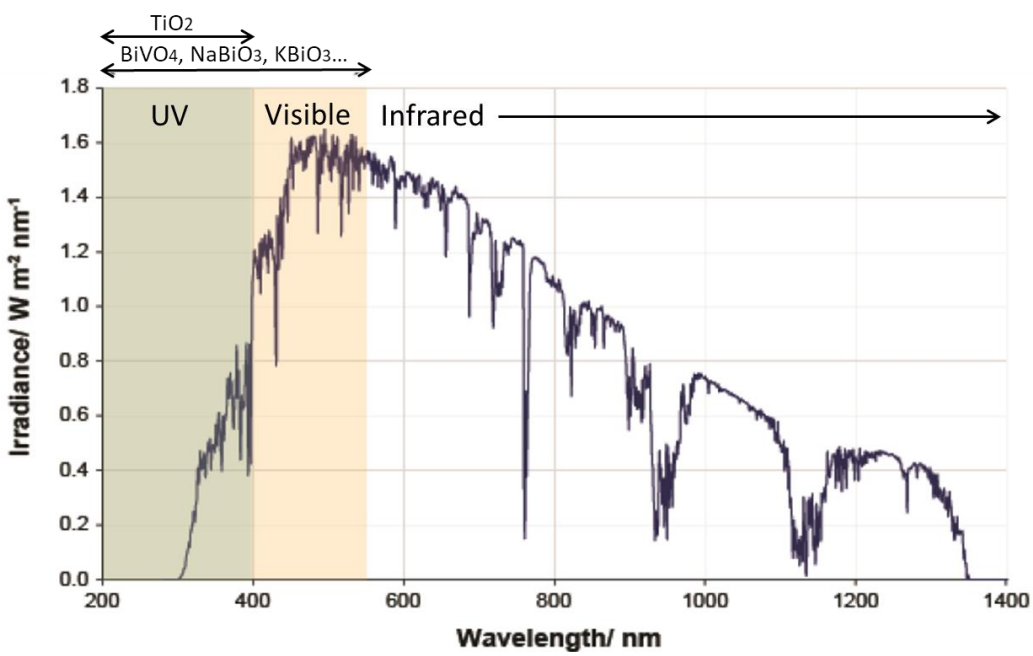

Figure 1.5 Solar spectral irradiance at AM1.5 [9]

Aside from the inefficiency of the TiO_2 in exploitation of visible light, the practical applications were also limited. It is due to the low adsorption capacity to hydrophobic contaminants, high aggregation tendency and difficulty in separation and recovery [10-12].

Despite of the efficiency of photocatalysis in the degradation of organic contaminants, the implementation in industrial application is still difficult and costly due to the difficulty of catalyst separation and recovery as well as the corrosion of the equipment used. In industrial wastewater treatment, especially the textile industries, a powder suspension system which uses photocatalyst in powder form is the most suitable method. This is because it provides more fine contact between catalyst particles and the organic substrates. Thus, we have chosen to study on two types of materials which are the alkali bismuthate which can decolorize effectively and the bismuth vanadate which can mineralized efficiently under visible light irradiation.

Besides that, the size of the particles played an important role as well. The nano-size photocatalytic materials have been proven to have a high degradation rate in degrading the organic contaminants, due to having a higher surface area, which provides more fine contact among catalyst particles and organic substrate, good dispersion and abundant active sites. However, recovery process becomes a drawback for this nano-size photocatalyst. The powder-like nano-photocatalyst often suffer from deactivation, agglomeration and difficulty in settling for catalyst recycling after the initial run. This makes the photocatalyst hard to be recycled, and non-recyclable photocatalytic materials will increase the operating cost, which significantly limits the applications in wastewater treatment. In most wastewater treatment, photocatalysts are suspended in aqueous solution. The separation of photocatalyst must be performed through settling by aid of gravity or mechanical centrifugation. Settling of ultrafine photocatalyst particles by the aid of gravity has been commonly observed to proceed very slowly.

Therefore, there are many methods that has been introduced to overcome this problem such as the coagulation method by ferrous sulfate [13]. Although it can solve the separation problems, the recyclability of the photocatalyst is another problem that arise.

By using the coagulation method, the photocatalyst powder became contaminated and cannot be reused. Thus, resulting in its inefficiency and increasing the process cost. Another method that has been introduced is creating a filter or membrane by embedding the powder on top of it. This can improve the recyclability of the photocatalyst powder, but it results in a loss of contact area between the catalyst particles and the organic substrate which reduce the degradation efficiency.

Thus, in order to overcome these problems, we chose to study on developing a microstructure photocatalyst as the micro-size is more easily to be separated as it can settle at the bottom of the reactor once we stop the process, which makes it recyclable for a couples of cycles. Besides, in order to reduce the cost of photocatalyst, the preparation and synthesis cost should be reduced. Therefore, we decided to develop a simple preparation method in synthesizing various structural and morphologies which will reduce the cost, besides having a higher and stable photocatalytic performance under visible light since visible light has a broader spectrum range compared to the ultraviolet light.

1.3 Research Objectives

In this study, the objective can be divided into three which are :-

1. To study and understand the relationship of the reactivity and stability of widely used sodium bismuthate in various pH condition in photocatalytic degradation of organic dye.
2. To synthesis and characterize alkali bismuthate material via solid state reaction by using sodium bismuthate as the starting material
3. To develop a simple and low-cost method in developing
   a) a various structures and morphologies of bismuth-based materials
   b) having high and stable photocatalytic performance under visible light in the degradation of anionic and cationic organic dyes

1.4 Significance of Study

This study will be a significant endeavor in promoting a basic study on material preparation and synthesis with various structure, even without the presence of highly equipped laboratories. Besides, we hope that by using a simpler preparation method, a highly efficient photocatalytic material can be produced, which results in a much lower production cost. Furthermore, by developing these photocatalysts, we expected the wastewater treatment by photocatalysis method would not require much modification towards the wastewater treatment system in implementing the technology. Thus, resulting in the affordability to implement the technology, not only in big and advanced industries, but in smaller industries as well. In the near future, we expected that this photocatalysis method in treating the industrial wastewater could be a common method and widely used by all.

1.5 Outline of Thesis

This thesis is composed of 8 chapters. Each chapter addresses different research issues.

Chapter 1: An outline of the global water pollution problem, especially water polluted by organic dyes in the textile industries. The problem statement, research objectives and the outlines of the thesis structure are also discussed.

Chapter 2: The history and basic concepts of photocatalyst, as well as bismuth based photocatalyst especially bismuth vanadate and bismuth alkali metals are reviewed. This chapter mainly discusses the fundamental knowledge of photocatalysis, the choice of photocatalysts, the mechanism, and the affecting factors in the reaction.

Chapter 3: The experimental part of the photocatalysis, which comprises of the chemicals and reagents, the instrument used and the standard experimental setup are explained. Besides, standard operating procedures are also included in this chapter. The schematic diagram and the photograph of the system are given. All the technical and analytical methods used in this research are addressed.

Chapter 4: The widely known hydrated sodium bismuthate, $NaBiO_3 \cdot 2H_2O$ reactivity and stability in cationic and anionic dyes degradation under different pH conditions are discussed.

Chapter 5: A new alkali bismuthate of potassium and lithium bismuthate were synthesis by solid state reaction, and its material characterization, optical properties and photocatalytic activity for cationic and anionic dyes are discussed in detail.

Chapter 6: A new bismuth vanadate, $Bi_{11}VO_{19} - VO_2$ microstructure which successfully synthesized by a simple precipitation method and its material characterization, optical properties and photocatalytic activity for cationic and anionic dyes are explained.

Chapter 7: A flower-like bismuth vanadate, $BiVO_4$ microspheres which successfully synthesized by a simple precipitation method and its material characterization, optical properties and photocatalytic activity for cationic dye are presented.

Chapter 8: The overall conclusions of the research and recommendations for potential future work is also addressed in this chapter.

1.6 References

1. World Health Organization, WHO
   Website : http://www.who.int/en/
2. Food and Agriculture Organizations of the United Nation, FAO
   Website : http://www.fao.org/home/en/
3. United Nations Educational, Scientific and Cultural Organization, UNESCO
   Website : http://en.unesco.org/
4. International Water Management Institute, IWMI
   Website : http://www.iwmi.cgiar.org/
5. United Nation water report
6. Rein Munter, Industrial Wastewater Characteristics, pp 185-194
7. United States Environmetal Protection Agency, US EPA

Website : https://www.epa.gov/sites/production/files/2015-09/documents/priority-pollutant-list-epa.pdf

8. Dimitris I. Kondarides, Catalysis – Photocatalysis, Encyclopedia of Life Support System
   Website : http://www.eolss.net/sample-chapters/c06/e6-190-16-00.pdf
9. Zhiming Wu, J., A beyond near-infrared response in a wide-bandgap ZnO/ZnSe coaxial nanowire solar cell by pseudomorphic layers, Mater. Chem. A, 2014, 2, 14571-14576.
10. A Bhattacharyya, S Kawi, MB Ray, Photocatalytic degradation of orange II by TiO_2 catalysts supported on absorbent, Catalysis Today, Volume 98, Issue 3, 2004, Pages 431-439.
11. Gao et al., On the true photoreactivity order of {001}, {010}, and {101} facets of anatase TiO_2 crystals, Angew Chem Int Ed Engl., Volume 50, Issue 9, 2011, Pages 2133-7.
12. Cui et al., Graphene oxide–TiO_2 composite filtration membranes and their potential application for water purification, Carbon, Volume 62, 2013, Pages 465-471.
13. C.Yu et al, Design and fabrication of microsphere photocatalysts for environmental purification and energy conversion, Chemical Engineering Journal, Volume 287, 2016, Pages 117-129

CHAPTER 2

LITERATURE REVIEW

This chapter provides the literature review of the history and fundamental of photocatalysis, organic dye pollutants, bismuth based photocatalyst, microstructure and its relationship towards photocatalysis

2.1 Photocatalysis and photocatalyst definition

Photocatalysis is a reaction which uses light to activate a substance which modifies the rate of a chemical reaction without being involved itself. It is a part of advanced oxidation process (AOPs) which involve the participation of photons in the reaction. On the other hand, photocatalyst is the substance which modify the rate of chemical reaction using light irradiation.

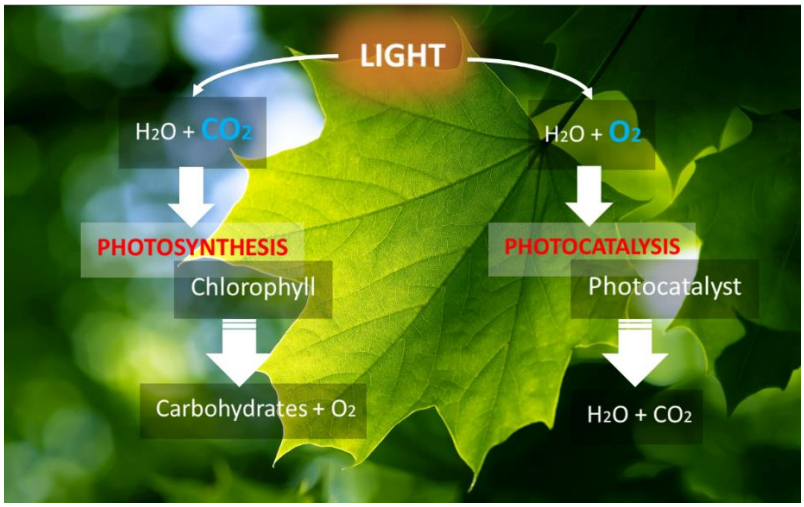

Figure 2.1 The general photosynthesis and photocatalysis mechanism

Photocatalysis can be compared with the natural photosynthesis that occurs in plants as shown in Figure 2.1. Chlorophyll of plants is the typical natural photocatalyst. The difference between chlorophyll photocatalyst to the man-made semiconductor photocatalyst; the chlorophyll captures sunlight to turn water and carbon dioxide into

oxygen and glucose, but on the contrary, semiconductor photocatalyst creates strong oxidation agent and electronic holes to breakdown the organic matter to carbon dioxide and water in the presence of photocatalyst, light and water.

2.1.1 History of photocatalysis

Photocatalysis was first discovered as early as 1911, by Eibner et al [1], Bruner and Kozak [2], and Landau [3] in 1913 which studies on the effect of the illumination of ZnO on the bleaching of Prussian blue [1] and degradation of oxalic acid under illumination in the presence of uranyl (UO_2^+) salts [2],[3]. In 1938, Doodeve and Kitchener [4] investigated for the first time the ability of TiO_2 to act as photosensitizer for the bleaching of dyes in the presence of oxygen. This work reported that UV absorption produces active oxygen species on the TiO_2 surface, causing the discoloration of organic chemicals by photooxidation, although TiO_2 itself remains unchanged after the process. However, due to the absence of practical applications, further study was not much being done and faded in following few decades as in Figure 2.2 [5] which shows the annual evolution of the number of articles of Scientific Citation Index (SCI) publications related to photocatalysis from 1910 to 1981. The dashed line marks the publication of the seminal article of Fujishima and Honda.

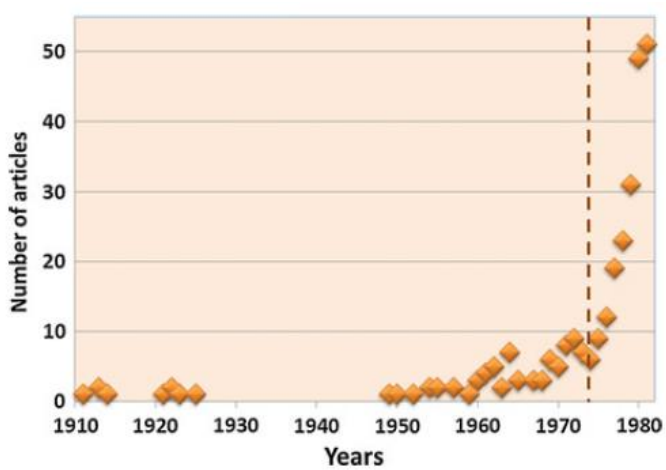

Figure 2.2 Annual evolution of the number of articles of Scientific Citation Index (SCI) publications related to photocatalysis from 1910 to 1981

In 1970s, due to the sudden increase of the crude oil prices which lead to the oil crisis, numerous researches in alternative energy sources had been conducted to find an alternative energy source to reduce the dependency on petroleum, which shows the skyrocketing numbers of articles being published in related field [5]. Fujishima and Honda had published an article in Nature in 1972 [6], on the electrochemical photolysis of water using a rutile electrode exposed to near-UV light and connected to a platinum counter electrode through an electrical load, which gave a perspective in the possibilities of producing a clean hydrogen using an abundant and inexpensive water and sunlight. Their work triggered the development of semiconductor photocatalysis for a wide range of environmental and energy applications.

2.1.2 Schematic diagram of semiconductor photocatalyst

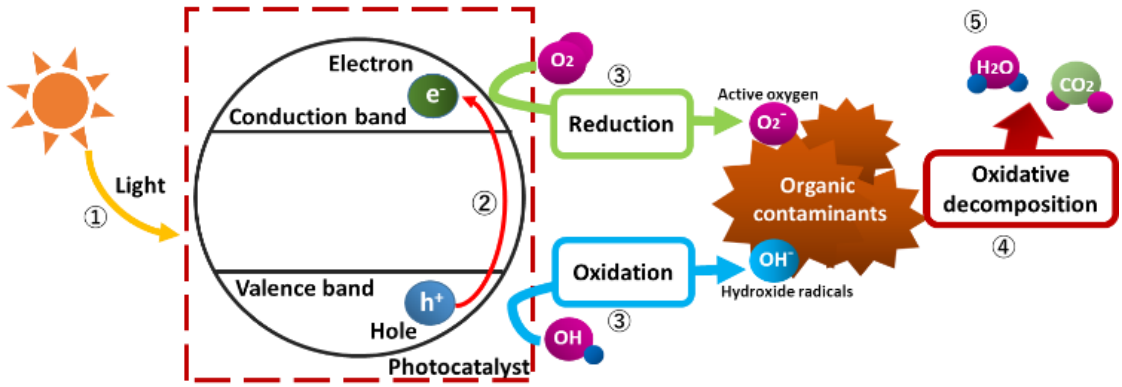

Figure 2.3 The overall mechanism of photocatalysis by semiconductor photocatalyst

A semiconductor material is characterized by two energy bands which separated by the band-gap energy, E_g (Figure 2.3). A semiconductor at absolute zero is insulator, because the valence band (lower energy level) is completely occupied and the conduction band (higher energy level) totally empty. In order to become a conductor, charge carriers need to be created, which usually by photoexcitation via irradiation of light. When a semiconductor surface is irradiated by light ($h\nu \geq Eg$), electron/hole pair (e^-/h^+) are generated by promoting electron from the valence band (VB) to the conduction band (CB). The oxidizing nature of the holes (h^+) in the valence band shows that OH radicals were being generated by the oxidation of the H_2O molecules or OH^- ions adsorbed on the semiconductor surface, that capable of oxidizing the organic molecules directly. The photoexcitation of semiconductor photocatalyst, *A* and possible oxidation of an organic compound are represented in the equations 1 to 4 and the overall mechanism can be seen in Figure 2.3.

$$Semiconductor\ photocatalyst + h\nu \rightarrow h^+ + e^- \quad (1)$$

$$h^+ + H_2O \rightarrow OH^{\cdot} + H^+ \quad (2)$$

$$h^+ + OH^- \rightarrow OH^{\cdot} \quad (3)$$

$$h^+ + dye \rightarrow semiconductor\ photocatalyst + dye^{\cdot +} \quad (4)$$

Although heterogeneous photocatalysis is a well understood process, and despite its promising results in water decontamination, its practical exploitation has been restricted by its low photonic efficiency, which is mainly due to recombination of the e^-/h^+ pair. Therefore, there are considerable efforts being made to obtain new processes able to separate charge carriers and minimize their recombination rate [7], [8].

2.2 Organic dye pollutants

Dyes may be defined as a substance that provide color when applied to a substrate by a process that alters, at least temporarily, any crystal structure of the colored substances [9, 10]. These substances with considerable coloring capacity are widely employed in the textile, pharmaceutical, food, cosmetics, plastics, photographic and paper industries [11], [12]. The dyes can adhere to compatible surfaces by solution and by forming covalent bond or complexes with salts or metals, by physical adsorption or by mechanical retention [9, 10]. Dyes can be classified based on its application and chemical structure. It composed of a group of atoms known as chromophores, which gives color to the dye. These chromophore-containing centers can be grouped based on diverse functional groups, such as the azo, anthraquinone, methine, nitro, arilmethane, carbonyl and others. In addition, electrons withdrawing or donating substituents so as to generate or intensify the color of the chromophores are denominated as auxochromes. The most common auxochromes are amine, carboxyl, sulfonate and hydroxyl [13-15].

It is estimated that over 10,000 different dyes and pigments are used industrially and over 700,000 tons of synthetic dyes are annually produced worldwide [11, 16, 17]. In the textile industry, up to 200,000 tons of these dyes are lost to effluents every year during the dyeing and finishing operations, due to the inefficiency of the dyeing process [17]. Unfortunately, most of these dyes escape conventional wastewater treatment processes and persist in the environment as a result of their high stability to light, temperature, water, detergents, chemicals, soap and other parameters such as bleach and perspiration [18]. However, environmental legislation obliges industries to eliminate color from their dye-containing effluents, before disposal into water bodies [17, 18].

Azo dyes are the largest group of colorants, constituting 60-70% of all organic dyes produced in the world [10, 19]. The success of azo dyes is due to the ease and cost effectiveness for synthesis as compared to natural dyes, and also their great structural diversity, high molar extinction coefficient, and medium-to-high fastness properties in relation to light as well as to wetness [10, 20]. They have a wide range of applications in the textile, pharmaceutical and cosmetic industries, and are also used in food, paper, leather and paints [21, 22]. However, some azo dyes can show toxic effects, especially carcinogenic and mutagenic events [23, 24].

One of the most difficult tasks confronted by the wastewater treatment plants of textile industries is the removal of the color of these compounds, mainly because dyes and pigments are designed to resist biodegradation, such that they remain in the environment for a long period of time. This is why the organic dye degradation has been one of the main subject of research in environmental remediation field in decades.

The photochemical treatment method has been one of the promising method to solve the problem since it used semiconductor photocatalysts which successfully decolorized the dye. Semiconductor such as TiO_2, ZnO, Bi_2O_3 and a few others react with the presence of light source to produce highly reactive species such as OH^- radicals and O^{2-} radicals which results in the decolorization of the dye pollutants in wastewater. Based on organic dye degradation by photocatalysis, organic dyes can be classified into two, which are the cationic dyes and anionic dyes [25].

Cationic dyes are referred to basic dyes due to the presence of positive ions in its molecule structure, while anionic dyes with negative charge on it shows the acidic properties [25, 26].

Therefore, in this study, we have chosen methylene blue (MB) dye which is made up of $C_{16}H_{18}ClN_3S$ for the cationic dye, and methyl orange (MO) dye which is from $C_{14}H_{14}N_3NaO_3S$ for the anionic dye group as a model dye for the photocatalysis study.

2.2.1 Cationic dye – methylene blue (MB)

Methylene blue powder may appear as a solid, odorless, dark green powder at room temperature that yields a blue solution when dissolved in water. It is a common type of azo dye which is used in photocatalytic studies due to its stability and solubility in water [27]. Besides, it is typically found in industrial wastewater and textile industries wastewater which indicates that it is a suitable candidate to be used as the organic pollutant in the study of photocatalytic degradation study. MB is a heterocyclic aromatic chemical compound which has a dark green color powder that yields a blue solution in aqueous solution. It is a cationic dye, with the maximum absorption of 664 nm (Figure 2.4).

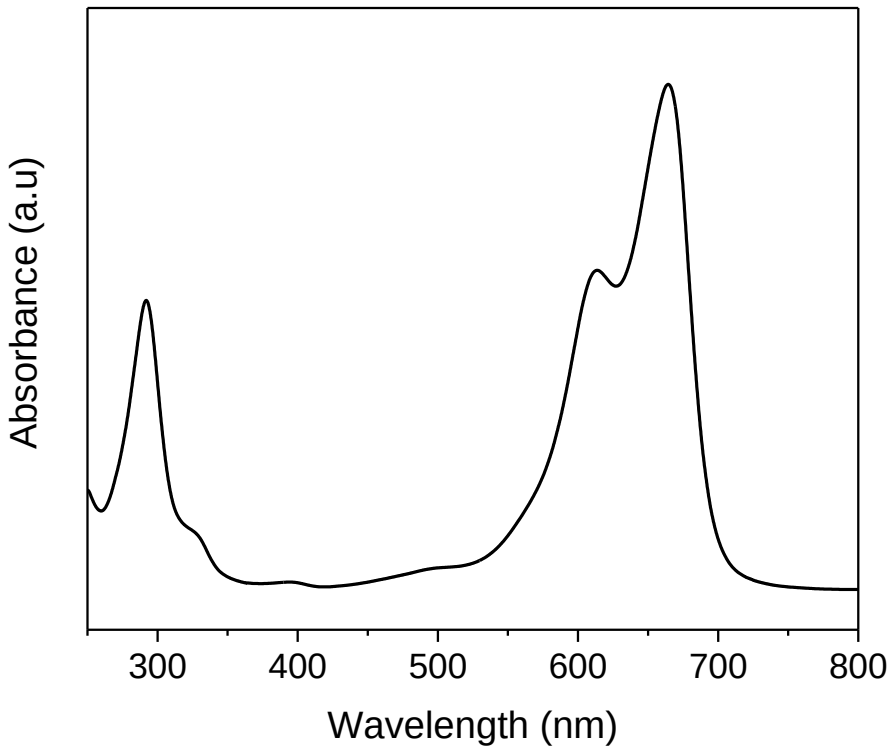

Figure 2.4 The absorption spectrum of methylene blue (MB) dye

The MB dye structure (Figure 2.5) has an equivalent amount of alternating double bonds. The positive charge is shared by the nitrogen and sulfur atoms and it is distributed across the whole cation and not localized at any particular atom. The physical properties of MB dyes are shown in Table 2.1.

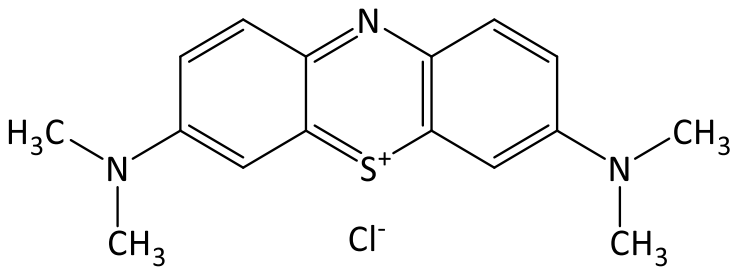

Figure 2.5 Chemical structure of methylene blue (MB) dye

Table 2.1 The physical and chemical properties of methylene blue (MB) dye [27]

IUPAC name	3, 7 bis(dimethylamino) phenothiazine-5-ium chloride
Molecular Formula	$C_{16}H_{18}ClN_3S$
Molecular Weight	319.851 gmol-1
Melting Point	180°C
Solubility in water	110mM
Maximum absorption	664nm

Hermann et.al [28] had described the MB degradation processes in Figure 2.6. It has been observed that the heterogeneous photocatalysis not only decolorized MB, but also completely mineralization it to CO_2, NO_x, SO_x and H_2O. MB degradation processes can be divided into four steps which are the

(1) Demethylation and/or deamination;

(2) Breaking of the MB central aromatic ring at the bonds of $C – S^+ = C$;

(3) Conversion of the above intermediates from the step to smaller organic species such as $R – NH^{3+,}$ aldehydic/carboxylate species, aniline, and phenol;

(4) Further minimization to ultimate products such as CO_2, NH^{4+}, NO^{3-} and SO_4^{2-} [29-32]

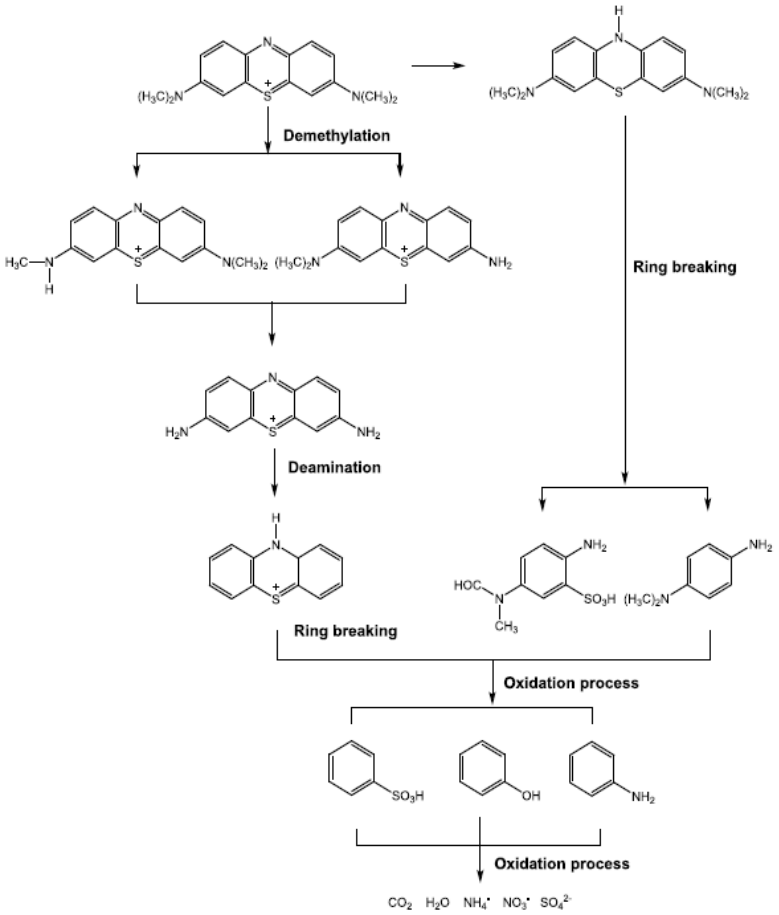

Figure 2.6 Possible photocatalytic degradation pathway of methylene blue (MB) dye as reported by Herrmann et al. [28]

2.2.2 Anionic dye – methyl orange (MO)

Methyl orange powder is in a yellowish orange color, and when dissolved in acidic solution, it turns red. When the solution becoming less acidic, methyl orange moves from red to orange and finally to yellow with the reverse occurring for a solution increasing in acidity.

It is another common type of azo dye which is used in photocatalytic studies. It is an anionic dye, with the maximum absorption of 464 nm (Figure 2.7).

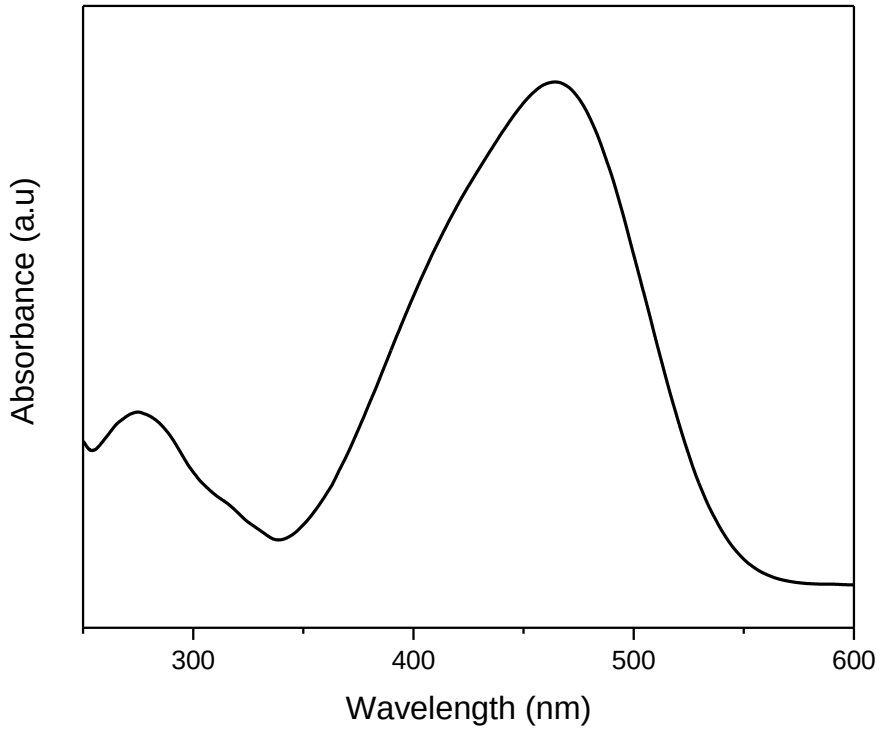

Figure 2.7 The absorption spectrum of methyl orange (MO) dye

MO dye structure (Figure 2.8) consists of negatively charged SO_3^- which is shared by the nitrogen atom. The physical properties of MO dyes are shown in Table 2.2.

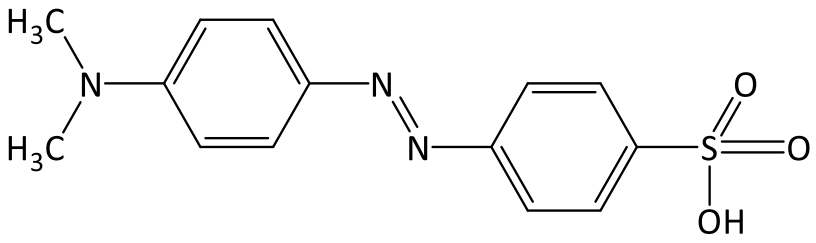

Figure 2.8 Chemical structure of methyl orange (MO) dye

Table 2.2 The physical and chemical properties of methyl orange (MO) dye

IUPAC name	4-dimethylaminoazobenzene-40-sulfonic acid sodium salt
Molecular Formula	$C_{14}H_{14}N_3NaO_3S$
Molecular Weight	327.334 gmol-1
Melting Point	300°C
Solubility in water	0.5 g/100 mL (20 °C)
Maximum absorption	464 nm

R.Comparelli et.al [33] had discussed on the degradation route of MO dye, which the first mechanism involves the homolytic rupture of the nitrogen–carbon bond of the aminic group, that giving rise to the substitution of methyl group with a hydrogen atom (Figure 2.9). The second mechanism is based on the aromatic ring substitution by one or more hydroxyl groups upon attack of hydroxyl radicals. Besides that, the OH substitution initially occurs on the benzene ring carrying the di-methylamino group due to its capability to stabilize the intermediate hydroxy-benzene radical, in contrast to the other benzene ring which, in fact, carries a $–SO_3H$. In addition, the ipso-substitution by a hydroxyl radical can also take place at the carbon position which carries the sulphonic moiety. Furthermore, the presence of by-products deriving from both hydroxyl substitution and photolysis, suggests that the mechanisms is independently active.

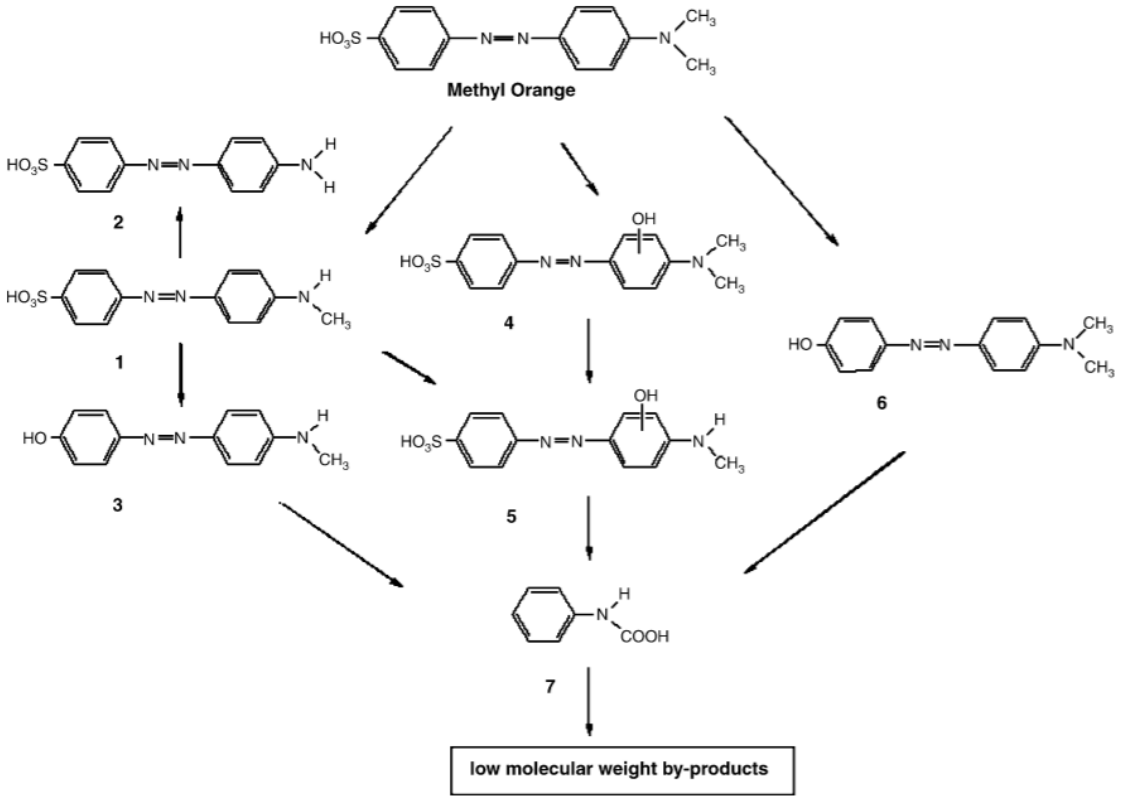

Figure 2.9 Possible photocatalytic degradation pathway of methyl orange (MO) dye [33]

2.3 Bismuth-based photocatalyst

Bismuth-based semiconductor are a promising material for visible light responsive photocatalysts. This is because it has an electronic structure which its valence band consists of hybrid orbitals of O 2p and Bi 6s. The Bi 6s orbitals results in increasing the mobility of its photo-generated charge carriers, besides decreasing the band gaps to less than 3.0 eV (Figure 2.10). Due to its potential, varieties of bismuth-based semiconductor have been studied for its photocatalytic activity such as Bi_2O_3, $BiVO_4$, $NaBiO_3$, BiOX (X= Cl, Br, and I) and others with various phases, morphologies, and various photocatalytic applications.

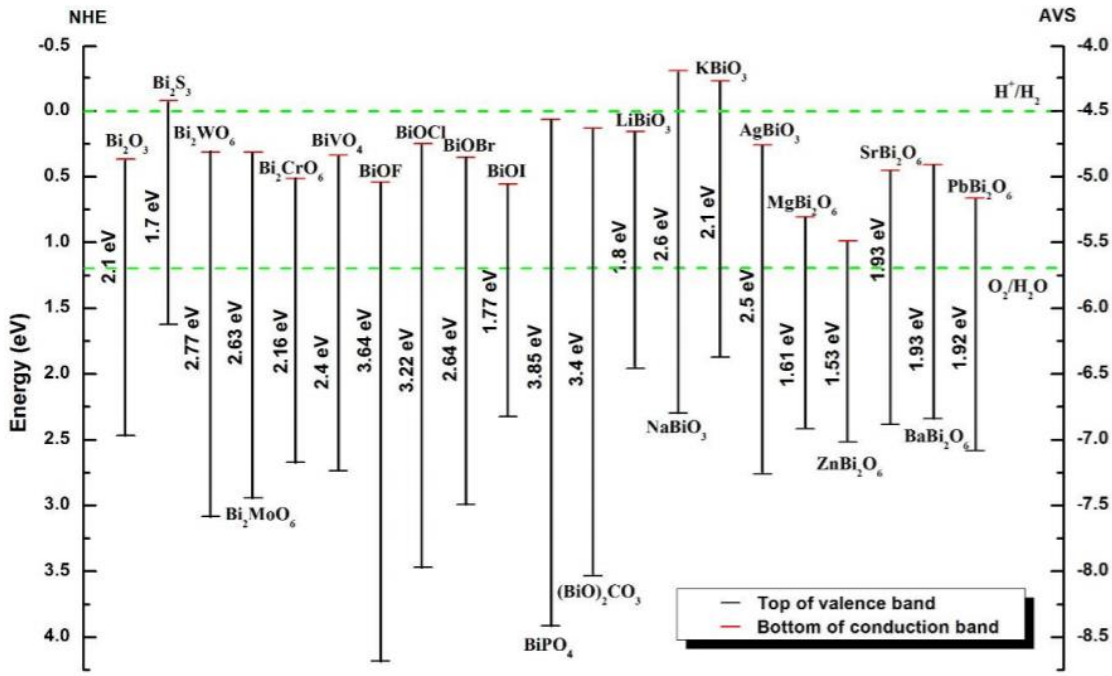

Figure 2.10 Bismuth-based photocatalytic materials and its flatband-edge positions [34]

2.3.1 Sodium bismuthate, $NaBiO_3$

$NaBiO_3$ structure was refined as an ilmenite-type under an ambient condition and the crystal structure was described by Kumada et al. [42]. The NaO_6 (AgO_6) octahedra and BiO_6 octahedra are stacked alternately along the c axis in a layer structure (Figure 2.11. The commercial $NaBiO_3$ (Wako Pure Chemical Industries Ltd., Japan) has a chemical structure of $NaBiO_3 \cdot 2H_2O$, which is a hydrated $NaBiO_3$. However, after calcination at 140°C for 5 hours as reported by Kako et al. [43], it loses the water and the structure changes to the ilmenite-type structure. When comparing these two types of $NaBiO_3$, the dehydrated $NaBiO_3$ has a slight higher efficiency when compared to the hydrated $NaBiO_3$.

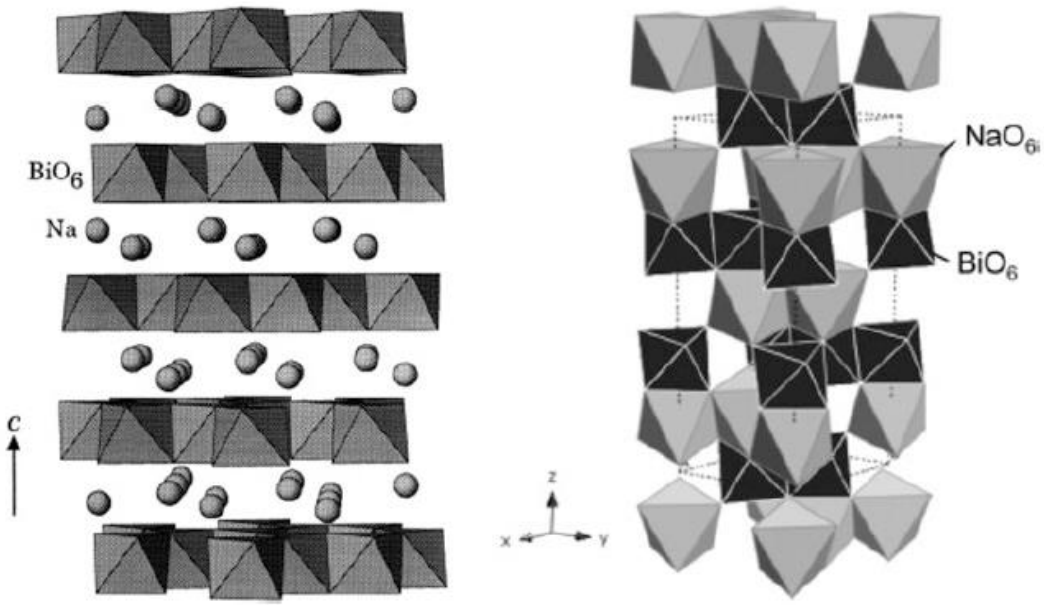

Figure 2.11 Crystal structure of $NaBiO_3$ from different view directions

Dias et al. [44] have also further determined the crystal structure of $NaBiO_3$ by measuring the phonon spectra via Raman and infrared spectroscopies. They have also conducted group theory calculations to confirm the trigonal R3, which is the most possible space group to describe the perovskite oxides, but with highly distorted structure because of the very small tolerance factor (t = 0.793) [44].

The first report on $NaBiO_3$ in photocatalysis application was published by Kako et al. [43], which uses dehydrated $NaBiO_3$ that was prepared by heating the commercialize $NaBiO_3 \cdot 2H_2O$ for 5 h. The calculated band gap value for the $NaBiO_3$ shows smaller value of 2.6 eV (indirect band gap), compared with typical trivalent bismuthates compound such as (2.8–2.9 eV), Bi_2WO_6 (2.8 eV), and $Bi_2W_2O_9$ (3.0 eV). The photocatalytic performance was determined by the decomposition of 2-propanol and methylene blue from air and aqueous solution, respectively. It was found that the $NaBiO_3$ can convert 2-propanol into acetone effectively under visible light, but cannot mineralize 2-propanol into CO_2 and H_2O at the irradiation time of less than 1 h, which might be due to the degradation pathway. However, $NaBiO_3$ exhibits superior photooxidation activity to methylene blue than N-doped TiO_2 and $BiVO_4$ photocatalysts which are commonly used in photocatalysis study. The photooxidation activity of $NaBiO_3$ shows a slight decrease after the reaction was cycled for 6 times, which correspond to the XRD data, which shows that $NaBiO_3$ were still detectable after recycling, indicating the good photostability of the $NaBiO_3$ catalyst.

Another study was reported by Yu et al. which shows a slight decrease in the photoactivity after five cycles of degrading Rhodamine B. It also shows that $NaBiO_3$ peak can still be detected after the cycles. [45]. Nonetheless, the instability of $NaBiO_3 \cdot 2H_2O$ under long time exposure was found by Eberl [46]. They found that the color of $NaBiO_3$ gradually changes from yellow to brown as the time of the photocatalytic reaction was extended. XRD results also showed that after a long time (about 20 h) of photocatalytic reaction, $NaBiO_3 \bullet 2H_2O$ was transformed into $(BiO)_2CO_3$ crystal finally. Moreover, Sepulveda-Guzman et al.'s study also showed the poor stability of $NaBiO_3$ under electron beam exposure. Selected Area Electron Diffraction (SAED) results showed that $NaBiO_3$ can be partially reduced to metallic Bismuth particles under electron beam irradiation [47].

2.3.2 Potassium bismuthate, $KBiO_3$ and lithium bismuthate $LiBiO_3$

$KBiO_3$ and $LiBiO_3$ exhibit tunnel structures and iso-structure with $KSbO_3$, which are different from ilmenite oxides of $ABiO_3$ (A=Na, Ag). However, both the $KBiO_3$ and $LiBiO_3$ with tunnel structures and ilmenite-type oxides of $ABiO_3$ (A=Na, Ag) are formed by edge-sharing octahedra. Such structures consist of BiO_6 octahedra pairs which are edge-shared to form Bi_2O_{10} clusters, resulting in the formation of tunnel structure (as shown in Figure 2.12 and 2.13). For $KBiO_3$, the potassium ion partially occupies three sites in the tunnel structure. Thermal gravimetric (TG) analysis results indicated that a sudden weight loss takes place above 500 °C, suggesting the decomposition of $KBiO_3$ into K_2O and Bi_2O_3 [48].

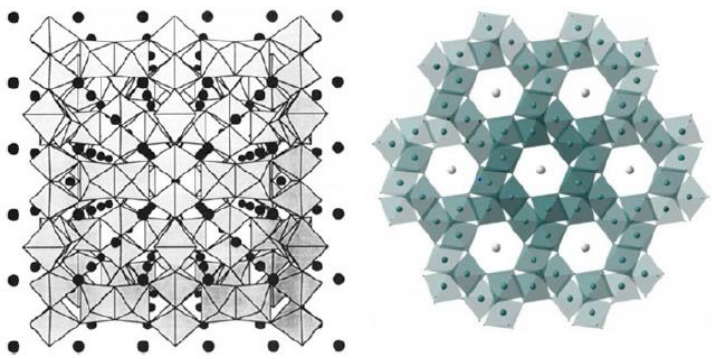

Figure 2.12 Crystal structure of $KBiO_3$ (shaded circles represent potassium atoms located along the [111] direction [48]; right: oxygen atoms are at the corner of the octahedron around Bi^{5+} while K^+ cations reside within the tunnels [49]

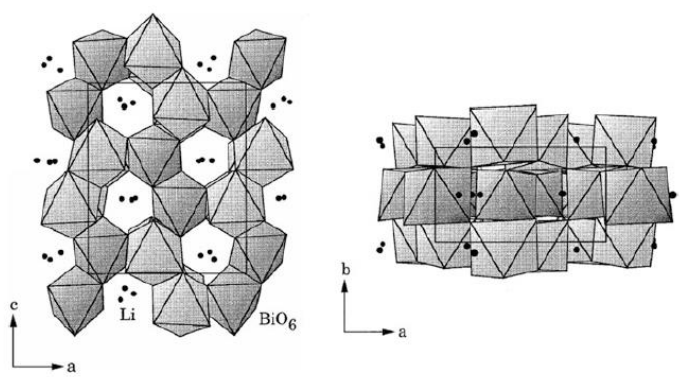

Figure 2.13 Crystal structure of $LiBiO_3$ [50]

The Goldschmidt's tolerance factor (t) of $KBiO_3$ and $LiBiO_3$ was calculated at 0.867 and 0.710 (as shown in Figure 2.14), respectively, indicating that only $KBiO_3$ can be considered as a stable perovskite oxide.

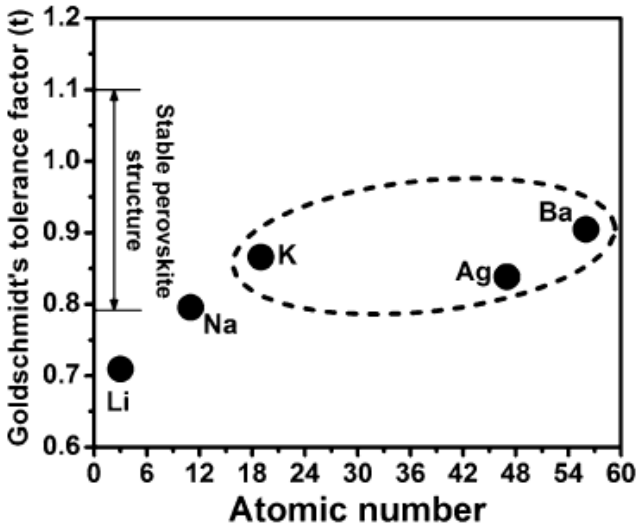

Figure 2.14 Calculated Goldschmidt's tolerance factors of various pentavalent bismuthates

Up to now, four kinds of lithium bismuth oxides containing pentavalent bismuth have been discovered, that is, Li_3BiO_4 [51], Li_7BiO_6 [52], Li_5BiO_5 [53], and $LiBiO_3$ [50]. Among them, $LiBiO_3$ has attracted more attention due to its potential applications in heterogeneous photocatalysis.

By means of neutron powder diffraction data, the structure of $LiBiO_3$ oxides with high purity was characterized and reported for the first time in 1996. The as-prepared $LiBiO_3$ crystal which crystallizes in the orthorhombic system was found to have the isostructure with $LiSbO_3$, because of the fact that array of hexagonally close-packed oxygen atoms with cations occupying two thirds of the octahedral sites can be observed in both structures. Thermal gravimetric and differential thermal analysis (TG-DTA) results show that $LiBiO_3$ is decomposed to $LiBiO_2$ after heating up to 300 °C [50].

Kikugawa et al. [54] investigated the photocatalytic degradation of methylene blue over as prepared $LiBiO_3$ under white fluorescent light exposure. Their results show that methylene blue can be completely decolorized after 4 hours reaction, and the mineralization efficiency can be reached to 70 %. The highest apparent photo-efficiency (PE) of 0.15 % could be obtained under 420 nm monochromatic light irradiation. The photocatalytic activity of $LiBiO_3$ was further confirmed by Ramachandran et al. [49]. Two cationic dyes of Rhodamine B and Methylene blue have been used as model compounds. Under UV and solar radiations, it was found that $LiBiO_3$ exhibits better photocatalytic activity of Methylene blue than Rhodamine B in terms of both degradation efficiency and reaction kinetics constant. The photocatalytic degradation of various anionic dyes, i.e., Orange G (OG), Amido black 10B (AB10B), Alizarin cyanine green (ACG), Indigo carmine (IC), and Coomassie brilliant blue R 250 (CBBr) over $KBiO_3$ from aqueous phase were investigated by Ramachandran et al. [49] as well. It was found that the overall photocatalytic degradation of CBBr and ACG are higher than that of OG and AB10B, possibly because of the more reactive of CBBr and ACG where sulfonyl group is attached to the benzene ring, but less reactive naphthalene leads to the less reactive of OG and AB10B.

2.3.3 Bismuth vanadate, $BiVO_4$

Bismuth vanadate ($BiVO_4$) has compelling physicochemical properties including ferro-elasticity and ionic conductivity. It has a theoretical band gap of 2.047 eV as calculated by DFT method [35]. The valence band of $BiVO_4$ mainly consists of O 2p and V 3d orbitals. Besides, $BiVO_4$ have three types of phases, like the bismuth oxide, Bi_2O_3 which makes it more interesting and varieties in exploring this material.

It has the monoclinic fergusonite, tetragonal scheelite and tetragonal zircon (Figure 2.15) while the reversible phase transition between monoclinic fergusonite and tetragonal scheelite occurs at 255℃ [36].

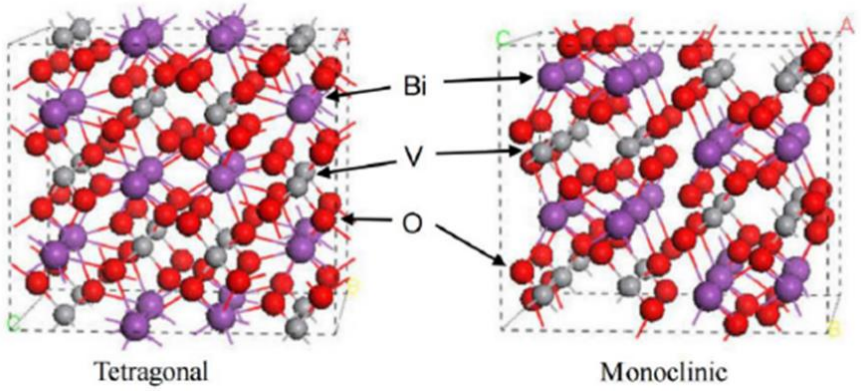

Figure 2.15 Two crystal structures of tetragonal and monoclinic $BiVO_4$ [37]

Various approaches in synthesizing $BiVO_4$ have been reported. A monoclinic $BiVO_4$ has successfully been prepared by solid state reaction (SSR) and by melting at a high temperature [38]. Whereas, a tetragonal $BiVO_4$ has been synthesized by a precipitation method at a room temperature [39]. The band gap for both phases also differs, which are 2.4 eV and 2.9 eV respectively, indicating that the monoclinic phase is at advantage for the visible-light region reaction. In addition, a simple aqueous process in preparing both monoclinic and tetragonal phase were also reported [40]. Besides, the use of hydrothermal process in creating various structural, morphologies and phase were also being reported. Since $BiVO_4$ can be prepared by using a simple method, it is one of the suitable candidates in the study of a low-cost synthesis method.

$BiVO_4$ has been widely used in various photocatalytic field such as organic dye degradation and hydrogen evolution by water splitting, under visible light irradiation. For example, in the organic degradation such as the Rhodamine B dye and phenol, $BiVO_4$ shows a higher removal efficiency when compared to N doped TiO_2 [41]. Besides, when compared to other materials such as the alkali bismuthate, even though the decolorization rate is slower, it is capable or degrading the compound better, which will be discussed in chapter 5 and 6.

2.4 Microstructure photocatalyst in enhancing the photocatalytic activity

Microsphere photocatalysts exhibited superior properties in aqueous photocatalytic reactions due to its low density, efficient light harvesting capability and carrier separation, excellent electronic and optical properties, high surface area, easy settling, good delivering ability, and surface permeability which improved the photocatalytic performances.

Although nanosize powder photocatalysts present superior properties in aqueous photocatalytic reactions because of its large surface area, good dispersion and abundant active sites, powder-like nano photocatalyst often suffer from deactivation, agglomeration and difficulty in settling for catalyst recycling after the initial run. This makes the photocatalyst hard to be recycle, and non-recyclable photocatalytic materials will increase the operating cost, which significantly limits the applications in wastewater treatment. In most wastewater treatment, photocatalysts are suspended in aqueous solution. The separation of photocatalyst must be performed through settling by aid of gravity or mechanical centrifugation. Settling of ultrafine photocatalyst particles by the aid of gravity has been commonly observed to proceed very slowly.

For example [55], for TiO_2 photocatalyst with the particle size of 10 to 22 nm, the average settling velocity was 3.3 mm/min. However, the average settling velocity of TiO_2 microspheres (size: 30 to 160 μm) was 2.5 to 15 mm/s. TiO_2 microspheres settled more quickly than the TiO_2 powder samples fabricated from the same raw materials. In real water purification, either in a batch-scale reactor or in a continuous reactor, the separation of photocatalysts from the aqueous phase is of great significance from an economic standpoint. The operating cost of the photocatalytic reaction mainly originates from the photocatalyst being once employed without recycling. For example, Liu et al. analyzed the economics of photocatalysts in water purification in detail [56]. The results illustrated that the cost of TiO_2 photocatalyst mainly depended on its dosage.

From the study, we can conclude that microsphere photocatalysts exhibit several distinct advantages in aqueous reactions compared to nano photocatalysts. Besides, it is

easy to be recycled after the separation from the reaction systems, which decrease the operating cost. Therefore, the design and fabrication of high-quality photocatalysts with desired morphologies and enhanced photocatalytic activities and stabilities are of significant fundamental and technological interest.

In the degradation of organic pollutants in water, photocatalytic process is commonly designed as a powder suspension system, and most photocatalysts are composed of ultrafine powders. The suspension system enables fine contact between the catalyst particles and organic substrates, and thus the illumination of the particles is ensured. However, the suspension reaction matrix suffers from the problem of photocatalyst recovery after use because photocatalysts are usually fabricated as nanosized particles which are easy to lose and difficult to separate from the reaction solution. To accelerate powder separation, certain additional measures are adopted. For example, coagulation through addition of ferrous sulfate is performed, but the photocatalyst is fouled and cannot be reused. Alternatively, the powder photocatalysts can be immobilized onto a solid support, such as glass, fiber, or stainless steel. However, a considerable loss of contact area between the immobilized photocatalyst and the light source occurs, thus evidently lowering the photocatalytic degradation efficiency of the organic substrate.

The problem of recycling photocatalyst requires a novel fabrication concept. Given that the suspension reaction system has high illumination efficiency because of the full contact between the photocatalyst particles and the light source, the advantage of this system is maintained. On the other hand, for easy recycling, the powder-like photocatalyst should be modified. Therefore, a microsphere photocatalyst appears to be ideal to overcome the disadvantages of its powder-like counterpart. Several works in this regard show that such microsphere photocatalysts can be applied successfully [57,58]. If the size of microspheres can be designed and the catalysts can be suspended by air bubbling or stirring, satisfactory contact with the light source can be maintained. Meanwhile, once air bubbling or mechanical stirring stops, the microspheres can rapidly settle to the reactor bottom under the force of gravity, so the treated aqueous phase can be decanted and easily separated from the microspheres. Thus, microspheres can be readily reused.

2.5 References

1. Eibner A, Action of light on pigments, I. Chem-Ztg 35, 1911, page 753–755.
2. Bruner L, Kozak J, Information on the photocatalysis I the light reaction in uranium salt plus oxalic acid mixtures. Z Elktrochem Angew P 17, 1911, page 354–360.
3. Landau M, Le phénomène de la photocatalyse. Compt Rend 156, 1913, page 1894–1896.
4. Doodeve CF, Kitchener JA, The mechanism of photosensitization by solids trans. Faraday Soc 34, 1938, page 902–912.
5. J. M. Coronado et al., Design of Advanced Photocatalytic Materials for Energy and Environmental Applications, Green Energy and Technology, 2013 page 1-4
6. Fujishima A, Honda K, Electrochemical photolysis of water at a semiconductor electrode, Nature 238, 1972, page 37–38.
7. S X.Z. Li, H. Liu, L.F. Cheng, H.J. Tong, Photocatalytic oxidation using a new catalytic TiO_2 microsphere for water and wastewater treatment, Environ. Sci. Technol. 37, 2003, page 3989-3994.
8. S C.Y. Song, W.J. Yu, B. Zhao, H.L. Zhang, C.J. Tang, K.Q. Sun, X.C. Wu, L. Dong, Y.Chen, Efficient fabrication and photocatalytic properties of TiO_2 hollow spheres, Catal. Commun. 10, 2009, page 650-654.
9. Kirk-Othmer. Encyclopedia of Chemical Technology, v. 7, 5th Edition. Wiley-Interscience, 2004.
10. Bafana A, Devi SS, Chakrabarti T. Azo dyes: past, present and the future. Environmental Reviews, 19, 2011, page 350–370.
11. Zollinger, H. Synthesis, Properties of Organic Dyes and Pigments. In: Color Chemistry. New York, USA: VCH Publishers, 1987, page 92-102.
12. Carneiro PA, Nogueira, RFP, Zanoni, MVB. Homogeneous photodegradation of C.I. Reactive Blue 4 using a photo-Fenton, Dyes and Pigments 74, 2007, page 127-132.
13. Christie R. Colour Chemistry. Cambridge, United Kingdom: The Royal Society of Chemistry; 2001.

14. Dos Santos AB, Cervantes FJ, van Lier JB. Review paper on current technologies for decolourisation of textile wastewaters: Perspectives for anaerobic biotechnology. Bioresource Technology, 98(12), 2007, page 2369-2385.
15. Arun Prasad AS, Bhaskara Rao KV. Physico chemical characterization of textile effluent and screening for dye decolorizing bactéria. Global Journal of Biotechnology and Biochemistry, 5(2), 2010, page 80-86.
16. Robinson T, McMullan G, Marchant R, Nigam P. Remediation of dyes in textile effluent: a critical review on current treatment technologies with a proposed alternative Bioresource Technology, 77(12), 2001, page 247-255.
17. Ogugbue CJ, Sawidis T. Bioremediation and Detoxification of Synthetic Wastewater Containing Triarylmethane Dyes by Aeromonas hydrophila Isolated from Industrial Effluent. Biotechnology Research International 2011
18. Couto SR. Dye removal by immobilised fungi. Biotechnology Advances, 27(3), 2009, page 227-235.
19. O'Neill C, Hawkes FR, Hawkes DL, Lourenço ND, Pinheiro HM, Delée W. Colour in textile effluents – sources, measurement, discharge consents and simulation: a review, Journal of Chemical Technology and Biotechnology, 74 (11), 1999, page 1009-1018.
20. Carliell CM, Barclay SJ, Shaw C, Wheatley AD, Buckley C A. The effect of salts used in textile dyeing on microbial decolourisation of a reactive azo dye. Environmental Technology, 19 (11), 1998, page 1133-1137.
21. Seesuriyachan P, Takenaka S, Kuntiya A, Klayraung S, Murakami S, Aoki K. Metabolism of azo dyes by Lactobacillus casei TISTR 1500 and effects of various factors on decolorization. Water Research, 41(5), 2007, page 985-992.
22. Ben Mansour H, Corroler D, Barillier D, Ghedira K, Chekir L, Mosrati R. Evaluation of genotoxicity and pro-oxidant effect of the azo dyes: Acids yellow 17, violet 7 and orange 52, and of their degradation products by Pseudomonas putida mt-2. Food and Chemical Toxicology, 45 (9), 2007, page 1670-1677.
23. Chung KT, Cerniglia CE. Mutagenicity of azo dyes: Structure-activity relationships, Mutation Research, 277 (3), 1992, page 201-220.

24. Pinheiro HM, Touraud E, Thomas O. Aromatic amines from azo dye reduction: status review with emphasis on direct UV spectrophotometric detection in textile industry wastewaters. Dyes and Pigments, 61 (2), 2004, page 121-139.
25. M. A. M. Salleh, D. K. Mahmoud, W. A. W. A. Karim and A. Idris, Cationic and anionic dye adsorption by agricultural solid wastes: A comprehensive review, Desalination, 280, 2011, page 1–13.
26. Tushar K Sen, et al., Review on Dye Removal from Its Aqueous Solution into Alternative Cost Effective and Non-Conventional Adsorbents, J Chem Proc Engg 1, 2014, page 1-7.
27. Eren, B Afsin, Y Onal ,Removal of lead ions by acid activated and manganese oxide-coated bentonite, Journal of Hazardous Materials 161 (2), 2009, pp 677-685
28. J. M. Herrmann, Heterogeneous photocatalysis: fundamentals and applications to the removal of various types of aqueous pollutants, Catalysis Today, 53, 1999, page 115–129.
29. H. Jiang, M. Nagai, and K. Kobayashi, Enhanced photocatalytic activity for degradation of methylene blue over V2O5/BiVO4 composite, Journal of Alloys and Compounds, vol. 479, no. 1-2, 2009, page 821–827.
30. P. Wang, M. Cheng and Z. Zhang, On different photodecomposition behaviors of rhodamine B on laponite and montmorillonite clay under visible light irradiation, Journal of Saudi Chemical Society, 18, 2014, page 308–316.
31. A. Houas, H. Lachheb, M. Ksibi, E. Elaloui, C. Guillard and J. M. Herrmann, Photocatalytic degradation pathway of methylene blue in water, Applied Catalysis B, 31, 2001, page 145–157.
32. R. Comparelli et al., UV-induced Photocatalytic Degradation of Azo Dyes by Organic-Capped ZnO Nanocrystals Immobilized onto Substrate, Applied Catalysis B: Environmental 60, 2005, page 1–11.
33. Xiangchao Meng, Zisheng Zhang, Bismuth based Photocatalytic Semiconductors: Introduction, Challenges and Possible Approaches, Journal of Molecular Catalysis A: Chemical, Volume 423, 2016, page 533-549.

34. Z. Zhao, W. Luo, Z. Li, Z. Zou, Density functional theory study of doping effects in monoclinic clinobisvanite BiVO4, Phys Lett A, 374, 2010, page 4919-4927.
35. J.D. Bierlein, A.W. Sleight, Ferroelasticity in BiVO4, Solid State Commun, 16, 1975, page 69-70.
36. R.a. He, S. Cao, P. Zhou, J. Yu, Recent advances in visible light Bi-based photocatalysts, Chinese J Catal, 35, 2014, page 989-1007.
37. M. Gotic, S. Music, M. Ivanda, M. Soufek, S. Popovic, Synthesis and characterisation of bismuth(III) vanadate, J Mol Struct, 744-747, 2005, page 535-540.
38. A. Kudo, K. Omori, H. Kato, A Novel Aqueous Process for Preparation of Crystal Form-Controlled and Highly Crystalline $BiVO_4$ Powder from Layered Vanadates at Room Temperature and Its Photocatalytic and Photophysical Properties, J Am Chem Soc, 121, 1999, page 11459-11467.
39. X. Zhang, Z. Ai, F. Jia, L. Zhang, X. Fan, Z. Zou, Selective synthesis and visible light photocatalytic activities of BiVO4 with different crystalline phases, Mater Chem Phys, 103, 2007, page 162-167.
40. M. Shang, W. Wang, J. Ren, S. Sun, L. Zhang, A novel $BiVO_4$ hierarchical nanostructure: controllable synthesis, growth mechanism, and application in photocatalysis, Crystengcomm, 12, 2010, page 1754-1758.
41. Kumada, N., Kinomura, N., Sleight, A.W.: Neutron powder diffraction refinement of ilmenite-type bismuth oxides: $ABiO_3$ (A=Na, Ag). Mater. Res. Bull 35, 2000, page 2397–2402.
42. Kako, T., Zou, Z.G., Katagiri, M., Ye, J.H.: Decomposition of organic compounds over NaBiO3 under visible light irradiation. Chem. Mater. 19, 2007, page 198–202.
43. Dias, A., Moreira, R.L.: Crystal structure and phonon modes of ilmenite-type $NaBiO_3$ investigated by Raman and infrared spectroscopies. J. Raman Spectrosc. 41, 2010, page 698–701.
44. Yu, K., Yang, S.G., He, H., Sun, C., Gu, C.G., Ju, Y.M.: Visible light-driven photocatalyticndegradation of rhodamine B over $NaBiO_3$: pathways and mechanism. J. Phys. Chem. A 113, 2009, page 10024–10032.

45. Eberl, J.: Visible light photo-oxidations in the presence of bismuth oxides. Dissertation, Friedrich-Alexander-Universität Erlangen-Nürnberg, 2008.
46. Sepulveda-Guzman, S., Elizondo-Villarreal, N., Torres-Castro, D.F.A., Gao, X., Zhou, J.P., Jose-Yacaman, M.: In situ formation of bismuth nanoparticles through electron-beam irradiation in a transmission electron microscope. Nanotechnology 18, 2007, page 335604.
47. Nguyen, T.N., Giaquinta, D.M., Davis, W.M., zur Loye, H.C.: Electrosynthesis of $KBiO_3$: a potassium ion conductor with the $KSbO_3$ tunnel structure. Chem. Mater. 5, 1993, page1273–1276.
48. Ramachandran, R., Sathiya, M., Ramesha, K., Prakash, A.S., Madras, G., Shukla, A.K.: Photocatalytic properties of $KBiO_3$ and $LiBiO_3$ with tunnel structures, Journal of Chemical Sciences 123(4), 2011, page 517-524.
49. Kumada, N., Takahashi, N., Kinomura, N.: Preparation and crystal structure of a new lithium bismuth oxide: $LiBiO_3$. J. Solid State Chem. 126, 1996, page 121–126.
50. Blasse, G.: On the structure of some compounds $Li_3Me^{5+}O_4$, and some other mixed metal oxides containing lithium. Z. Anorg. Allgem. Chem. 331, 1964, page 44–50.
51. Nomura, E., Greenblatt, M.: Ionic conductivity of Li_7BiO_6. Journal of Solid State Chemicals, 52, 1984, page 91–93.
52. Greaves, C., Katib, S.M.A.: The structures of Li_5BiO_5 and Li_5SbO_5 from powder neutron diffraction. Mater. Res. Bull 24, 1989, page 973–980.
53. Kikugawa, N., Yang, L.Q., Matsumoto, T., Ye, J.H.: Photoinduced degradation of organic dye over $LiBiO_3$ under illumination of white fluorescent light. J. Mater. Res. 25, 2010, page 177–181.
54. Yu C L, Zhou W Q, Liu H, et al., Design and fabrication of microsphere photocatalysts for environmental purification and energy conversion, Chemical Engineering Journal, 287, 2016, page 117–129.
55. H. Liu, C.L. Yu, C. Wang, Economics and its implication of photocatalyst recycling for water purification, handbook of photocatalysts: preparation, structure and applications, Chapter 19, 2009, page 527-534.

56. C.L. Yu, J.C. Yu, M. Chan, Sonochemical fabrication of fluorinated mesoporous titanium dioxide microspheres, Solid. State. Chem. 182, 2009, page 1061-1069.
57. J.C. Yu, J.G. Yu, L.Z. Zhang, W.K. Ho, Enhancing effects of water content and ultrasonic irradiation on the photocatalytic activity of nano-sized TiO_2 powders, J. Photochem. Photobiol. A: Chem. 148, 2002, page 263-271.

CHAPTER 3

RESEARCH METHODOLOGY

This chapter focuses on the experimental part of the photocatalysis, which comprises of the chemicals and reagents, the instrument used and the standard experimental setup. Standard operating procedures are also included in this chapter. The schematic diagram and the photograph of the systems are given. All the technical and analytical methods used in this research are addressed.

3.1 Chemicals and Reagents

In this study, we have used methylene blue dye powder from Waldeck GmbH & Co. KG, methyl orange dye powder, sodium bismuthate ($NaBiO_3$), potassium hydroxide (KOH), lithium hydroxide monohydrate ($LiOH{\cdot}H_2O$), bismuth dioxide (Bi_2O_3), bismuth nitrate pentahydrate ($Bi(NO_3)_3{\bullet}5H_2O$) crystal, sodium metavanadate ($NaVO_3$), bismuth titanate($Bi_2O_3{\bullet}2TiO_2$), titanium dioxide P25 (TiO_2), hydrochloric acid (HCl), nitric acid (HNO_3), Tert-butanol and EDTA were purchased from Wako Pure Chemical Industries, bismuth vanadate ($BiVO_4$) from Alfa Aesar and sodium hydroxide (NaOH) granule was bought from Kanto Chemical Co., Inc. Ultrapure water was used in all experiments. All chemicals were analytical grade and used as received without further purification.

3.2 Synthesis of photocatalysts

Sodium bismuthate ($NaBiO_3$), bismuth vanadate ($BiVO_4$), bismuth dioxide (Bi_2O_3), bismuth titanate ($Bi_2O_3{\bullet}2TiO_2$) and titanium dioxide (TiO_2) were further used without any further purification for the pilot study. However, for further study in the next chapter, sodium bismuthate was calcined at 140°C for 6 hours. Potassium bismuthate and lithium bismuthate were prepared via solid state reaction method, which will be discussed in

detail in chapter 5 while bismuth vanadate, $Bi_{11}VO_{19}$ and $BiVO_4$ were prepared by using the simple precipitation method that will be explained in chapter 6 and 7.

3.3 Photocatalytic degradation of dyes

In this study, we have chosen two different types of organic dye to be used which are the methylene blue (MB) dye from cationic dye group and methyl orange (MO) dye from anionic dye group. These two dyes act as the organic contaminants for the study of photocatalytic degradation.

3.3.1 Photocatalysis set up, rate of degradation and TOC

4mL of dye solution was placed in a 100 mL Pyrex vessel. Then, 96mL of ultrapure water was added to the aqueous solution. After that, 0.3 g of photocatalyst sample was added for each experiment. The experiments were conducted under the presence of visible light (λ > 400nm). The solution was magnetically stirred to ensure uniformity. The samples were then filtered by using syringe membrane filter (Millex: Millipore Corp., United States) to remove the photocatalyst particles. Samples were taken from the solution for every 10 minutes for MB dye and 30 minutes for MO dye and placed inside a UV-Vis spectrophotometer cell in order to measure the maximum absorption of wavelength for the dye and the rate of degradation. The experiment setup is shown in Figure 3.1.

The percentage of degradation was calculated by C/C_0. Here, C is the concentration of remaining MB solution at each irradiated time interval, while C_0 is the initial concentration. The degradation efficiency of the dye wastewater was defined as the following equation (Eq. 1).

$$\textit{Degradation rate (\%)} = (C_0 - C_t)/ C_0 \times 100\% \quad (1)$$

where C_0 was the initial concentration of the MB or MO and C_t was the concentration of the MB or MO at certain irradiation time t (min). Besides, a study using Total Organic

Carbon (TOC) analysis was also performed to measure the level of organic molecules or contaminants in the wastewater. The total organic carbon can be defined as the following equation (Eq.2).

TC (Total Carbon) – TIC (Total Inorganic Carbon) =

TOC (Total Organic Carbon) (2)

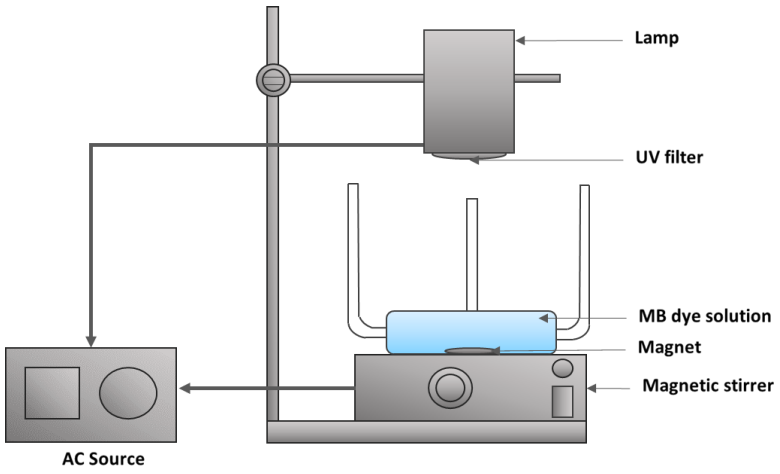

Figure 3.1 Photocatalysis set up for MB or MO dye degradation

3.4 Analysis

After synthesizing the photocatalytic materials, various analyses were conducted to provide a better understanding towards the new developed materials. Analyses part can be divided into two parts, which are the structural analysis and the physical analysis.

3.4.1 Structural Analysis

In structural analysis, we have conducted 4 analyses by using XRD to study on the compound formed, the uv-vis diffuse reflectance spectrometer for the wavelength absorbance, the FTIR for the study of synthesized materials bonding character, the raman spectra analysis and fluorescence spectrometer.

For XRD analysis (Figure 3.2), the samples were analyzed with an x-ray diffractometer (XRD, RINT 2000; Rigaku, Corp., Japan) operated at 30 kV and 40 mA with Cu Kα radiation (λ=1.54178Å). Data were collected in the angular range of 2θ=15–80°.

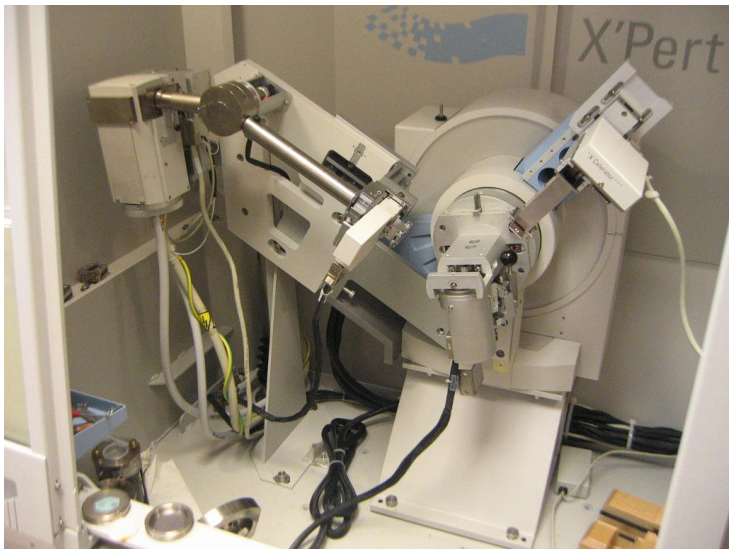

Figure 3.2 XRD

For UV-visible diffusion reflectance spectra, the measurement was conducted at a room temperature, with a UV-Vis-NIR Spectrophotometer JASCO V-7200 (Figure 3.3). The reflectance was then converted to absorbance by using the Kubelka–Munk method.

Figure 3.3 UV-Visible Spectrophotometer

FTIR identifies chemical bonds in a molecule by producing an infrared absorption spectrum. The spectra produce a profile of the sample, a distinctive molecular fingerprint that can be used to screen and scan samples for many different components. It is an effective analytical instrument for detecting functional groups and characterizing covalent bonding information. In this study, Fourier Transform Infrared Spectroscopy Thermoscientific Nicolet 4700 was used. The details of the covalent bond and functional group can be seen in Figure 3.4 and Table 3.1.

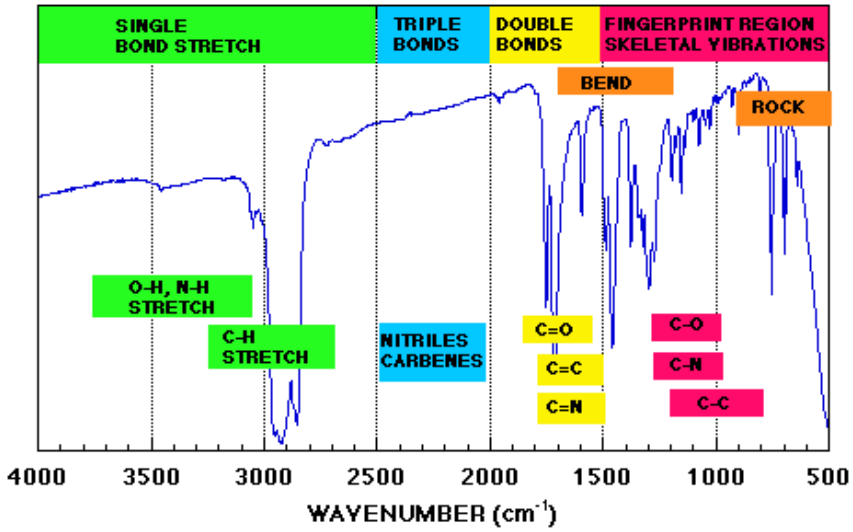

Figure 3.4 FTIR covalent bond analysis chart

Table 3.1 Typical vibrational frequencies of functional groups for FTIR analysis

Table 10.1 Typical vibrational frequencies of functional groups		
Bond	**Molecule**	**Wavenumber (cm^{-1})**
C–O	Alcohols, ethers, esters, carboxylic acids, etc.	1300 – 1000
C=O	Aldehydes, ketones, esters, carboxylic acids	1750 – 1680
C=O	Amides	1680 – 1630
N–H (Stretching)	Amines and amides	3500 – 3100
–N–H (Bending)	Amines and amides	1640 – 1550
O–H	Alcohols	3650 – 3200
C–N	Amines	1350 – 1000
S–H	Mercaptans	2550

Raman analysis was conducted to study the ionic bonding formed that could not be detected by the FTIR (Figure 3.5). Raman frequencies of common chemical functional group can be seen in Table 3.2.

Figure 3.5 Micro Raman Spectrometer

Table 3.2 Typical vibrational frequencies of functional groups for raman analysis

Functional Group	**Position (cm^{-1})**	**Remarks**
>S-S<	500-550	
C-C	~1060 and 1127	Polyethylene
C-C	700-1260	Highly mixed in complex molecule
Aromatic ring	~1000	Monosubstituted
Aromatic ring	~1000	1,3 disubstituted
Aromatic ring	~1000	1,3,5 trisubstituted
Aromatic ring	~860	1,4 disubstituted
CH_3 umbrella mode	~1375	
CH_3 and CH_2 deformations	1410-1460	
>C=C<	~1650	
>C=C<	~1623	Ethylene
>C=O mixed with NH deformation	1620-1690	Amide I
>C=O	1710-1745	Changes for ketone, aldehyde, and ester
C≡C	2100-2300	
SH	2540-2600	
$>CH_2$	2896 and 2954	Ethane
$>CH_2$	2845 and 2880	Polyethylene
CH_3	2870 and 2905	Polypropylene
$R_1R_2R_3CH$	2880-2890	Methine CH
CH	~2900	Cellulose
CH	~3015	Olefinic CH
CH	~3065	Aromatic CH
CH	3280-3340	Acetylenic CH
NH	3150-3340	Broadened and shifted by H-bonding
OH	3000-3600	Broadened and shifted by H-bonding

Whereas, the Fluorescence Spectrometer JASCO, FP8500 (Figure 3.6) was used to determine the recombination rate of the electron in the compound at a certain excitation wavelength, λ_{ex}. It has a main specifications emission of 200 - 750nm, excitation of 200 - 750nm, at a temperature range of 0 -100℃. The sample in liquid, powder and film can be used in this measurement.

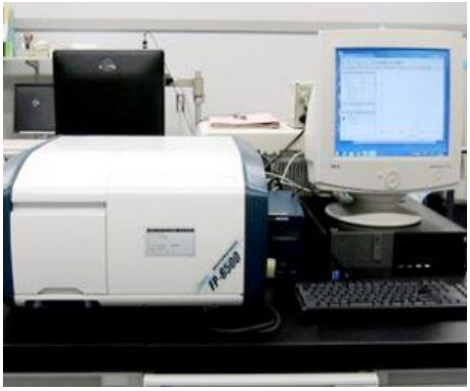

Figure 3.6 Fluorescence Spectrometer

3.4.2 Physical Analysis

In physical analysis, we used the Hitachi FESEM S4800 with EDX Horiba and Hitachi FESEM SU8000 (Figure 3.7) to study the morphologies and compositions of the materials.

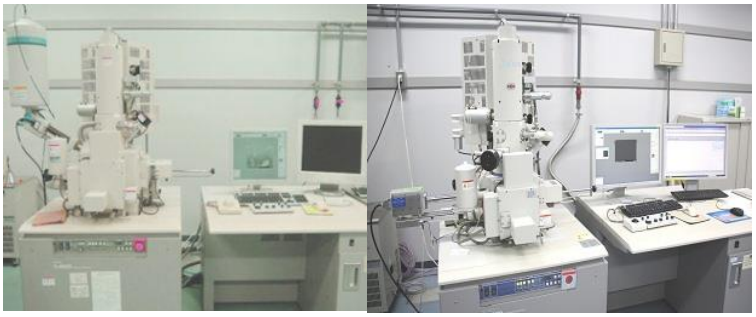

Figure 3.7 FESEM EDX S-4800 EDX, (HORIBA) and Hitachi FE-SEM SU8000, EDX (Bruker)

CHAPTER 4

CATIONIC AND ANIONIC DYE DEGRADATION BY $NaBiO_3$ PHOTOCATALYST UNDER VISIBLE LIGHT IRRADIATION

In this chapter, the widely known hydrated sodium bismuthate, $NaBiO_3 \cdot 2H_2O$ reactivity and stability in cationic and anionic dyes degradation under different pH conditions are discussed.

4.1 Introduction

Based on the pilot study we have conducted (Figure 4.1) [1], it shows that sodium bismuthate $NaBiO_3$ is the best photocatalyst and has high rate of degradation compared to the other four photocatalysts which are the bismuth vanadate ($BiVO_4$), bismuth (III) oxide (Bi_2O_3), bismuth titanate ($Bi_2O_3 \cdot 2TiO_2$) and titanium dioxide P25 (TiO_2). $NaBiO_3$ was first reported by Kako et al, which shows it has a high photocatalytic activity towards methylene blue dye degradation, and since than various study has been conducted on this material.

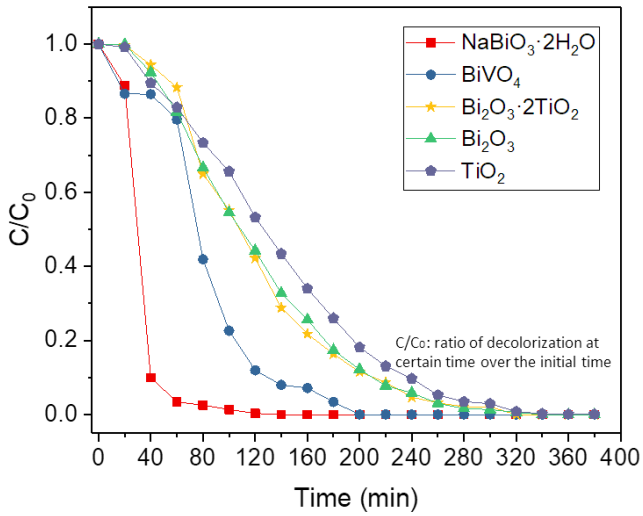

Figure 4.1 Pilot study on five difference types of bismuth compound in methylene blue dye degradation under visible light irradiation

However, to the best of our knowledge, there is not much study has been done on the optimum condition for this material to function at its best. In this study, we are trying to find an optimum condition for the sodium bismuthate by creating three different pH conditions which are the acidic condition (pH 3), neutral condition (pH 7) and alkaline condition (pH 11), with and without the presence of visible light.

As for the dye contaminants, we have chosen two dyes, which are the cationic methylene blue (MB) dye, and the anionic methyl orange (MO) dye. Both of these dyes were chosen because it is one of the frequently used dyes in the industries. The MB dye and MO dye has the chemical structure of $C_{16}H_{18}N_3SCl$ and $C_{14}H_{14}N_3NaO_3S$ each.

4.2 Objective

In this study, we are going to study and understand how the decolorization and degradation of each dye works under different type of experimental conditions such as the pH of the system with the presence and absence of light. This study is important in order to understand the stability of the photocatalyst and to figure out whether does degradation occurs or only decolorization take place. This experiment will give us the understanding as a basic and core for the further study in the next chapter.

4.3 Experimental Procedure

Hydrated sodium bismuthate ($NaBiO_3 \cdot 2H_2O$), bismuth dioxide (Bi_2O_3), methyl orange (MO) dye powder and hydrochloric acid (HCl) were purchased from Wako Pure Chemicals Industries Ltd.. Sodium hydroxide (NaOH) granule was bought from Kanto Chemical Co., Inc and methylene blue (MB) dye powder was from Waldeck GmbH & Co. KG. Ultrapure water was used in all the experimental procedure and all chemicals were analytical grade and used as received without any further purification.

Hydrated sodium bismuthate was used in all experiments in this chapter, was used as it is without further intervention. The reaction rate for each study might be differs for each chapter.

4.4 Characterization

The samples were analyzed with an x-ray diffractometer (XRD, RINT 2000; Rigaku, Corp., Japan) operated at 30 kV and 40 mA with Cu Kα radiation (λ=1.54178Å). Data were collected in the angular range of 2θ=10–80°. FESEM images were obtained from Hitachi FE-SEM SU8000. UV-visible diffusion reflectance spectra were measured at a room temperature, with a UV-Vis-NIR Spectrophotometer JASCO V-7200. The reflectance was then converted to absorbance by using the Kubelka–Munk method.

4.5 Photocatalytic Evaluation Test

Photocatalytic evaluation test was conducted as follows. 4 mL of methylene blue solution with a concentration of 0.3mg/100mL was placed in a 100 mL. Then, 96mL of ultrapure water was added to the aqueous solution. After that, 0.3g of photocatalyst sample was added for each experiment. The pH conditions of the solution were controlled by HCl and NaOH. The experiments were conducted under the presence of visible light (λ > 400nm) and with the absence of light. The solution was magnetically stirred for 40 minutes without the irradiation of light to ensure uniformity. The light was on after 40 minutes. The samples were then filtered by using syringe membrane filter (Millex: Millipore Corp., United States) to remove the photocatalyst particles. Samples were taken from the solution for every 20 minutes for MB and MO dye and placed inside a UV-Vis spectrophotometer cell in order to measure the maximum absorption of wavelength for the dye and the rate of degradation.

4.6 Results and discussion

4.6.1 Materials Characterization

Figure 4.2 shows the X-ray diffraction patterns of the commercial $NaBiO_3 \bullet 2H_2O$ powder before photocatalytic reaction. The strong characteristic peaks of $NaBiO_3$ can be observed from the (0 0 1), (1 0 0), (1 0 1), (1 1 0) and (1 1 1) planes. Table 4.1 shows the detail of crystallographic parameters for this photocatalyst. It has a tetragonal crystal system of P3 space group.

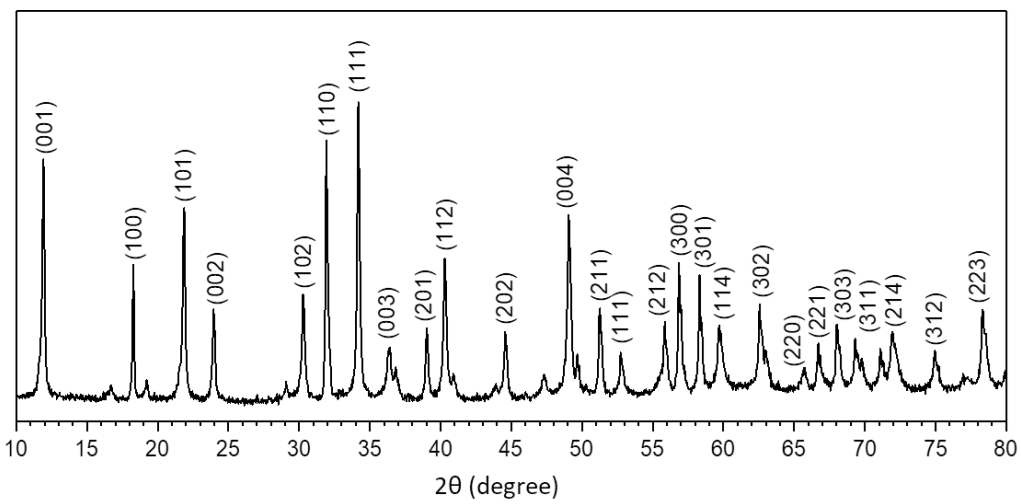

Figure 4.2 The XRD analysis for $NaBiO_3 \bullet 2H_2O$ powder

Table 4.1 Crystallographic parameters for $NaBiO_3 \bullet 2H_2O$

Formula	$NaBiO_3 \bullet nH_2O$
Crystal System	Tetragonal
Space Group	P3
Space Group Number	143
a (A)	5.6050
b (A)	5.6050
c (A)	7.4250
Alpha	90.0000
Beta	90.0000
Gamma	120.0000
Volume of cell (10^6 pm^3)	202.01
RIR	5.50

Figure 4.3 shows the morphology of the commercial $NaBiO_3 \cdot 2H_2O$ powder under a field-emission SEM microscope. The FESEM analysis indicated that the commercial $NaBiO_3 \cdot 2H_2O$ consists of tetragonal clumps made up of multiple nano-sheets. The lengths of the nano-sheets flakes which have the thickness off about 100 nm and length about 1 μ m.

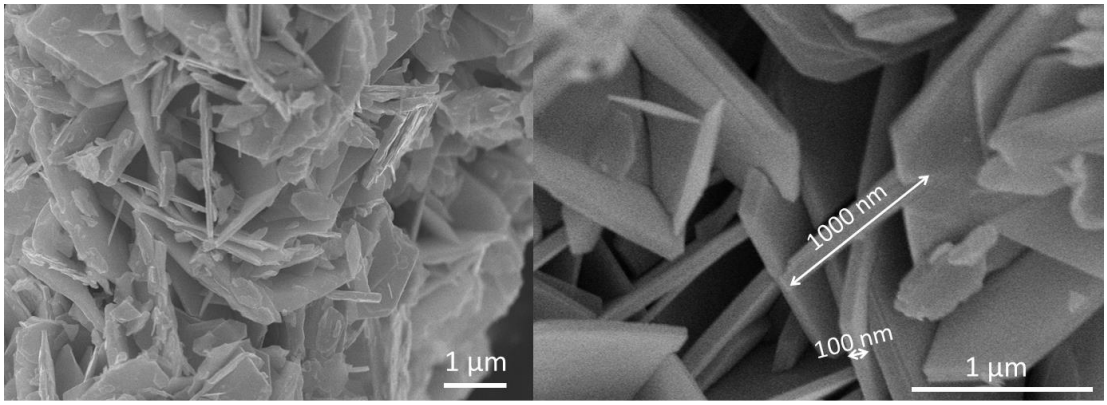

Figure 4.3 FESEM images of $NaBiO_3$ powder

4.6.2 Optical properties

The optical absorption spectrum of the commercial $NaBiO_3 \cdot 2H_2O$ was also measured, in order to evaluate the photooxidation activity, as shown in Figure 4.4. The $NaBiO_3 \cdot 2H_2O$ spectrum was characterized by the sharp decrease around 450 nm due to the band gap transition and up to about 800 nm which is probably caused by the *lattice defects*, such as oxygen vacancies. The optical band gap was estimated to be about 2.70 eV from the onset of the absorption edge, which slightly smaller than the Bi_2O_3 which was about 2.80 eV.

Lattice defect - An ideal crystalline solid exhibit a periodic crystal structure with the positions of atoms or molecules occurring on repeating fixed distances, determined by the unit cell parameters. However, the arrangement of atoms or molecules in most crystalline materials is not perfect and the regular patterns are interrupted by crystallographic defects. Lattice structures (or crystals) are more prone to defects when their temperature is greater than 0 K.

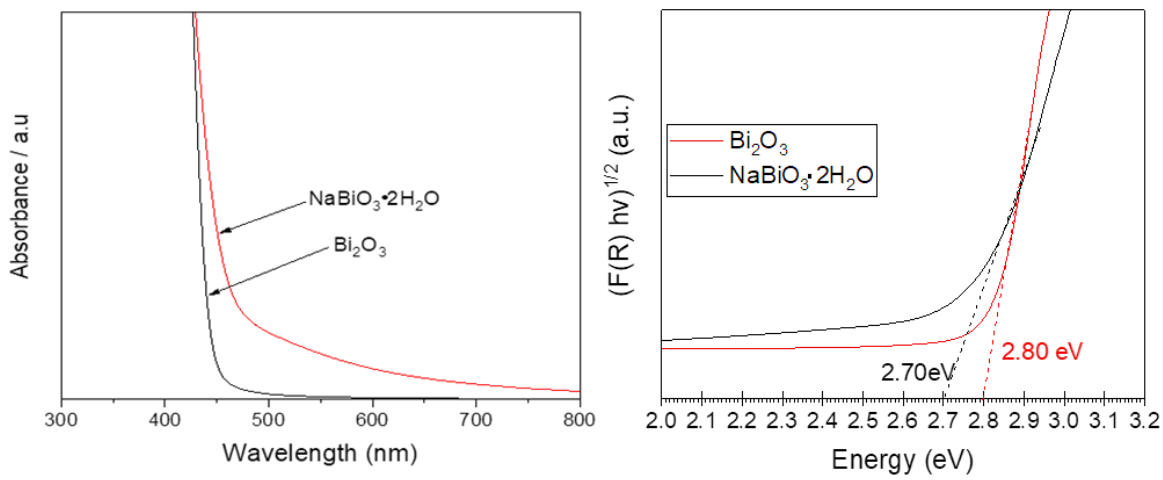

Figure 4.4 Optical absorption spectra of the commercial $NaBiO_3 \cdot 2H_2O$ with Bi_2O_3 as a comparison & band gap by Kubelka-Munk derivation for the the commercial $NaBiO_3 \cdot 2H_2O$ with Bi_2O_3 as a comparison

4.6.3 Photocatalytic Activity

The photocatalytic activity for $NaBiO_3$ was tested by the degradation of methylene blue and methyl orange dye, under different pH conditions with and without the presence of light.

4.6.3.1 Rate of degradation

In MB dye, the degradation rate was slightly faster compared to the MO dye. For each of the condition, the rate of reactions was different. The rate of degradation for MB dye can be seen in Figure 4.5 and 4.6. The decolorization rate was fastest in the acidic condition, pH 3, followed by pH 7 and finally the alkaline condition, pH 11.

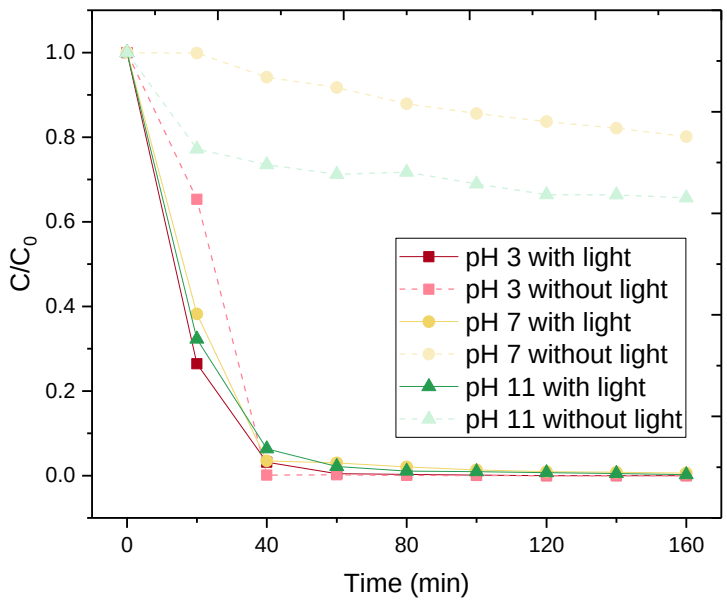

Figure 4.5 The absorbance rate for methylene blue dye in pH 3, pH 7 and pH 11

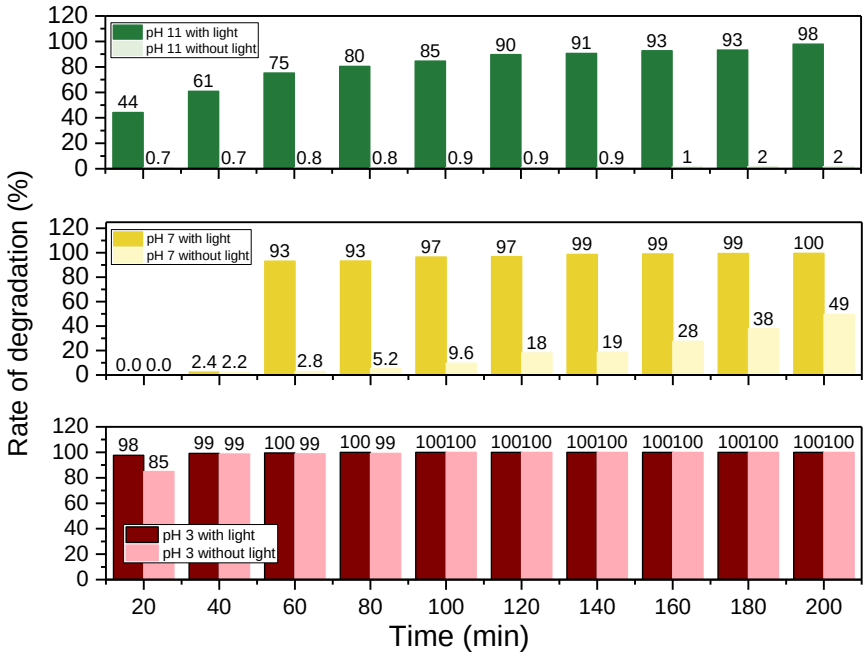

Figure 4.6 Rate of degradation for methylene blue dye in pH 3, pH 7 and pH 11

However, when the light was absence, the rapid decolorization still occurred in pH 3, but only a slight decolorization occurred in pH 7 and moderate in pH 11. This can be contributed by the absorbance of the dye onto the photocatalyst. In pH 3, it is hard to say that the degradation occurred in this reaction, instead, only decolorization take place. This is because even without the presence of light, which photocatalysis did not take place, the decolorization still occurred. Thus, $NaBiO_3 \cdot 2H_2O$ can be concluded to be not stable under acidic condition. Normally, as in pH 7, only a slight decolorization occurs during the absence of light, which indicates the stability of the photocatalyst.

On the other hand, in the degradation of MO dye, which the results shown in Figure 4.7 and 4.8, it took a little longer time to decolorize compared to MB dye. Usually, MO took a longer time than MB dye to decolorize, due to its more complex structure. But in this study, $NaBiO_3 \bullet 2H_2O$ only took about 3 hours to fully decolorize under neutral condition.

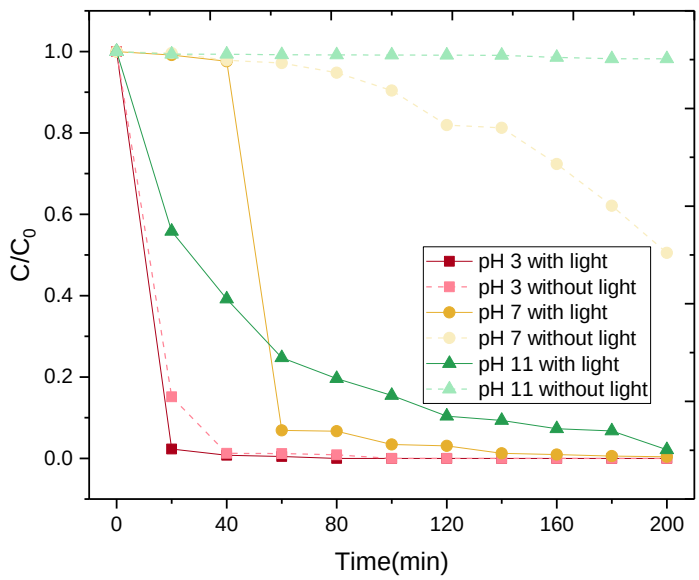

Figure 4.7 The absorbance rate for methyl orange dye in pH 3, pH 7 and pH 11

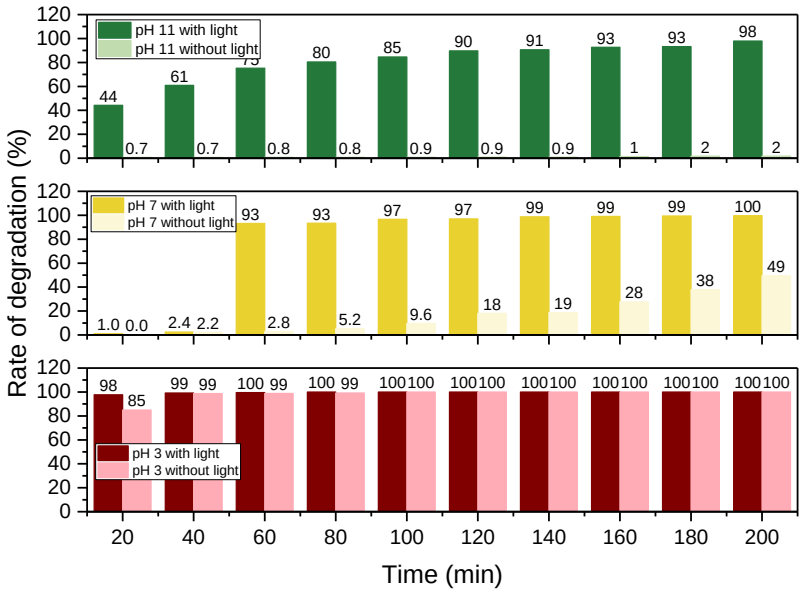

Figure 4.8 Rate of degradation for methyl orange dye in pH 3, pH 7 and pH 11

In pH 3, we can see the same trend as what occurred in the MB dye degradation. Thus, this justify a stronger hypothesis and evidence that the $NaBiO_3 \cdot 2H_2O$ only absorbed the dye, instead of degrading it. Another hypothesis is that, with the excess presence of HCl in the system, the active species of radical H^+ increases, which contributed to the rapid decolorization of the dyes, even without the presence of light.

The results achieved are influence by the pH value of the experiment condition. This is because, in a low pH value (acidic condition, which in this study is pH 3), the hydroxyl radicals can be formed by the reaction between the hydroxide ions and the positive holes. Furthermore, the positive holes presence considered as the major oxidation. However, in a neutral (pH 7) or high pH value. It has been reported in previous study that the alkaline condition, has a higher probability of the hydroxyl radical (•OH) formation, which is an oxidant. Therefore, it increases the efficiency of the degradation of the dye [2]. But, there is also a Coulombic repulsion between the negative charged surface of photocatalyst and the hydroxide anions which can prevent the formation of •OH and thus decrease the photooxidation [3], which leads on why it took a longer time to degrade the MO dye in the alkaline condition.

4.6.3.2 Stability

In order to study for the stability of the photocatalyst used, we conducted the XRD analysis after running the photocatalytic experiment for each condition. The results shown as in Figure 4.9. From the figure, we can see that there were no distortion or changes in the characteristic peaks of $NaBiO_3 \cdot 2H_2O$ after the experiment at pH 7 and pH 11. Thus, it shows the stability of the photocatalyst in the neutral and alkaline solution. However, after the experiment in pH 3, the characteristic peaks were badly distorted and destroyed. As a result, it limits the repeatability and recyclability of the photocatalyst in the acidic solution. This shows that $NaBiO_3 \cdot 2H_2O$ photocatalyst could not be used in an acidic solution and alternative ways and improvement should be made in increasing the efficiency and stability.

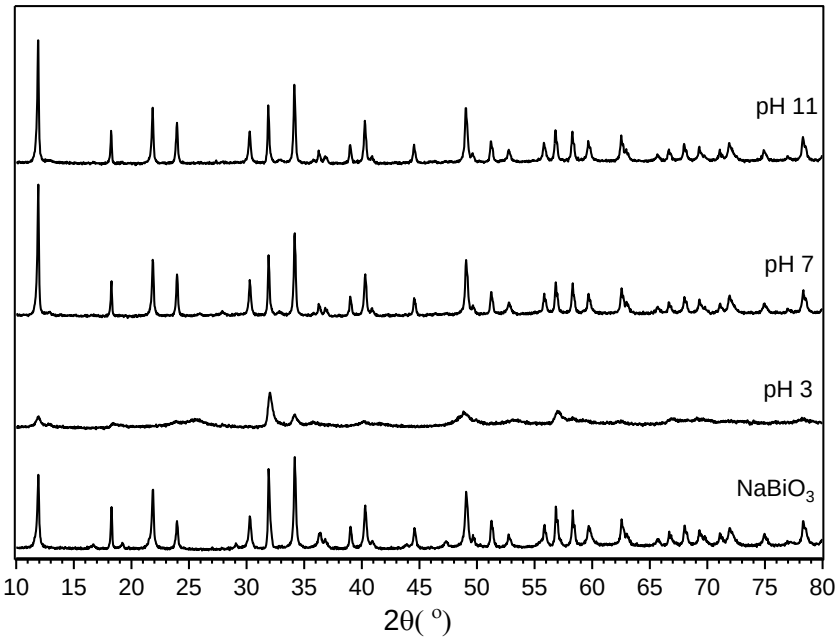

Figure 4.9 The XRD analysis after photocatalytic activity in pH 3, pH 7 and pH 11

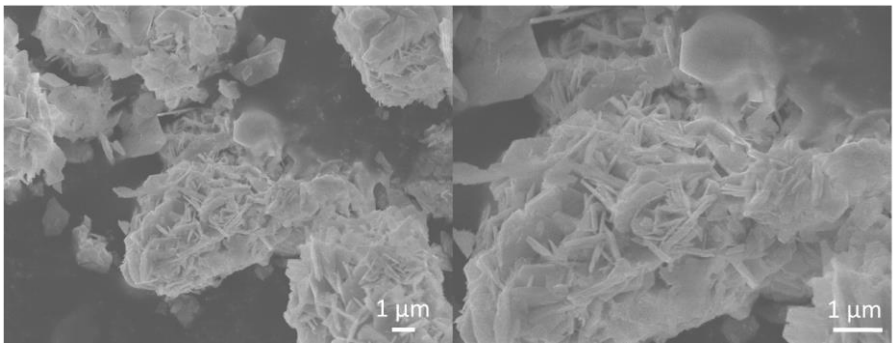

Figure 4.10 FESEM images of $NaBiO_3$ powder after reaction in pH 3 condition

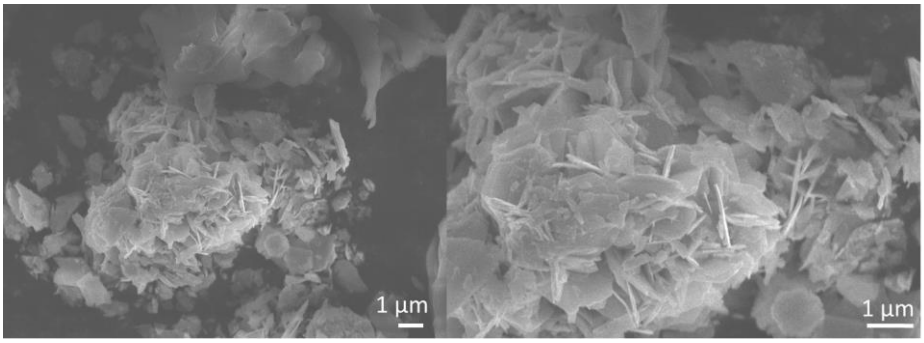

Figure 4.11 FESEM images of $NaBiO_3$ powder after reaction in pH 7 condition

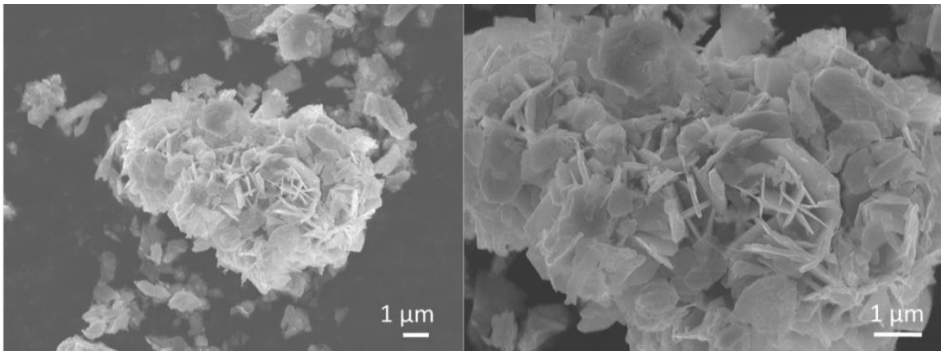

Figure 4.12 FESEM images of $NaBiO_3$ powder after reaction in pH 11 condition

4.7 Conlusion

In this study, we can conclude that the sodium bismuthate works best in decolorizing the dye under the acidic (pH 3) condition, with the presence of visible light for both dyes. Nonetheless, the stability and resistant towards acidic solution was very low. For a long-term run, the used of this materials under acidic solution is not recommended. Besides, in the degradation of MO dye, it took a longer time compared to the degradation of methylene blue (MB) dye, which shows that difference target contaminant structural compound may affected the performance of the photocatalyst.

4.8 References

1. Arini Nuran, Akira Fujiki, A Comparison of Five Different Photocatalysts in the Degradation of Methylene Blue Dye, Recent Advances on Energy and Environment, 2015, page 33-36.
2. T. Zhang, T. Oyama, S. Horikoshi, H. Hidaka, J. Zhao, N. Serpone, Photocatalyzed N-demethylation and degradation of methylene blue in titania dispersions exposed to concentrated sunlight, Sol. Energy Mater. Sol. Cells, Volume 73, 2002, page 287–303.

3. U.G. Akpan, B.H. Hameed, Parameters affecting the photocatalytic degradation of dyes using TiO_2-based photocatalysts: A review, Journal of Hazardous Materials, Volume 170, 2009.
4. Arini Nuran Zulkifili, Akira Fujiki, A Basic Study on the Organic Dye Degradation by $BiNaO_3$ Photocatalyst, International Journal of Advances in Science Engineering and Technology, 2321-9009, Volume 4, Issue 2, Special Issue 2, 2016, page 109-112.
5. Yaobin Ding et al., In situ H+-mediated formation of singlet oxygen from $NaBiO_3$ for oxidative degradation of bisphenol A without light irradiation: Efficiency, kinetics, and mechanism, Chemosphere, Volume 141, 2015, page 80-86.
6. Chung-Shin Lu et al., Photocatalytic Degradation of Acridine Orange over $NaBiO_3$ Driven by Visible Light Irradiation, Catalysts, Volume 3, 2013, page 501-516.
7. Xiaofeng Chan et al,. Photocatalytic decomposition of 4-t-octylphenol over NaBiO3 driven by visible light: Catalytic kinetics and corrosion products characterization, Journal of Hazardous Materials, Volume 173, 2010, page 765-772.
8. Yaobin Ding et al., Visible-light photocatalytic degradation of bisphenol A on $NaBiO_3$ nanosheets in a wide pH range: A synergistic effect between photocatalytic oxidation and chemical oxidation, Chemical Engineering Journal, Volume 291, 2016, page 149-160.

CHAPTER 5

SYNTHESIS OF ALKALI BISMUTHATE BY USING $NaBiO_3$ AS A STARTING MATERIAL VIA SOLID STATE REACTION METHOD

In this chapter, a new alkali bismuthate of potassium and lithium bismuthate were synthesis by solid state reaction, and its material characterization, optical properties and photocatalytic activity for cationic and anionic dyes are discussed in detail.

5.1 Introduction

A number of researchers has reported about bismuth-based semiconductor photocatalyst such as Bi_2O_3, $BiVO_4$, $NaBiO_3$, and a few others. There is also study on alkali metal bismuthate, $MBiO_3$ (M : K, Na, Li) photocatalyst [1-5]. Although some research has been carried out on this, the reports are limited to characterization without focusing on the synthesis method and its photocatalytic performance. Besides, the reports limited to only theoretical study and not much of study had been done. In this study, we are focusing on three types of alkali metal bismuthate which are potassium, sodium and lithium bismuthate. $NaBiO_3$ was reported by Kako et.al and shows a high photocatalytic performance in degrading methylene blue dye and propanol. In this study, we chose one type of dye for each cationic dye and anionic group dye. For cationic dye, we used methylene blue and methyl orange for anionic dye. The stability and recyclability of each photocatalyst for each dye were also studied.

5.2 Objective

The objectives of this study are :-

1. To synthesis and characterize alkali bismuthate material via solid state reaction by using sodium bismuthate as the starting material

2. To develop a simple and low-cost method in developing

a) a various structures and morphologies of bismuth based materials

b) high and stable photocatalytic performance under visible light in the degradation of anionic and cationic organic dyes

5.3 Experimental Procedure

5.3.1 Chemicals and reagents

Sodium bismuthate ($NaBiO_3$•$2H_2O$), potassium hydroxide (KOH), lithium hydroxide monohydrate ($LiOH$•H_2O) and methyl orange (MO) dye powder were purchased from Wako Pure Chemicals Industries Ltd.. Methylene blue (MB) dye powder was from Waldeck GmbH & Co. KG. Ultrapure water was used in all photocatalysis reaction and all chemicals were analytical grade and used as received without further purification.

5.3.2 Synthesis method

The three types of alkali bismuthate compounds were prepared via a simple synthesis method. At first, we prepared $NaBiO_3$ by dehydrating the commercial $NaBiO_3$•$2H_2O$ from Wako Pure Chemicals Industries Ltd., by heating in air at 413K for 5 hours as been reported by Kako et.al [1]. The $NaBiO_3$ was then further used in the preparation of $KBiO_3$ and $LiBiO_2$. Both of these compounds were prepared by a solid state reaction (SSR) method.

In $KBiO_3$, we prepared 8 samples with $NaBiO_3$ and KOH in 4:1, 3:1, 2:1, 1:1, 1:1.75, 1:2, 1:3 and 1:4 weight ratio. Both of the substances were grind in a mortar for 10 minutes. Then, it was transferred into a crucible and was heat at a heating rate of 250°C in 30 minutes and hold for 6 hours, before cooling to room temperature. The samples were then grind for a few minutes before further used. Among these samples, the sample

where the $NaBiO_3$ weight ratio is 1.75 to 1 of KOH shows the highest rate of reaction. Since the KOH is highly hygroscopic, a fine powder could not be achieved for weight ratio less than 1.75.

For $LiBiO_2$ preparation, we prepared 4 samples with different weight ratio of $NaBiO_3$ to $LiOH{\bullet}H_2O$ of 1:4, 1:3, 1:2 and 1:1. Both of the substances were grind in a mortar for 10 minutes. Then, it was transferred into a crucible and was heat at a heating rate of 315°C in 30 minutes and hold for 6 hours, before cooling to room temperature. The samples were then grind for a few minutes before further used. In this study, the weight ratio 1($NaBiO_3$) to 4($LiOH \cdot H_2O$) shows the highest rate of reaction, compared to the others.

5.4 Characterization

The samples were analyzed with an x-ray diffractometer (XRD, RINT 2000; Rigaku, Corp., Japan) operated at 30 kV and 40 mA with Cu Kα radiation (λ=1.54178Å). Data were collected in the angular range of 2θ=10–90°. FESEM images were obtained from Hitachi FE-SEM SU8000. UV-visible diffusion reflectance spectra were measured at a room temperature, with a UV-Vis-NIR Spectrophotometer JASCO V-7200. The reflectance was then converted to absorbance by using the Kubelka–Munk method. FTIR and raman spectra were also used in this study.

5.5 Photocatalytic Evaluation Test

4mL of dye solution was placed in a 100mL Pyrex vessel. Then, 96mL of ultrapure water was added to the aqueous solution. After that, 0.3g of photocatalyst sample was added for each experiment. The experiments were conducted under the presence of visible light (λ> 400nm) and with the absence of light. The solution was magnetically stirred for 40 minutes without the irradiation of light to ensure uniformity. The light was on after 40 minutes. The samples were then filtered by using syringe membrane filter (Millex: Millipore Corp., United States) to remove the photocatalyst particles. Samples were taken

from the solution for every 10 minutes for MB and MO dye and placed inside a UV-Vis spectrophotometer cell in order to measure the maximum absorption of wavelength for the dye and the rate of degradation.

5.6 Results and discussion

5.6.1 Materials Characterization

In this study, we have prepared 8 samples with $NaBiO_3$ and KOH in 4:1, 3:1, 2:1, 1:1, 1:1.75, 1:2, 1:3 and 1:4 weight ratio and only 4:1, 3:1, 2:1 and 1.75:1 samples can be used for further study. When the amount of KOH increases (weight ratio less than 1.75:1), the samples started to turn into a paste instead of powder due to the low melting point of KOH which is highly hygroscopic (Figure 5.1). Thus, 1:1, 1:2, 1:3 and 1:4 samples were not suitable to be synthesis via solid state reaction preparation.

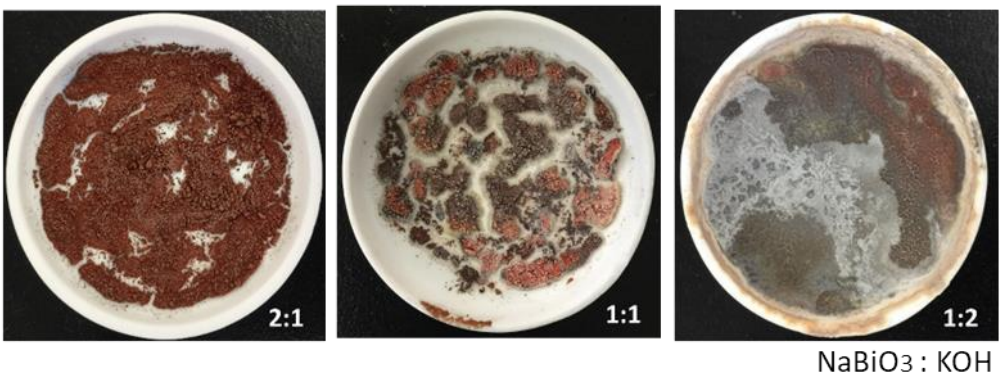

Figure 5.1 Samples of $KBiO_3$ 2:1, 1:1 and 1:2 after calcination

In addition, we have conducted XRD analysis for further analysis (Figure 5.2). Unfortunately, as the ratio of $NaBiO_3$ increases, the end product shows the presence of $NaBiO_3$ as well. However, the strong characteristic peak of $NaBiO_3$ getting weaker as the amount of KOH increases, indicating the starting of $KBiO_3$ formation.

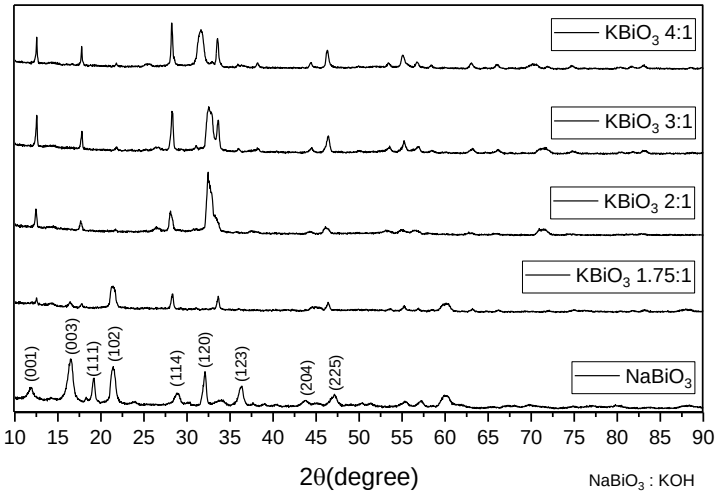

Figure 5.2 XRD analysis for $KBiO_3$ 4:1, 3:1, 2:1 and 1.75:1 with $NaBiO_3$ as the reference

We have also studied on the morphologies of the $KBiO_3$ powder. From the FESEM images, we can see that as the amount of KOH ratio increases, the structure started to be getting bulkier and the KOH melts can be seen clearly. There were no specific structures that can be seen, and the presence of $NaBiO_3$ structure could not be found in these images.

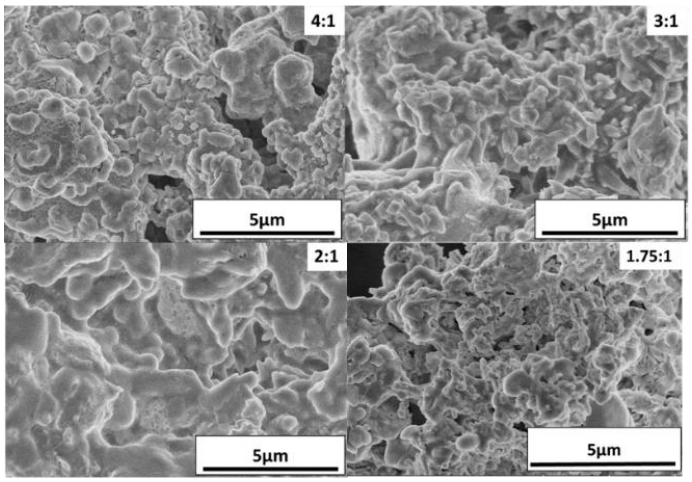

Figure 5.3 FESEM images for $KBiO_3$ 4:1, 3:1 and 2:1 at 5K magnification.

Further analyses were made by using the EDX in order to confirm the elements presence and the percentage of the elements. The EDX analyses were summarized into Table 5.1. We can conclude that as the amount of sodium decreases, the percentage of potassium in this compound will increases. Although a pure $KBiO_3$ powder could not be formed from this method, we can conclude that this method can still be used as the powder formed dramatically changes its color from light yellowish brown to bright red, indicating the formation of $KBiO_3$ compound.

Table 5.1 $KBiO_3$ samples for EDX composition of samples A to D

Sample	K (wt%)	Bi (wt%)	O (wt%)	Na (wt%)
A (4:1)	6.30	55.57	19.61	18.52
B (3:1)	11.10	26.33	44.92	17.64
C (2:1)	16.34	25.84	43.41	14.40
D (1.75:1)	35.57	14.20	38.43	11.80

To understand this compound more, we made a further analysis by using FTIR and raman spectra. From Figure 5.4 and 5.5, we found the presence of potassium characteristic peak from the graph obtained in the analysis.

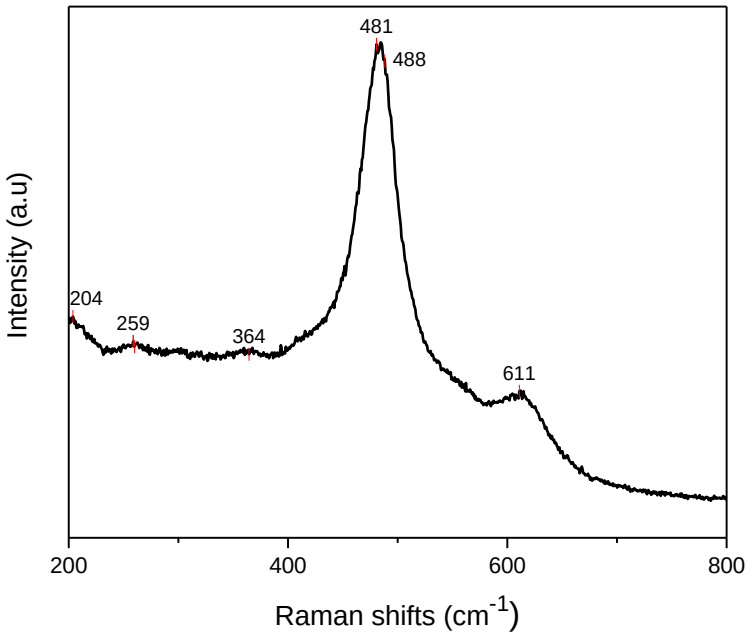

Figure 5.4 Raman analysis for $KBiO_3$

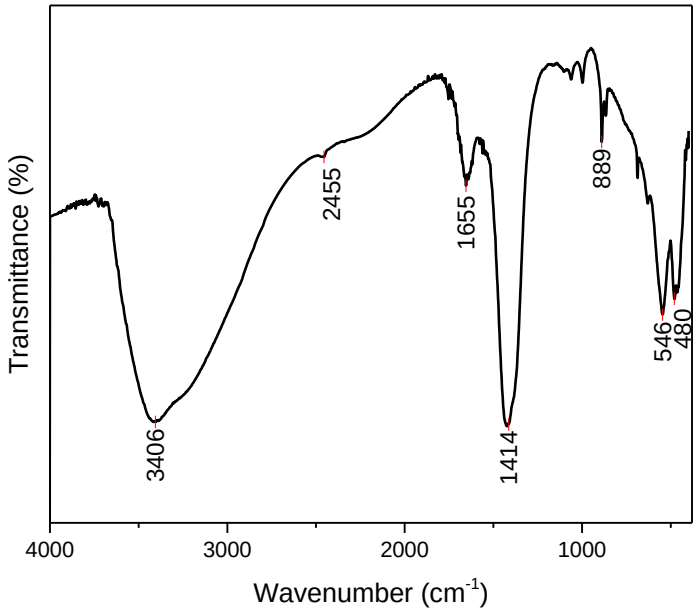

Figure 5.5 FTIR analysis for $KBiO_3$

In addition, we have conducted XRD analysis for $LiBiO_2$ (Figure 5.6). As the ratio of $LiOH•H_2O$ increases, the $NaBiO_3$ characteristic peaks were also decreases.

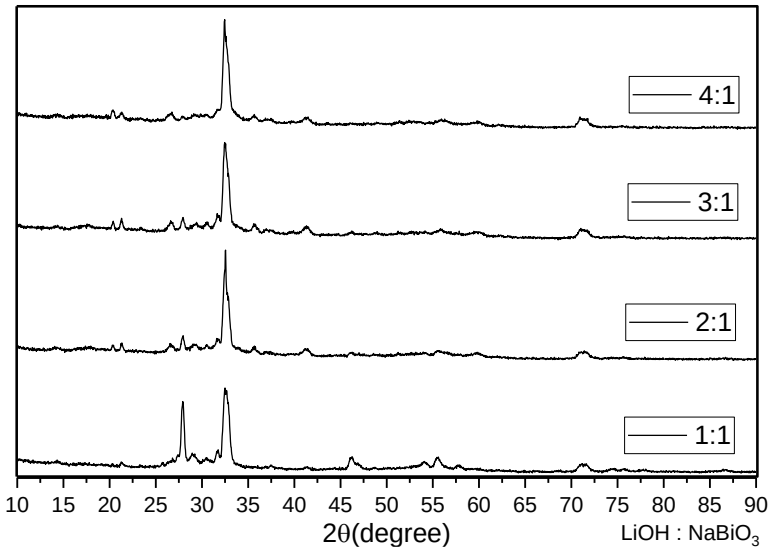

Figure 5.6 XRD analysis for $LiBiO_2$ 4:1, 3:1, 2:1 and 1:1

Besides, we conduct a FESEM observation to study for the morphologies of the compound formed (Figure 5.7). As the ratio of $LiOH•H_2O$ increases, the compound becomes more porous and thus increases the surface area available, thus, increases the efficiency of the compound as a photocatalyst.

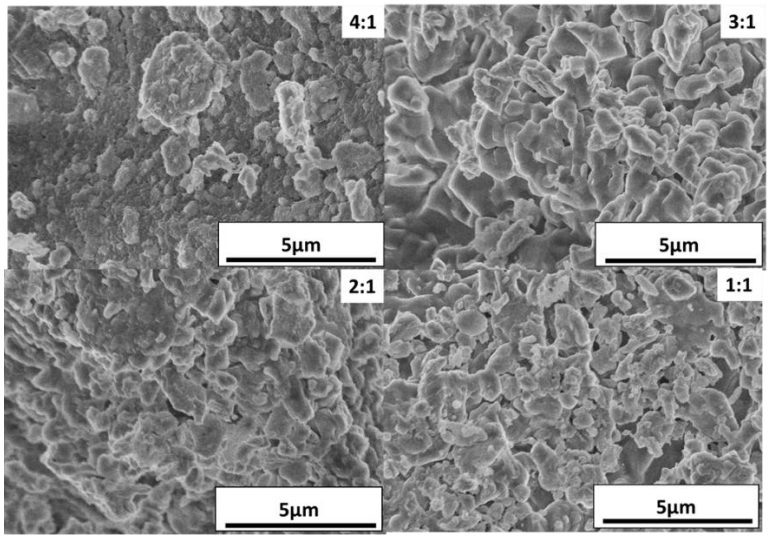

Figure 5.7 FESEM images for $LiBiO_2$ 4:1, 3:1, 2:1 and 1:1 at 5K magnification.

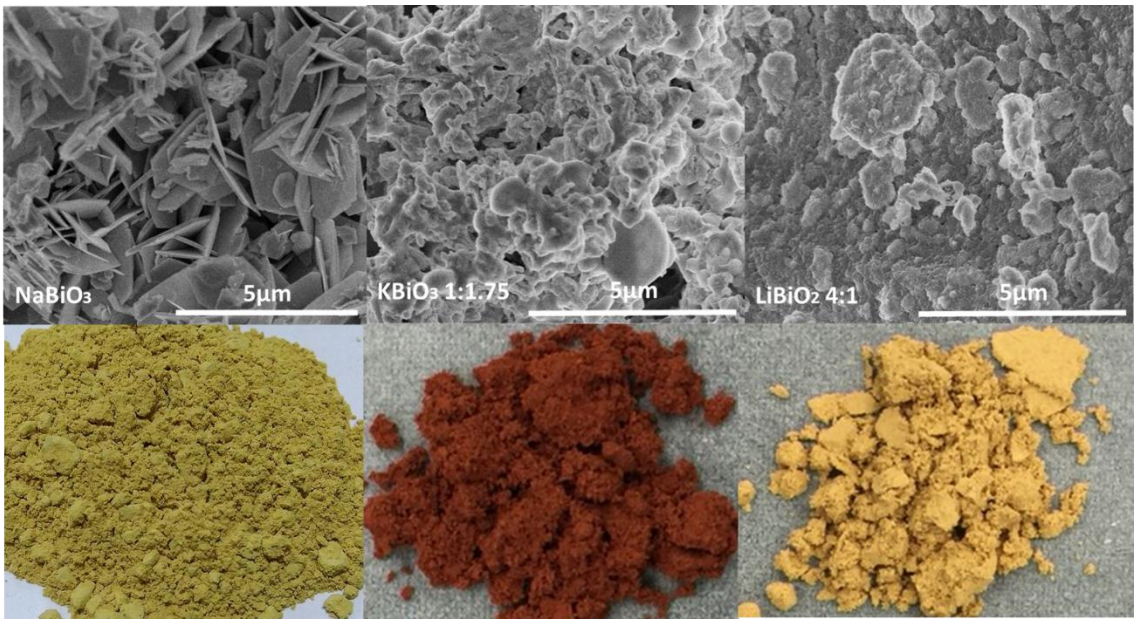

Figure 5.8 FESEM images and powder images for $NaBiO_3$, $KBiO_3$, and $LiBiO_2$

Furthermore, we further analyze the materials by raman analysis. From the raman scattering spectra in Figure 5.9, a strong characteristic peak of lithium can be seen at 514cm^{-1} and 633cm^{-1}. However, a slight peak of $NaBiO_3$ peak bond could be observed at 474cm^{-1}.

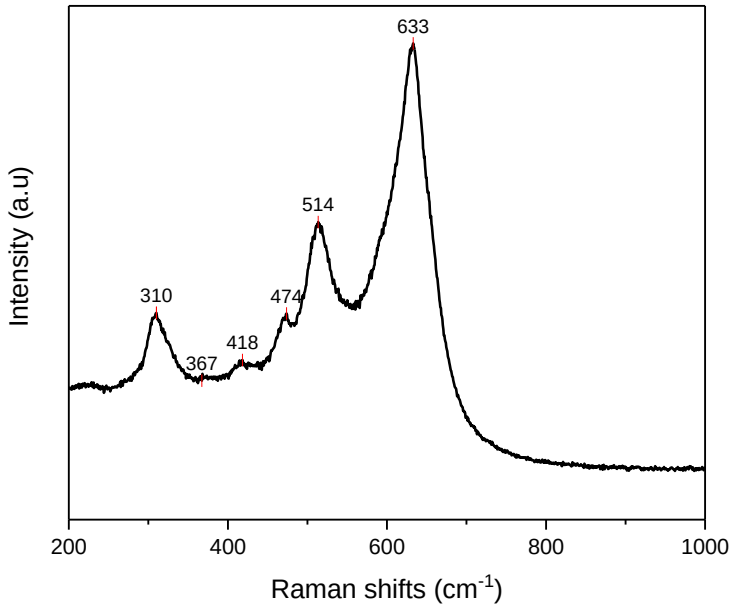

Figure 5.9 Raman analysis for $LiBiO_2$

We also have made further analysis by using FTIR. From Figure 5.10, we found the presence of lithium characteristic peak from the graph obtained in the analysis.

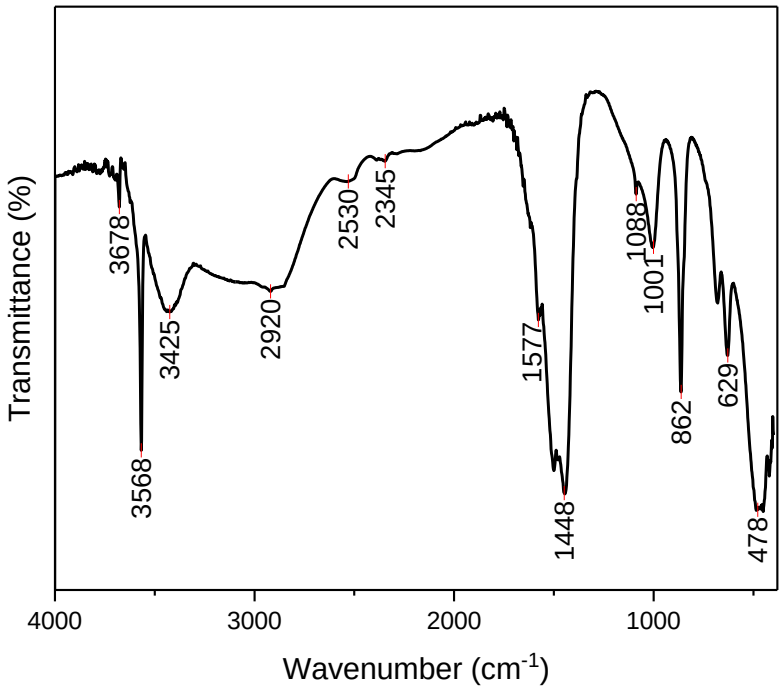

Figure 5.10 FTIR analysis for $LiBiO_2$

5.6.2 Optical properties

Besides that, we also conducted a UV-vis diffuse reflectance spectrum to determine the band gap of the samples. The band gap was found to be not much difference between the ratio which is 2.05eV for 4:1 and 2.03eV for 3:1. The small band gap indicates that it is a perfect candidate for the degradation of organic contaminants under visible light irradiation (Figure 5.10 and 5.11).

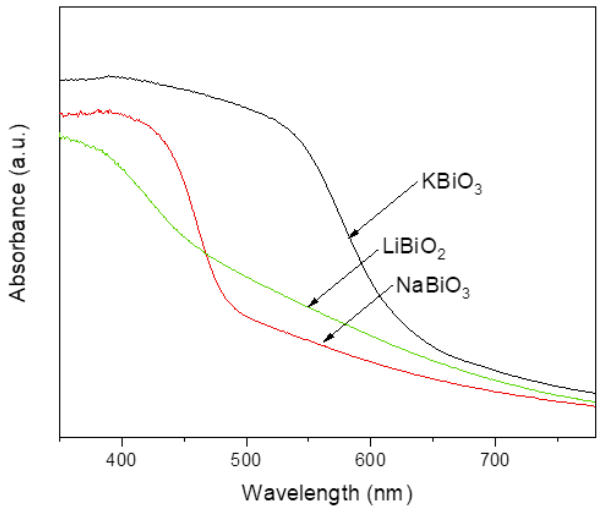

Figure 5.10 Uv-vis diffuse reflectance spectrum for $NaBiO_3$, $KBiO_3$, and $LiBiO_2$

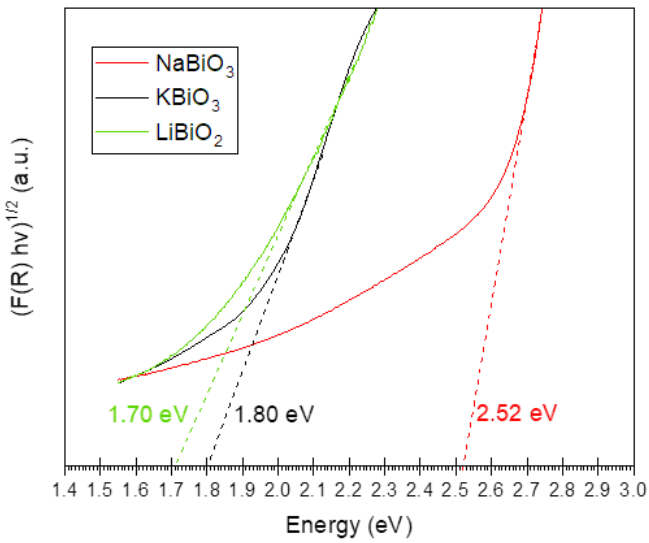

Figure 5.11 Band gap via Kubelka-Munk derivation for $NaBiO_3$, $KBiO_3$, and $LiBiO_2$

5.6.3 Photocatalytic Activity

5.6.3.1 Rate of degradation

For the organic contaminant degradation of the dye study, we have chosen methylene blue dye (cationic dye) as the degradation target. The experiment was conducted under visible light irradiation for 6 hours. From the graph in Figure 5.12, the lower the ratio of $NaBiO_3$ to KOH, the higher the rate of the degradation of the dye.

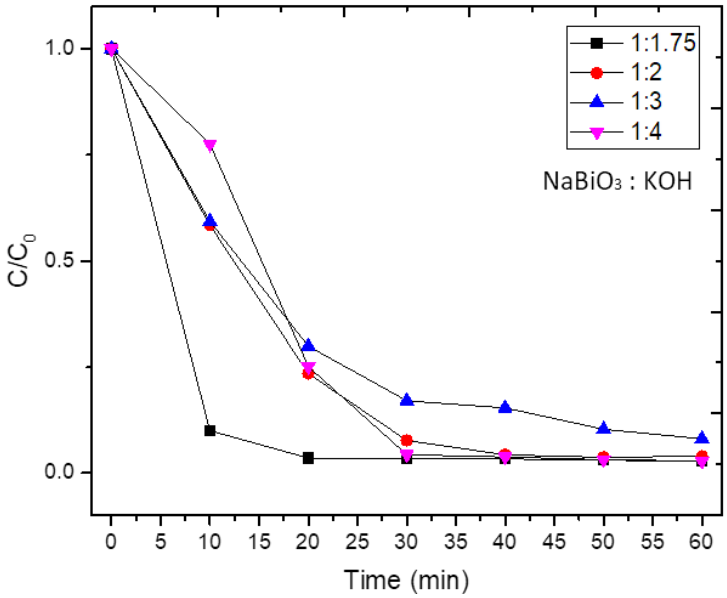

Fig. 5.12 The rate of absorbance of methylene blue dye by $KBiO_3$

For the $LiBiO_2$ study, we have chosen methylene blue dye (cationic dye) as the degradation target. The experiment was conducted under visible light irradiation for 6 hours. From the graph in Figure 5.13, the lower the ratio of $NaBiO_3$ to KOH, the higher the rate of the degradation of the dye. The reactivity of the photocatalysts are shown in Figure 5.14.

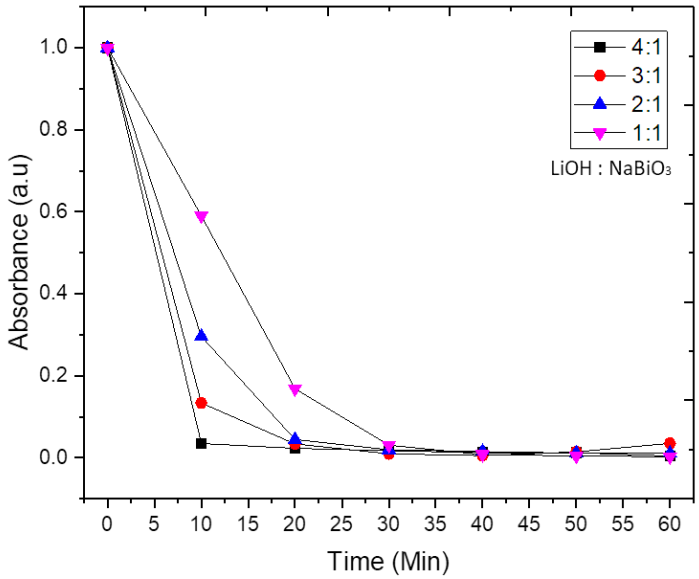

Fig. 5.13 The rate of absorbance of methylene blue dye by $LiBiO_2$

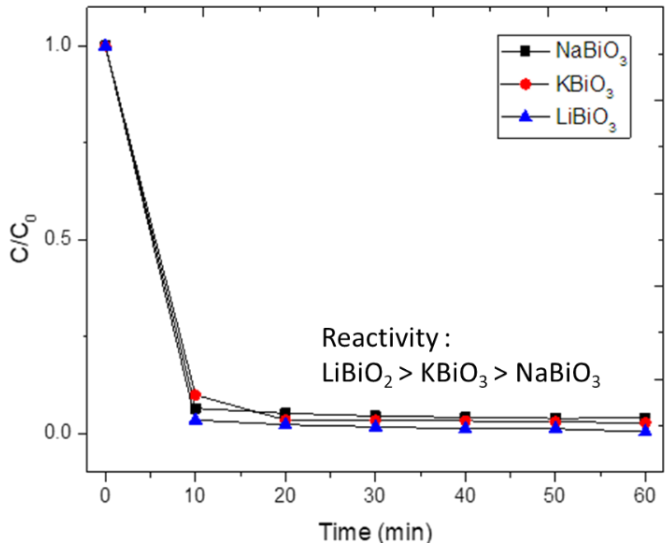

Fig 5.14 The reactivity rate of degradation of methylene blue dye by $LiBiO_2$, $KBiO_3$ and $NaBiO_3$

5.7 Conlusion

In this study, we can conclude that the alkali bismuthate can be prepared by the SSR method. However, a pure compound and a fine powder could not be achieved by this method, but an increase in the efficiency of degradation of the dye can be seen. The choices of the starting materials and helps of other types of reagents in the SSR method played a vital role. Therefore, the addition of other reagents should be studied in order to achieve a pure and fine powder of the alkali bismuthate since it have a good reactivity in the decolorization of the dyes. Besides, creating a heterojunction of these compounds might increase the stability and efficiency of decolorization and degradation of dyes.

5.8 References

1. Kako, T., Zou, Z.G., Katagiri, M., Ye, J.H.: Decomposition of organic compounds over $NaBiO_3$ under visible light irradiation. Chem. Mater. 19, 198–202 (2007)
2. Nguyen, T.N., Giaquinta, D.M., Davis, W.M., zur Loye, H.C.: Electrosynthesis of $KBiO_3$: a potassium ion conductor with the KSbO3 tunnel structure. Chem. Mater. 5, 1273–1276 (1993)
3. Ramachandran, R., Sathiya, M., Ramesha, K., Prakash, A.S., Madras, G., Shukla, A.K.: Photocatalytic properties of $KBiO_3$ and $LiBiO_3$ with tunnel structures. J. Chem. Sci.
4. Kumada, N., Takahashi, N., Kinomura, N.: Preparation and crystal structure of a new lithium bismuth oxide: $LiBiO_3$. J. Solid State Chem. 126, 121–126 (1996)
5. Kikugawa, N., Yang, L.Q., Matsumoto, T., Ye, J.H.: Photoinduced degradation of organic dye over $LiBiO_3$ under illumination of white fluorescent light. J. Mater. Res. 25, 177–181 (2010)

CHAPTER 6

$Bi_{11}VO_{19}$ -VO_2 MICROSTRUCTURE AND ITS VISIBLE LIGHT DRIVEN PHOTOCATALYTIC PERFORMANCE IN ORGANIC DYE DEGRADATION

In this chapter, a new bismuth vanadate, $Bi_{11}VO_{19}$ – VO_2 microstructure which successfully synthesized by a simple precipitation method and its material characterization, optical properties and photocatalytic activity for cationic and anionic dyes are explained.

6.1 Introduction

Bismuth vanadate with varieties of structures and morphologies has been the subject of research since decades in the photocatalysis field. This is due to its high potential for visible-light-driven photocatalysis. It is well known that bismuth vanadate has three main phases, namely, monoclinic scheelite (s-m), tetragonal scheelite (s-t) and tetragonal zircon (zt), and its photocatalytic properties are strongly dependent on its crystal structure. Among these three crystal phases, the monoclinic phase shows the highest photocatalytic activity [1-3]. In this chapter, we tried to synthesis bismuth vanadate microstructure by using a simple precipitation method, at a low temperature. From this method, we managed to achieved a bismuth vanadate, $Bi_{11}VO_{19}$ with a monoclinic VO_2 microstructure. Based on our knowledge, there was only one report based on this material, which was conducted by Yuting Lu et al.[4]. They prepared a δ-Bi_2O_3-structural $Bi_{11}VO_{19}$ nanoparticles by Pechini method and tested the photocatalytic performance by the photodegradation of the methylene blue (MB) under visible light irradiation.

Therefore, in this study, we conducted various analyses to further understand this material. In the photocatalytic performance study, we have chosen two dyes, which are the cationic methylene blue (MB) dye, and the anionic methyl orange (MO) dye. Both of these dyes were chosen because it is one of the frequently used dyes in the industries. The

MB dye and MO dye has the chemical structure of $C_{16}H_{18}N_3SCl$ and $C_{14}H_{14}N_3NaO_3S$ each.

6.2 Objective

To develop a simple and low-cost method in developing

1. a various structures and morphologies of bismuth based materials
2. high and stable photocatalytic performance under visible light in the degradation of anionic and cationic organic dyes

6.3 Experimental Procedure

6.3.1 Chemical Reagents

Bismuth nitrate pentahydrate ($Bi(NO_3)_3 \bullet 5H_2O$) crystal and nitric acid (HNO_3) were purchased from Wako Pure Chemical Industries. Sodium hydroxide (NaOH) granule was bought from Kanto Chemical Co., Inc, sodium metavanadate ($NaVO_3$) from Wako Pure Chemical Industries and methylene blue dye powder from Waldeck GmbH & Co. KG. Ultrapure water was used in all experiments. All chemicals were analytical grade and used as received without further purification.

6.3.2 Synthesis Method

The $Bi_{11}VO_{19}$-VO_2 microstructure were synthesized by a simple precipitation method at 65°C for 24 hours. 4.2 g of $Bi(NO_3)_3.5H_2O$ and 1 mmol to 6 mmol of $NaVO_3$ were dissolved in a 60 mL of HNO_3 with a concentration of 4molL^{-1}. Ultrapure water was added until it gave a final volume of 300 mL. The solution was stirred until a clear solution formed. Then, the pH of the solution was adjusted to pH 10.7 by adding the NaOH concentration. The solution will change its color from clear solution to pale

yellowish precipitate which indicates the formation of bismuth vanadate. The suspension was inserted into an oil bath at 65°C for 24 hours without stirring. The resulting pale-yellow precipitate was retrieved by centrifugation, washed several times with distilled water and absolute ethanol. The yellow precipitate was then dried at 70°C for 12 hours and was calcined at a different temperature (400°C, 500°C and 600°C) for further study.

6.4 Characterization

The samples were analyzed with an x-ray diffractometer (XRD, RINT 2000; Rigaku, Corp., Japan) operated at 30 kV and 40 mA with Cu Kα radiation (λ=1.54178Å). Data were collected in the angular range of 2θ=10–80°. FESEM images were obtained from Hitachi FE-SEM SU8000. UV-visible diffusion reflectance spectra were measured at a room temperature, with a UV-Vis-NIR Spectrophotometer JASCO V-7200. The reflectance was then converted to absorbance by using the Kubelka–Munk method. FTIR and raman spectra were also used in this study.

6.5 Photocatalytic Evaluation Test

Photocatalytic evaluation test was conducted as follows. 4 mL of methylene blue solution with a concentration of 0.3mg/100mL was placed in a 100 mL. After that, 0.3 g of $Bi_{11}VO_{19}$-VO_2 powder was added for each experiment. The experiments were conducted under the presence of visible light (λ> 400nm). The solution was magnetically stirred to ensure uniformity. The samples were then filtered by using syringe membrane filter (Millex: Millipore Corp., United States) to remove the photocatalyst particles. Samples were taken from the solution for every 30 minutes and placed inside a UV-Vis spectrophotometer cell in order to measure the maximum absorption of wavelength for the dye and the rate of degradation. The percentage of degradation was calculated by the formula of $[1-(C/C_0)]$ x 100%, where C_0 is the initial concentration of the dye solution, and C is the concentration of the dye for every 30 minutes interval. In order to determine the active species that involve in the photodegradation of the dye, scavenger method was

implemented. Benzoquinone for O_2^- radical trapping and tert-butanol for OH^- radicals trapping.

6.6 Results and Discussions

6.6.1 Material characterization

The obtained light yellowish powder of $Bi_{11}VO_{19}$-VO_2 was characterize by XRD at two theta range from 10° to 80°. Figure 6.1 shows the XRD pattern for the $Bi_{11}VO_{19}$-VO_2 microstructures. The XRD pattern shows that the sample was well crystallized with a pure $Bi_{11}VO_{19}$, phase together with two vanadium oxide peak(VO_2) at 011 and 110. $Bi_{11}VO_{19}$ crystallizes in the Fm3m space group with a fluorite-type cubic cell. The details of the crystallographic parameters of $Bi_{11}VO_{19}$ and VO_2 are shown in Table 6.1. The presence of VO_2 monoclinic is expected to be one of the contribution to the good efficiency of the photocatalyst. This is because, based on previously reported works, monoclinic scheelite phase possessed a superior photocatalytic [5-7] activity compared to others besides having a better conductivity [4].

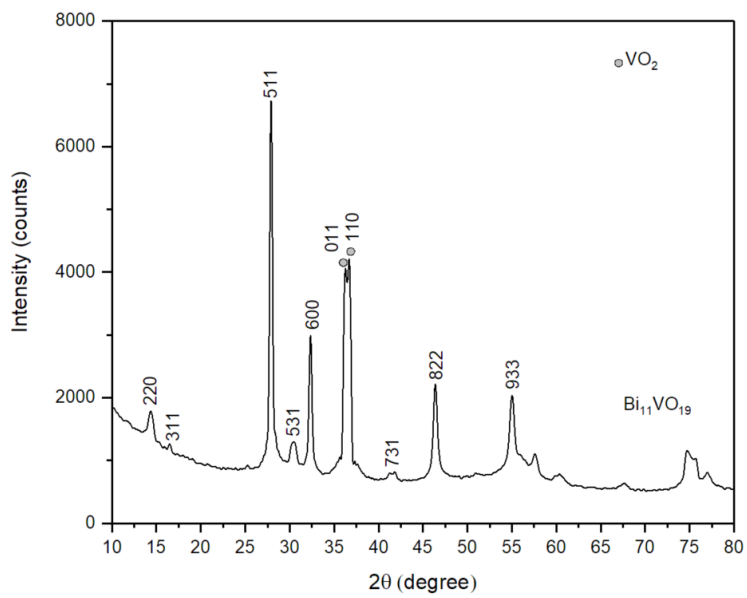

Figure 6.1 X-ray diffraction profiles for $Bi_{11}VO_{19}$-VO_2 microstructure

Table 6.1 Crystallographic parameters for $Bi_{11}VO_{19}$ and VO_2

Formula	$Bi_{11}VO_{19}$	VO_2
Crystal System	Cubic	Monoclinic
Space Group	Fm-3m	P2/m
Space Group Number	225	10
a (A)	16.6434	4.5060
b (A)	16.6434	2.8990
c (A)	16.6434	4.6170
Alpha	90.0000	90.0000
Beta	90.0000	91.7900
Gamma	90.0000	90.0000
Volume of cell (10^6 pm^3)	4610.27	60.28
RIR	4.60	1.76

The FESEM images of $Bi_{11}VO_{19}$-VO_2 microstructures are shown in Figure 6.2. The sample shows a coral-like structure which is made up of average 200 nm cubic particles mixed with nanosheets.

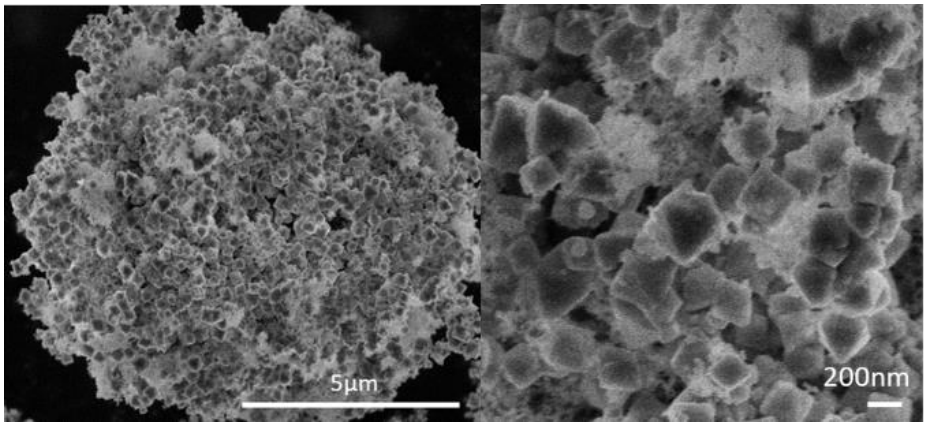

Figure 6.2 FESEM images and particle size for $Bi_{11}VO_{19}$-VO_2 microstructure

The size distribution of the particles is shown in Figure 6.3 which shows the average of 849.5 nm in size with a large error bar due to some loose structure formed from the excess vanadium oxide, VO_2. Besides that, as the temperature increases, the size of the particles also increases.

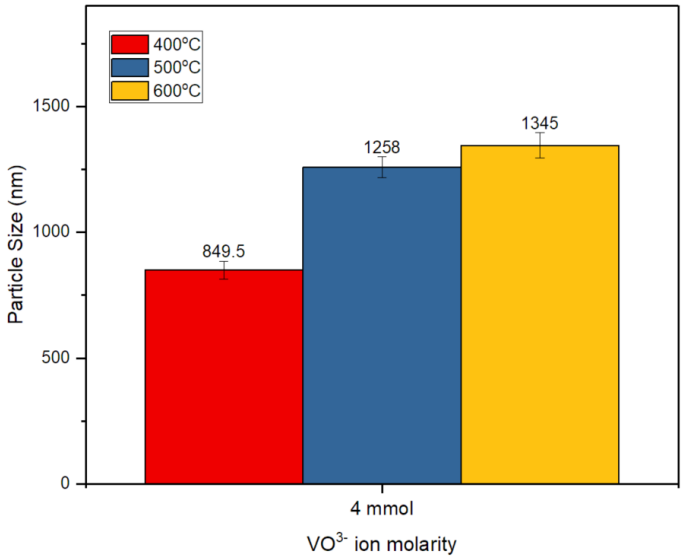

Figure 6.3 Particle size distribution depending on the molarity of VO^{3-} ions

In addition, we had varied the VO^{3-} ions molarity by increasing the molarity and it shows that the morphologies of the compounds were also changed. The size of the microstructure kept increasing with the increases of the molarity. Furthermore, it started to get bulky, and have lesser porosity as what we can see from Figure 6.4.

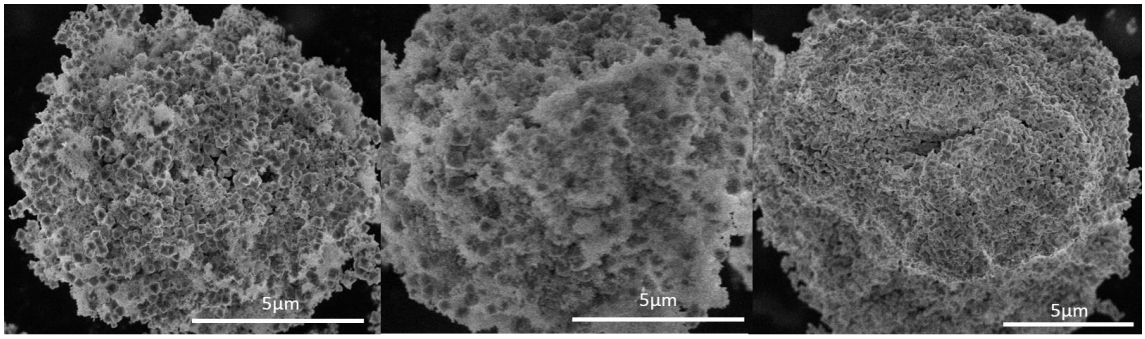

Figure 6.4 FESEM images on the morphological changes as the molarity of VO^{3-} ions increases

We have also conduct a measurement on the energy dispersive X-ray spectra, EDX to examine the elemental compositions and its percentage in the synthesized photocatalyst. The EDX spectrum is shown in Figure 6.5. The Bi/V ratio is almost tally to the XRD analysis, which is the theoretical formula of $Bi_{11}VO_{19}$ with VO_2 compound.

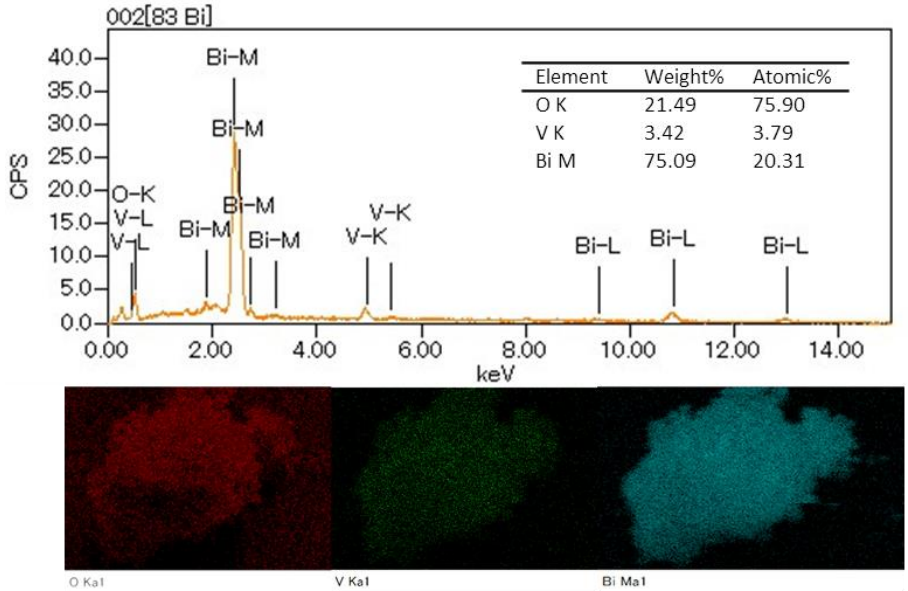

Fig. 6.5 EDX analysis for $Bi_{11}VO_{19}$-VO_2 microstructure

6.6.2 Optical properties

The UV-Vis optical absorption spectrum of $Bi_{11}VO_{19}$-VO_2 microstructure was measured as shown in Figure 6.6. A broad absorption spectrum could be seen from 250 nm to 370 nm. At around 370 nm, an abrupt cutoff absorption edge was observed. In this structure, there are three possible optical activators such as the V^{5+}, V^{+} and Bi^{3+}.

Correspondingly, the 400 nm to 500 nm band-gap absorption is the transition of the 6s electrons of Bi^{3+} to the empty 3d orbitals of V^{5+}. In this case usually the Bi^{3+} 6s orbitals can hybridize with O-2p in VB [10].

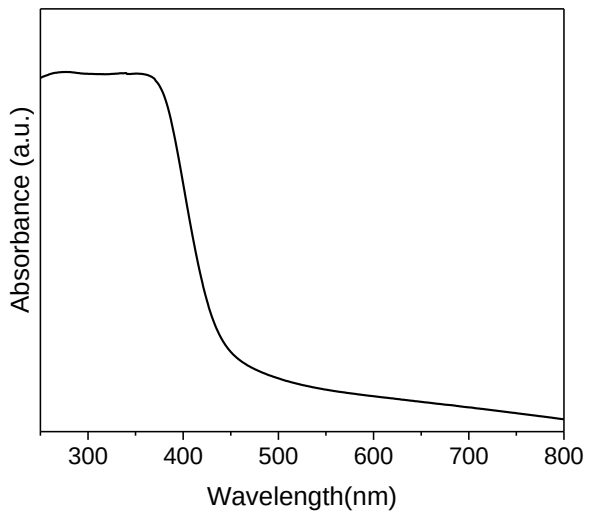

Figure 6.6 UV-vis absorbance for $Bi_{11}VO_{19}$-VO_2 microstructure

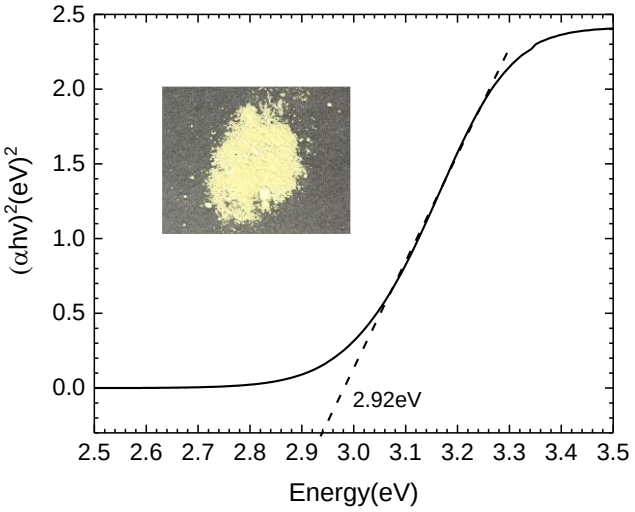

Figure 6.7 UV-vis diffuse reflectance spectra for $Bi_{11}VO_{19}$-VO_2 microstructure

The absorption band contains a tail extending rightwards until about 800 nm. This may result from the crystal defects formed during the growth of the $Bi_{11}VO_{19}$-VO_2 microstructure. The band gap energy was determined by Kubelka-Munk derivation (Figure 6.7). The band gap of this photocatalyst is 2.92 eV and has the light yellowish colored powder. It is slightly broader than the reported $Bi_{11}VO_{19}$ nanoparticles [4] which is only 2.23 eV. However, since the band gap is less than 3.2 eV, it can still work efficiently under visible light irradiation. Besides, the presence of VO_2 monoclinic which

possess a superior photocatalytic activity will enhance the photocatalytic character of this photocatalyst.

Furthermore, in Figure 6.8, the photoluminescence spectra at the excitation wavelength of 325 nm shows a peak at 712 nm with an intensity of 80 which indicated that it has a moderate recombination rate. Thus, results in a better efficiency and higher recyclability.

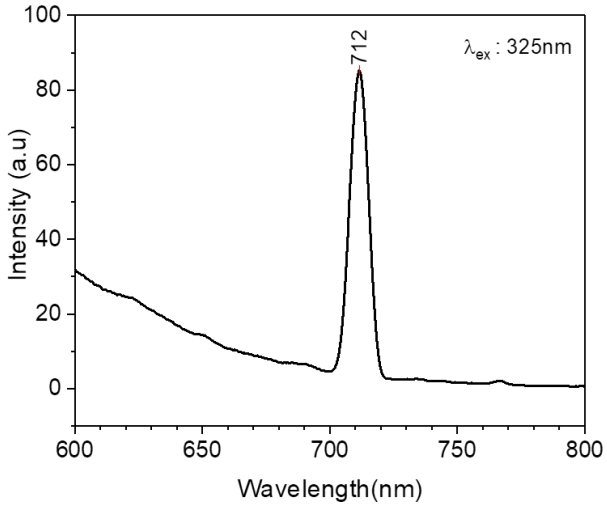

Fig. 6.8 Photoluminescence at the excitation wavelength of λ_{ex} : 325nm for $Bi_{11}VO_{19}$-VO_2 microstructure

From the FTIR analysis spectrum in Figure 6.9, at 1,093cm^{-1}it shows an unshared V=O stretching vibrations, at 769cm^{-1}, an antisymmetric stretching vibrations of the bound oxygen which are shared by two vanadium atoms (V–O–V), 501cm^{-1}, a symmetric stretching mode of V–O–V units, finally at 3,454 and 1,630cm^{-1}, an O-H stretching and bending vibration of lattice water molecules are found.

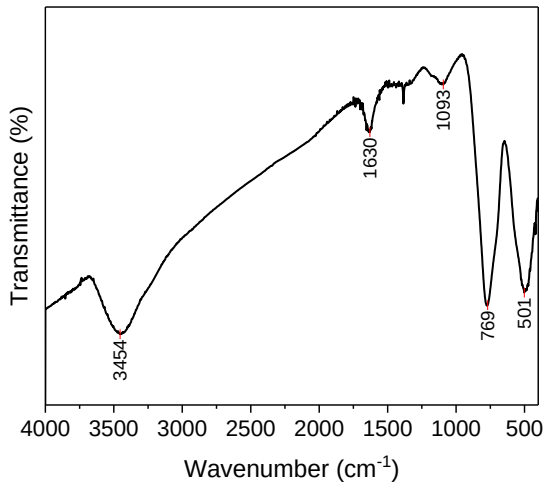

Figure 6.9 FTIR analysis for $Bi_{11}VO_{19}$-VO_2 microstructure

In raman spectra analysis in Figure 6.10, it shows an anti-symmetric bending vibration of the VO_4^{3-} tetrahedron at 305cm^{-1} and a symmetric V-O stretching mode at 824 cm^{-1}.

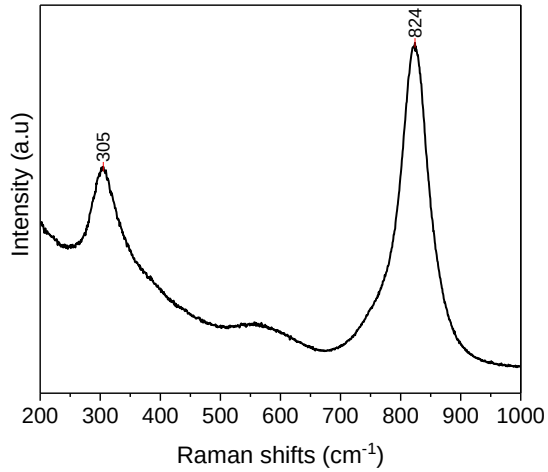

Figure 6.10 Raman analysis for $Bi_{11}VO_{19}$-VO_2 microstructure

6.6.3 Photocatalytic activity

In the photocatalytic study, we have run the degradation experiments on two types of dyes, the cationic dye, MB and anionic dye, MO. In MB dye degradation, it shows a good and stable photocatalytic activity. However, in MO dye degradation, there is only a slight amount of MO degraded in 270 minutes experiment. This shows that this photocatalyst is good in degrading the cationic dye, but not for anionic dye. For degrading the anionic dye, further modification needs to be done to increase the efficiency of the photocatalyst.

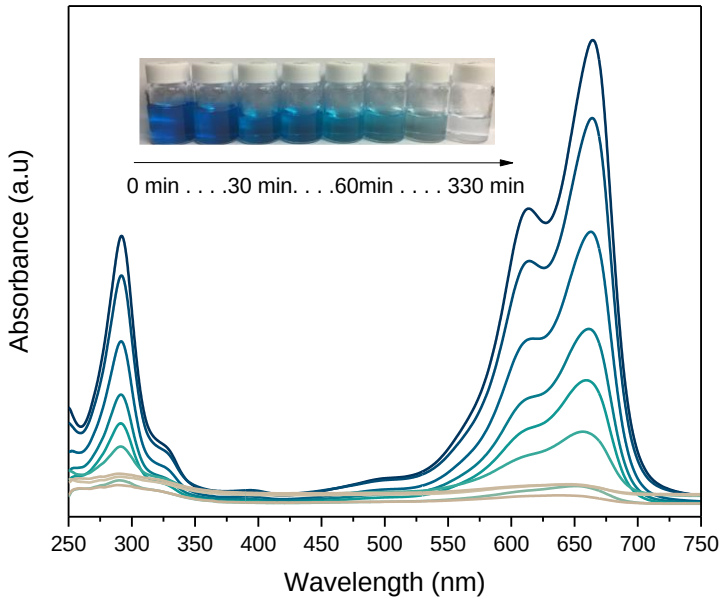

Figure 6.11 The absorbance rate of degradation of methylene blue dye for $Bi_{11}VO_{19} – VO_2$ microstructure

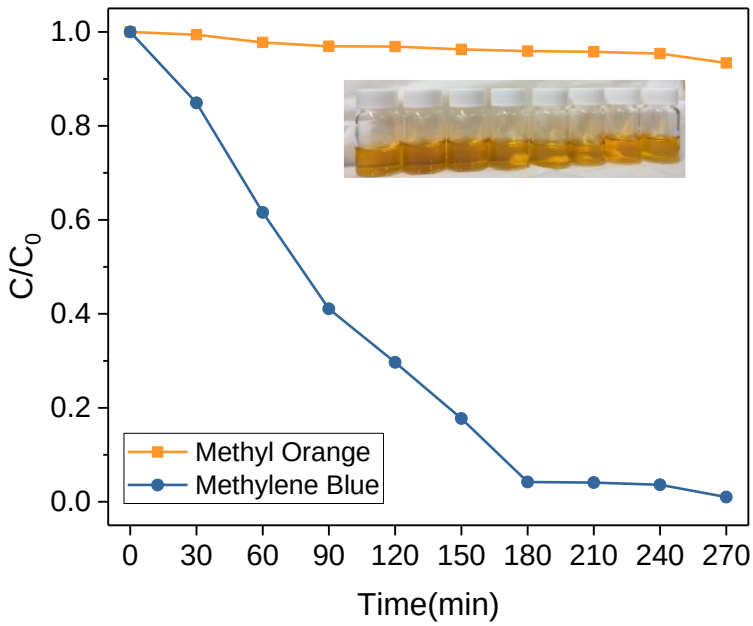

Figure 6.12 The absorbance rate of degradation of methylene blue dye and methyl orange dye for $Bi_{11}VO_{19}$-VO_2 microstructure

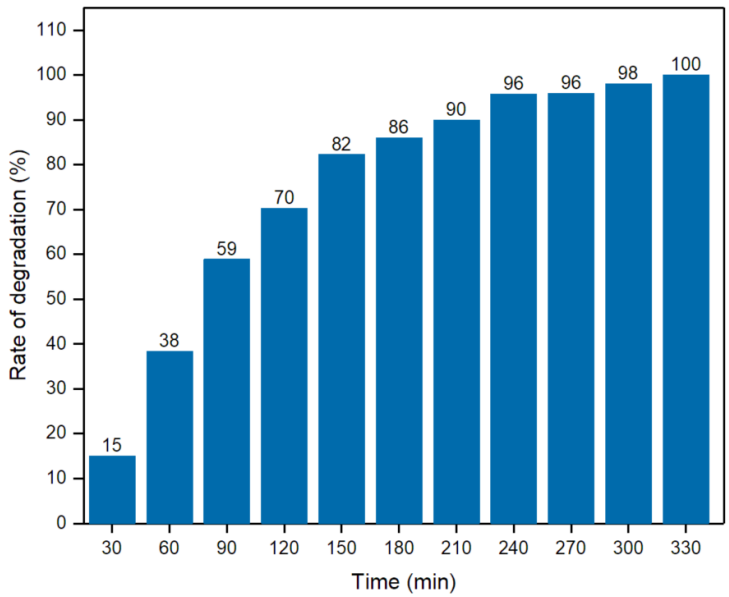

Figure 6.13 The degradation rate of methylene blue dye for $Bi_{11}VO_{19}$-VO_2 microstructure

Besides, we also conducted the study in order to identify of active species by in situ capture experiments. Benzoquinone was used to capture the O_2^- radicals and tert-butanol for OH^- radicals. From the graph in Figure 6.14, it shows that the OH^- radicals act as the main active species in the photocatalytic degradation of MB dye.

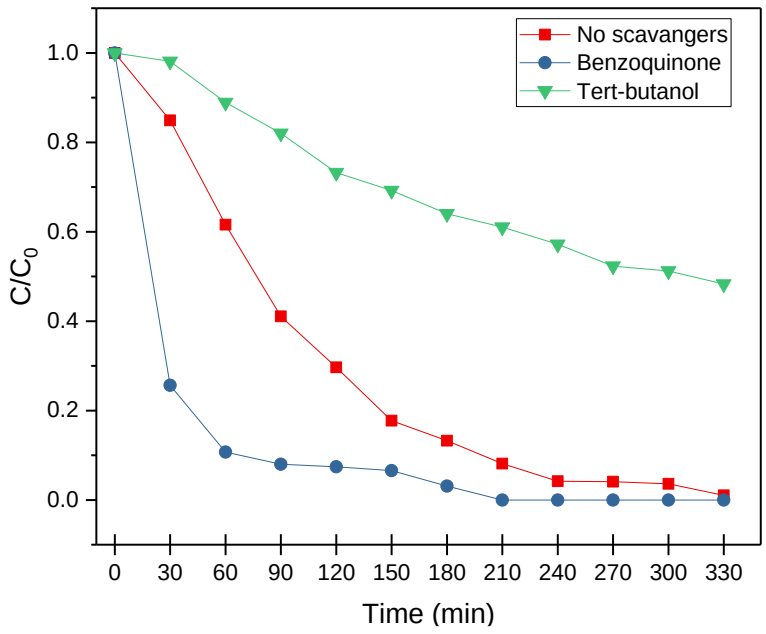

Figure 6.14 The identification of active species involved by in-situ capture experiment in the degradation of methylene blue dye for $Bi_{11}VO_{19}$-VO_2 microstructure

Furthermore, a study on recyclability and stability was also conducted. From the result in Figure 6.15, it shows that it has quite a good stability since after the 4th run, just a slight amount of efficiency decreases. Therefore, it is a good photocatalyst in the visible light range. However, the recyclability in terms of easy settlement reduces as the particles started to dispersed into smaller particles after each run.

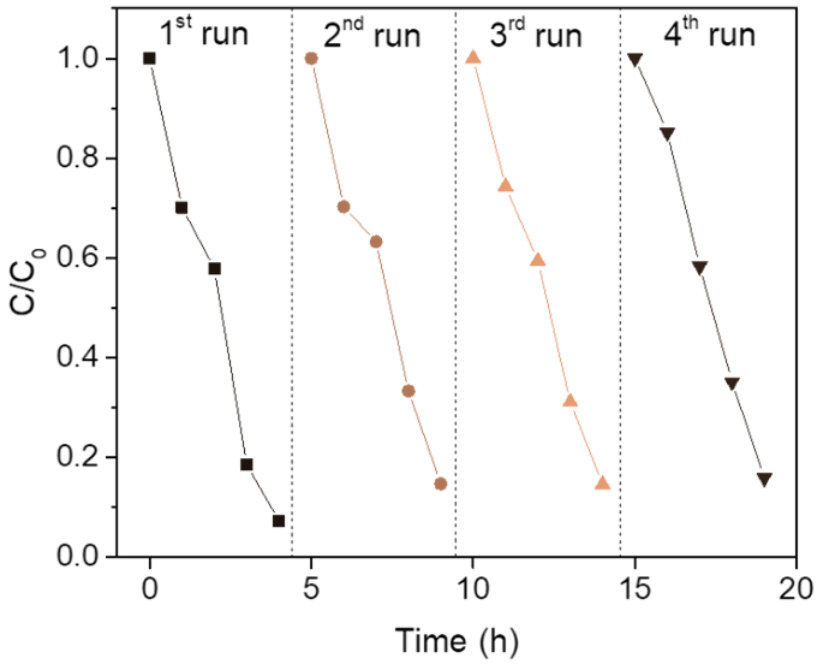

Figure 6.15 The recyclability of degradation of methylene blue dye in 4 cycles for $Bi_{11}VO_{19}$-VO_2 microstructure

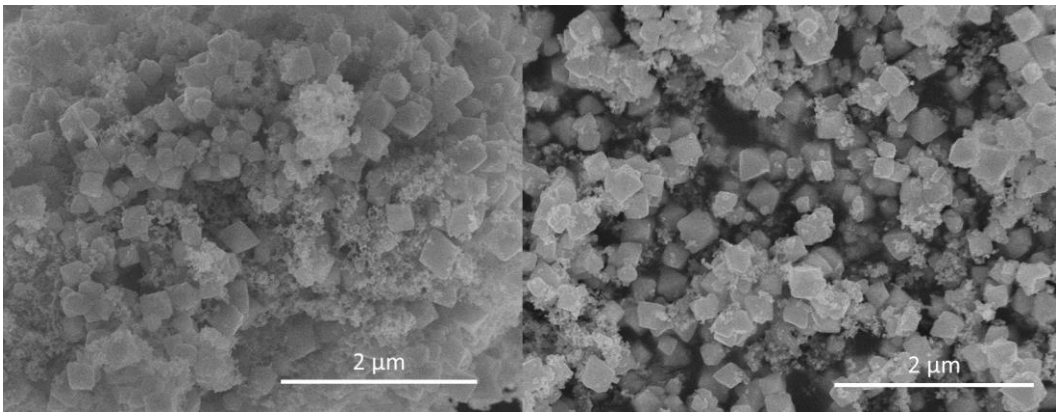

Figure 6.16 FESEM images of $Bi_{11}VO_{19}$-VO_2 microstructure powder after experiment

6.7 Conclusions

In a conclusion, we have successfully synthesized the $Bi_{11}VO_{19}$ -VO_2 microstructure via s simple precipitation method at 65℃. Besides, it possessed a good photocatalytic activity in degrading cationic type dye, the MB dye. It also has a good stability and can be recyclable. However, it could not function very well in an anionic type dye, which is the MO dye. Only a slight amount of degradation was observed. Therefore, further study on the modification in degrading anionic type of dye is important to increase its efficiency more.

6.8 References

1. D.N. Ke, T.Y. Peng, L. Ma, P. Cai, K. Dai, Effects of hydrothermal temperature on the microstructures of BiVO4 and its photocatalytic O2 evolution activity under visible light, Inorg. Chem. 48, 2009, page 4685–4691.
2. C.G. Li, G.S. Pang, S.M. Sun, S.H. Feng, Phase transition of BiVO4 nanoparticles in molten salt and the enhancement of visible-light photocatalytic activity, J. Nanopart. Res. 12, 2010, page 3069–3075.
3. N.C. Castillo, A. Heel, T. Graule, C. Pulgarin, Flame-assisted synthesis of nanoscale amorphous and crystalline, spherical BiVO4 with visible-light photocatalytic activity, Appl. Catal. B Environ. 95, 2010, page 335–347.
4. Y.Lu et al., Optical properties and visible light-driven photocatalytic activity of $Bi_{11}VO_{19}$ nanoparticles with d-Bi_2O_3-structure, Journal of Alloys and Compounds 640, 2015, page 226-232.
5. Kudo, A.; Miseki, Y. Heterogeneous Photocatalyst Materials for Water Splitting, Chem. Soc. Rev., 38, 2009, page 253−278.
6. L. Ren et al., Template-free synthesis of BiVO4 nanostructures: I. Nanotubes with hexagonal cross sections by oriented attachment and their photocatalytic property for water splitting under visible light, Nanotechnology, 20, 2009, page 115603.

7. G. Xi and J. Ye, Synthesis of bismuth vanadate nanoplates with exposed {001} facets and enhanced visible-light photocatalytic properties, Chemical Communications, Issue 11, 2010, page 1893–1895.
8. M.R. Hoffmann, S.T. Martin, W. Choi, D.W. Bahnemann, Environmental Applications of Semiconductor Photocatalysis, Chemical Reviews, 95(1), 1995, page 69–96.
9. N. Kumagai, T. Fujiwara, K. Tanno, T. Horiba, Physical and Electrochemical Characterization of Quaternary Li‐Mn‐V‐O Spinel as Positive Materials for Rechargeable Lithium Batteries, Journal of Electrochemical Society, 143, 1996, page 1007–1013.
10. D. Prakash, Y. Masuda, C. Sanjeeviraja, Synthesis and structure refinement studies of LiNiVO4 electrode material for lithium rechargeable batteries, Ionics 19, 2013, page 17–23.

CHAPTER 7

FLOWER-LIKE BISMUTH VANADATE ($BiVO_4$) MICROSPHERES AND ITS VISIBLE LIGHT DRIVEN ACTIVITY

In this chapter, a flower-like bismuth vanadate, $BiVO_4$ microspheres which successfully synthesized by a simple precipitation method and its material characterization, optical properties and photocatalytic activity for cationic dye are presented.

7.1 Introduction

A flower-like $BiVO_4$ photocatalyst was synthesized by a simple template-free precipitation method at 60°C for 24 hours. The purpose of this study is to explore for a low cost and simple method in synthesizing the self-assembled structural in order to enhance the photocatalytic performance under visible light irradiation (λ>420nm). In this study, the morphology, structure and photo-absorption of flower-like $BiVO_4$ were characterized, and the effects of the photocatalytic performance were analyzed. The formation of the hierarchical microspheres was also proposed. Besides, the as-obtained samples were then calcined under a different temperature (200 ^{o}C, 300 ^{o}C, 400 ^{o}C, 500 ^{o}C, and 600 ^{o}C) to study the effect of calcination towards the structure and how it affects the photocatalytic performance. The photocatalytic performance was then evaluated by the decolorization of methylene blue (MB) dye under visible-light irradiation.

As for the dye contaminants, we have chosen two dyes, which are the cationic methylene blue (MB) dye, and the anionic methyl orange (MO) dye. Both of these dyes were chosen because it is one of the frequently used dyes in the industries. The MB dye and MO dye has the chemical structure of $C_{16}H_{18}N_3SCl$ and $C_{14}H_{14}N_3NaO_3S$ each.

7.2 Objective

To develop a bismuth-based hierarchical structure microspheres via a simple precipitation method at a low synthesis temperature which have :-

- High surface area
- More stability
- Higher efficiency

in degrading the organic contaminants in aqueous solution.

7.3 Experimental Procedure

7.3.1 Chemicals and reagents

Bismuth nitrate pentahydrate ($Bi(NO_3)_3{\cdot}5H_2O$) crystal and nitric acid (HNO_3) were purchased from Wako Pure Chemical Industries. Sodium hydroxide (NaOH) granule was bought from Kanto Chemical Co., Inc, vanadium(III) acetylacetonate ($C_{10}H_{14}O_5V$) crystal from Strem Chemicals Inc. and methylene blue dye powder from Waldeck GmbH & Co. KG. Ultrapure water was used in all experiments. All chemicals were analytical grade and used as received without further purification.

7.3.2 Synthesis method

The 3D flower-like $BiVO_4$ microspheres were synthesized by a simple template-free homogeneous precipitation method at 60°C for 24 hours. 4.2 g of $Bi(NO_3)_3{\cdot}5H_2O$ and 0.27g of $C_{10}H_{14}O_5V$ were dissolved in a 100 mL of HNO_3 with a concentration of $4molL^{-1}$. Ultrapure water was added until it gave a final volume of 500mL. The solution was stirred until a clear light blue solution was formed. Then, the pH of the solution was adjusted to pH 12 by adding the NaOH. The solution will change its color from clear light blue to blueish precipitate and brownish precipitate which indicates the changes from

acidic to neutral to alkaline state. The suspension was inserted into an oil bath at 60°C for 24 hours without stirring. The resulting yellow precipitate was retrieved by centrifugation, washed several times with distilled water and absolute ethanol. The yellow precipitate was then dried at 60°C for 24 hours and was calcined at a different temperature (300°C, 400°C, 500°C and 600°C) for further study.

7.4 Characterization

The samples were analyzed with an x-ray diffractometer (XRD, RINT 2000; Rigaku, Corp., Japan) operated at 30 kV and 40 mA with Cu Kα radiation (λ=1.54178Å). Data were collected in the angular range of 2θ=15–80°. FESEM images were obtained from Hitachi FE-SEM SU8000. UV-visible diffusion reflectance spectra were measured at a room temperature, with a UV-Vis-NIR Spectrophotometer JASCO V-7200. The reflectance was then converted to absorbance by using the Kubelka–Munk method. The size of the particles was recorded by a Zeta Potential and particle analyzer Otsuka Electronics ELSZ-2000 at a room temperature by using ultrapure water as a solution. FT-IR (Fourier Transform Infrared Spectroscopy) Thermoscientific Nicolet 4700, Micro Raman Spectrometer Horiba-Jovin Yvon T64000 and Fluorescence Spectrometer JASCO FP8500 was also used for further analyses.

7.5 Photocatalytic Evaluation Test

Photocatalytic evaluation test was conducted as follows. 4 mL of methylene blue solution with a concentration of 0.3mg/100mL was placed in a 100 mL. Then, 96mL of ultrapure water was added to the aqueous solution. After that, 0.3g of BiVO4 powder was added for each experiment. The experiments were conducted under the presence of visible light (λ> 400nm). The solution was magnetically stirred to ensure uniformity. The samples were then filtered by using syringe membrane filter (Millex: Millipore Corp., United States) to remove the photocatalyst particles. Samples were taken from the solution for every 30 minutes and placed inside a UV-Vis spectrophotometer cell in order to measure the maximum absorption of wavelength for the dye and the rate of degradation.

The percentage of degradation was calculated by the formula of [1-(C/C0)] x 100%, where C0 is the initial concentration of the dye solution, and C is the concentration of the dye for every 30 minutes interval.

7.6 Results and Discussion

7.6.1 Material Characterization

XRD was used to characterize the phase structure of the obtained samples. Figure 7.1 shows the XRD pattern of the as-prepared $BiVO_4$ microspheres for each calcination temperature. The XRD pattern at 400 °C indicates that the sample composed mainly of monoclinic phase which exhibits high photocatalytic activity compared to other phases. Besides, a well and definite sharp peak can be seen after calcination at 300°C. This indicates that the sample has achieved a well-defined organizational structure which leads to a better photocatalytic activity.

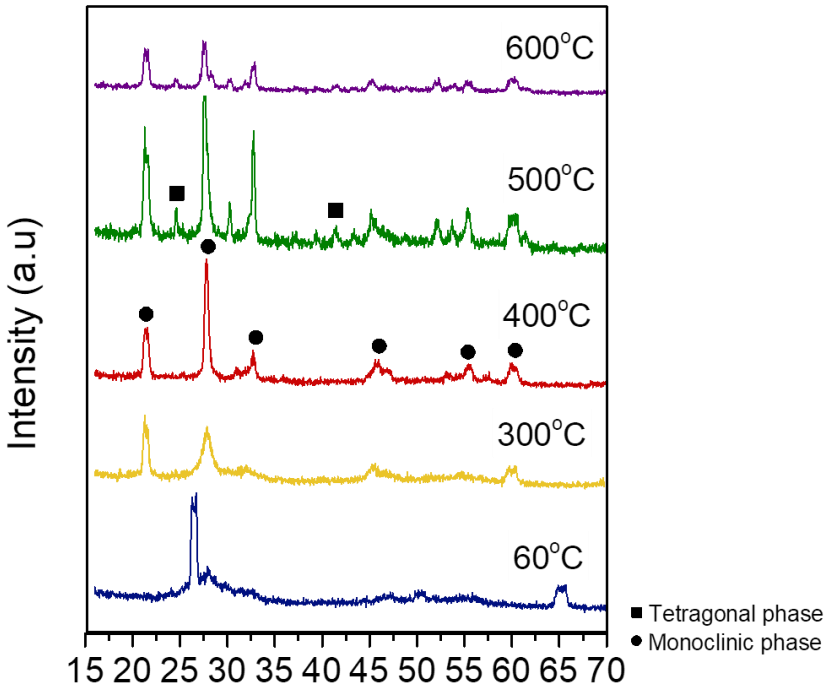

Figure 7.1 XRD analysis for $BiVO_4$ microspheres under different calcination temperature

From the SEM observation images in Figure 7.2(a) and (b), after calcination at 400°C, the products formed were uniformed. The SEM images of commercial $BiVO_4$ can be seen as bulky and not much surface area is available (Figure 7.2(c)).

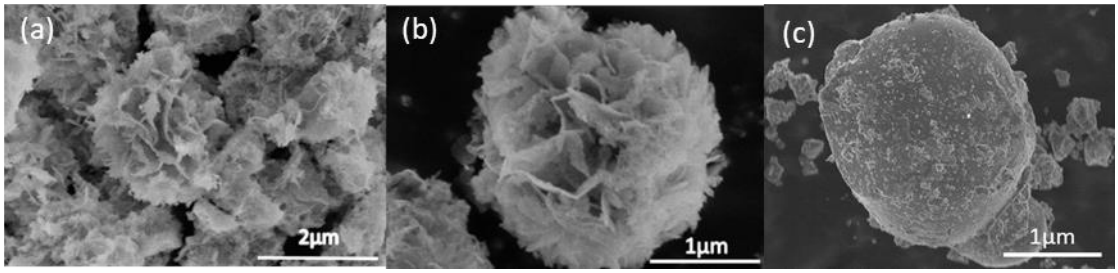

Figure 7.2 (a), (b) FESEM images of flower-like BiVO4 and (c) Commercial BiVO4

However, at 500 °C (Figure 7.5), the mixture of flowerlike structural and agglomerates started to form while at 600°C, the particles started to form only agglomerates, and no flowerlike structures were found.

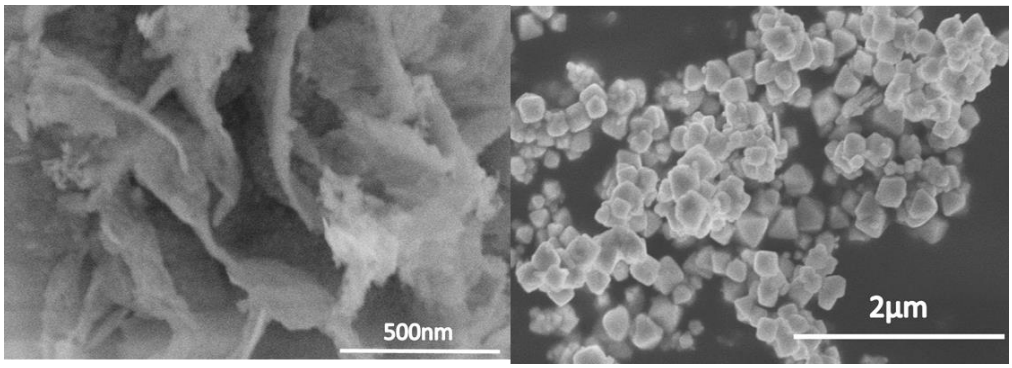

Figure 7.3 High magnification of flower-like $BiVO_4$ and the results obtained under synthesis condition of pH more than 12

To study more on the morphology structure, we observed the samples under high magnification SEM in Figure 7.2, and the flowerlike structures of the sample were composed of numerous 2D nanosheets with the thickness of about 100nm. The 2D nanosheets intercross each other to form a flowerlike microsphere via the self-assembly and Ostwald ripening process. These 3D structures resulting in the increase of the surface area which leads to a better photocatalytic performance compared to the commercial $BiVO_4$ that has a bulky structure and low surface area. Besides that, due to a large surface

area provided by the flowerlike structure, it can allow a more rapid diffusion of the reactants and products to take place during reaction process. Besides, if we increased the pH of the synthesis condition to be more than pH 12, the flowerlike structure could not be formed, and only microspheres/microcubes can be observed.

Figure 7.4 Schematic illustration of the proposed formation of flowerlike $BiVO_4$ microspheres structure

We also proposed the formation mechanism of the flowerlike BiVO4 microspheres as shown in Figure 7.4. A precipitation process occurred by the nucleation and growth of the second phase from a supersaturated solution. When a two phase of mixture composed of dispersed second phase in a system, the mixture does not appease the thermodynamic equilibrium state. This is due to the smaller particles which have a higher surface ratio having a higher energy state that leads to the excess surface energy. Thus, it does not satisfy the requirement of a minimum energy configuration. Therefore, the total energy of this system need to be decreased by increasing the size scale of the second phase which decrease the total interfacial area. This will result in the continuous nucleation and growth process until a single precipitate particle formed which introduce a new particle of a given size class which in this case, the flowerlike microspheres structure [5][6].

The particle mean size for the obtained samples were also studied by using the Zeta potential and particle analyzer. Based on Figure 7.3, 400°C shows the smallest size which is 2566 nm with a slight error value. At a 60°C and 300°C, the sample consist of impurities which lead to a larger mean particle size. However, at 500°C, the mean particle size is getting larger than at 400°C because of the mixture of 3D microspheres structure and agglomerates started to form. The mean particle size become the largest with a substantial error value at 60°C due to most of the sample were made up of large agglomerates, which contributes to a poor photocatalytic performance.

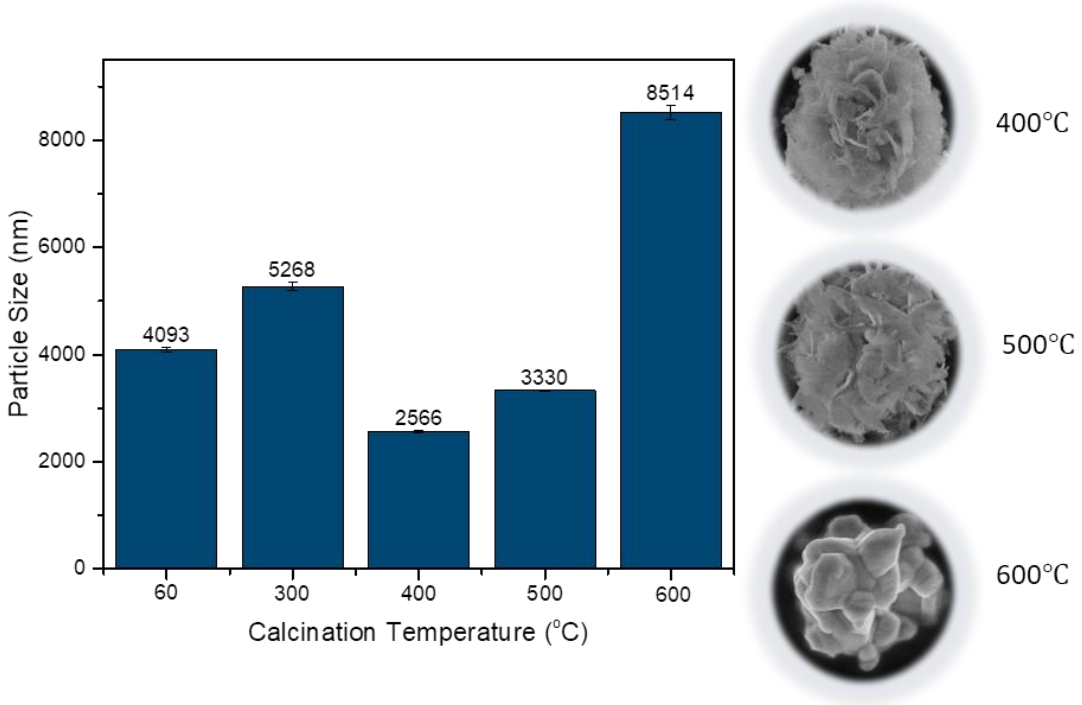

Figure 7.5 Particle size analysis of BiVO4 microspheres under calcination temperature of 60°C, 300°C, 400°C, 500°C and 600°C

7.6.2 Optical properties

The UV-Vis optical absorption spectrum of $BiVO_4$ microsphere was measured and compared with the commercial $BiVO_4$ and as-synthesized $BiVO_4$ microsphere as shown in Figure 7.6. A broad absorption spectrum could be seen from 300 nm to 400 nm. At around 420 nm, an abrupt cutoff absorption edge was observed.

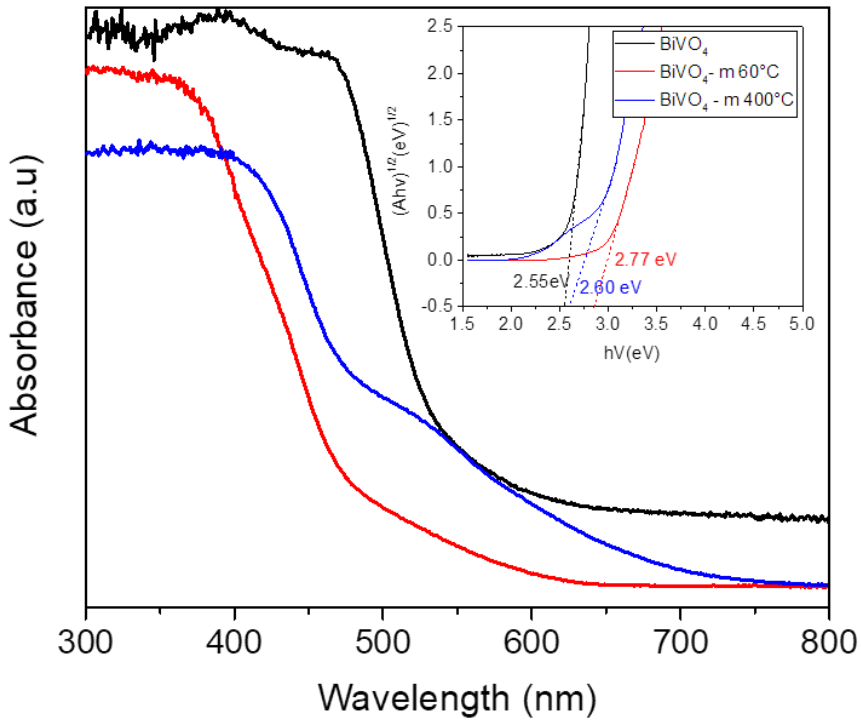

Figure 7.6 UV-Vis diffuse reflectance spectra of $BiVO_4$ microspheres and band gap via Kubelka-Munk derivation for $BiVO_4$ microspheres

The absorption band contains a tail extending rightwards until about 800 nm. This may result from the crystal defects formed during the growth of the $BiVO_4$ microsphere. The band gap energy was determined by Kubelka-Munk derivation (Figure 7.6). The band gap of this photocatalyst is 2.60 eV and has the yellowish colored powder. This shows that this photocatalyst can work efficiently under visible light irradiation. Besides, the presence of monoclinic phase which possess a superior photocatalytic activity contributed to the enhancement of the photocatalytic character of this photocatalyst.

Photoluminescence spectra analysis was studied at the excitation wavelength, λ_{ex} = 325 nm. In Figure 7.7, a strong peak could be seen at around 560 nm for both synthesized microspheres and the commercialize $BiVO_4$. The strong emission at 560nm, is correspond to the recombination of the hole formed from the hybrid orbitals of Bi 6s and O 2p and the electron generated from the V 3d orbitals. Besides, the emission bands of $BiVO_4$–m have blue shift, in comparison with the commercial $BiVO_4$, which could be associated with the particle size and shape effects of the sample. Based on the intensity, compared to the $Bi_{11}VO_{19}$ in previous chapter, the rate of recombination is higher, which influence to the photocatalytic activity.

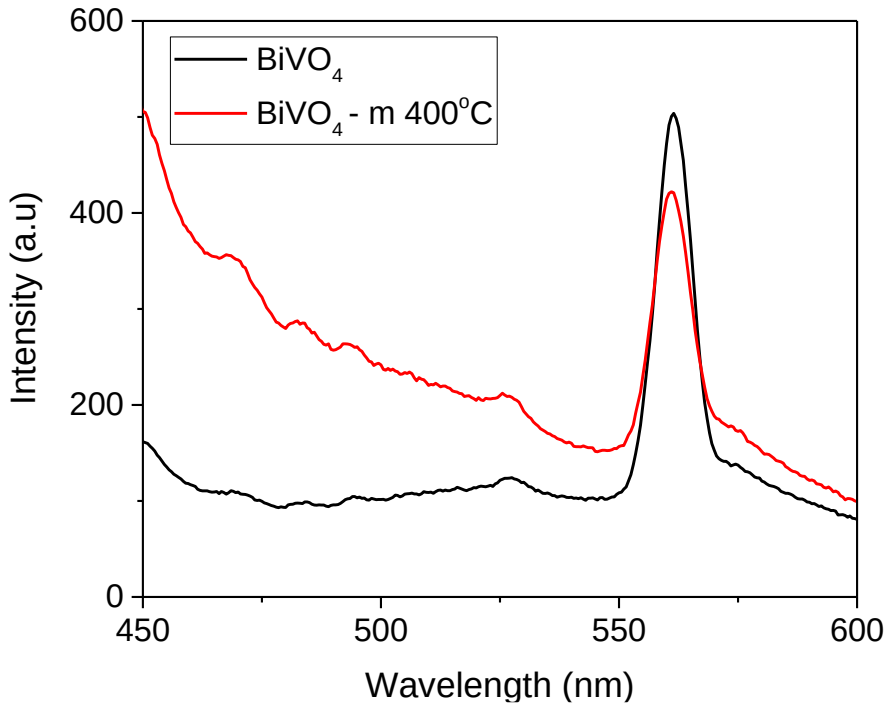

Figure 7.7 Photoluminescence spectra at the excitation wavelength of λ_{ex}: 325nm for $BiVO_4$ microspheres

The Raman analysis study was also investigated as shown in Fig. 7.8. The Raman bands at 313 cm^{-1} is the typical vibrations of $BiVO_4$ and can be assigned to the asymmetric and symmetric deformation modes of the VO_4^{3-} tetrahedron [29]. It was reported that there were two Raman bands at 710 cm^{-1} and 805 cm^{-1} which attributed to the stretching modes of two different types of V–O bands in the Raman spectrum of $BiVO_4$ [29]. However, only one band around 805 cm^{-1} is found in our case. The absence of 710 cm^{-1} band might be attributed to the local structure of porous microspheres that is composed of nanosheets. Besides that, the Raman band at 517 cm^{-1} indicates the characteristic of monoclinic scheelite $BiVO_4$ which made up this microsphere structures.

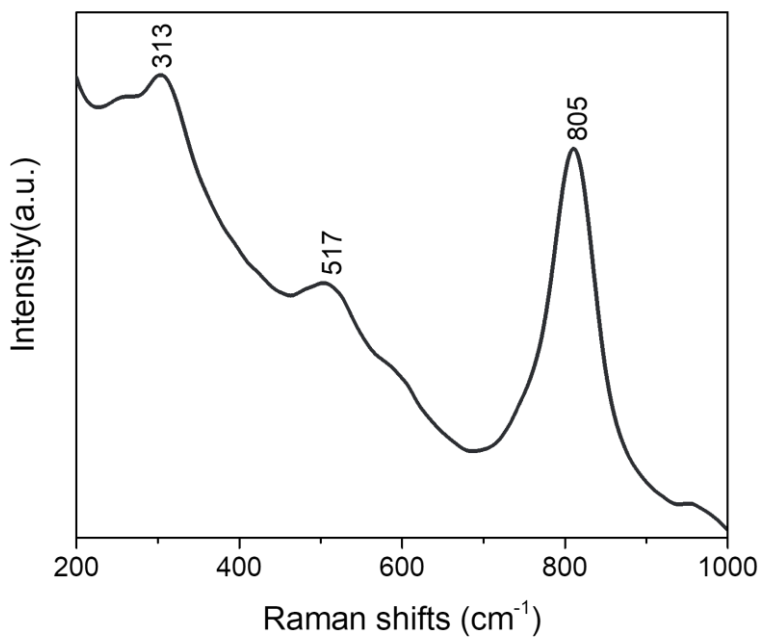

Figure 7.8 Raman analysis of $BiVO_4$ microspheres

From the FTIR analysis (Figure 7.9) we have conducted, we can understand the bonding group presence in this $BiVO_4$ microspheres. At 1,021cm^{-1}, there is an unshared V = O stretching vibrations, followed by 833cm^{-1} which shows the presence of an antisymmetric stretching vibrations of the bound oxygen that are shared by two vanadium atoms (V–O–V). Furthermore, at 523cm^{-1}, a symmetric stretching mode of V–O–V unit presence and finally at 3,402 cm^{-1} and 1,627cm^{-1}, it shows an O-H stretching and bending vibration of the lattice water molecules.

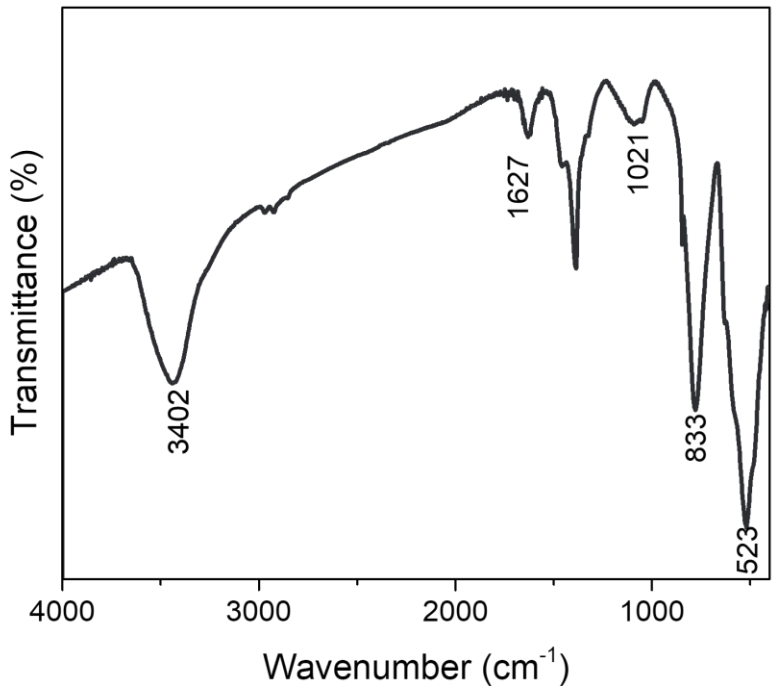

Figure 7.9 FTIR analysis of $BiVO_4$ microspheres

We have also conducted the zeta potential analysis to study the stability of this flowerlike BiVO4 in terms of the colloidal dispersion as shown in Figure 7.10. It shows that it has a high stability compared to the commercialize $BiVO_4$ since it possessed a higher + zeta potential value. When the potential is small, attractive forces may exceed this repulsion and the dispersion may break and flocculate. Therefore, colloids with high zeta potential (negative or positive) are electrically stabilized while colloids with low zeta potentials tend to coagulate or flocculate [7][8].

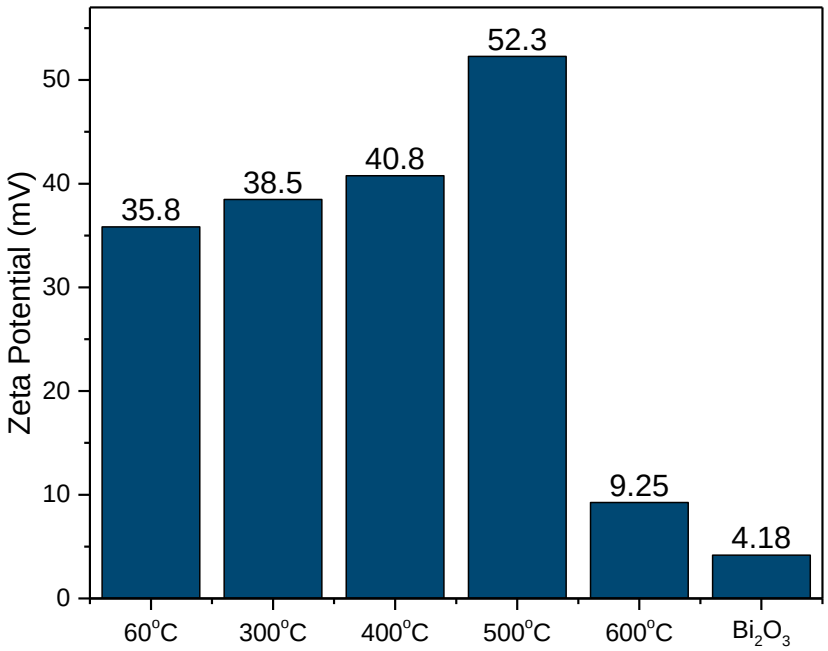

Figure 7.11 Zeta potential analysis of BiVO4 microspheres

7.6.3 Photocatalytic properties

The photocatalytic performance of the samples were evaluated by decolorization of MB aqueous solution under visible light irradiation, and the results are shown in Figure 7.12 and 7.13. The absorption of MB aqueous solution at λ=664nm was used to monitor the MB dye decolorization rate process. The decolorization rate sequence can be concluded as 400℃, 500℃, 60℃, 300℃, and follow by 600℃. The improved

performance was observed for 60℃, 300℃, 400℃ and 500℃. However, due to the presence of only agglomeration and bulk structure at 600℃, the reaction rate has declined.

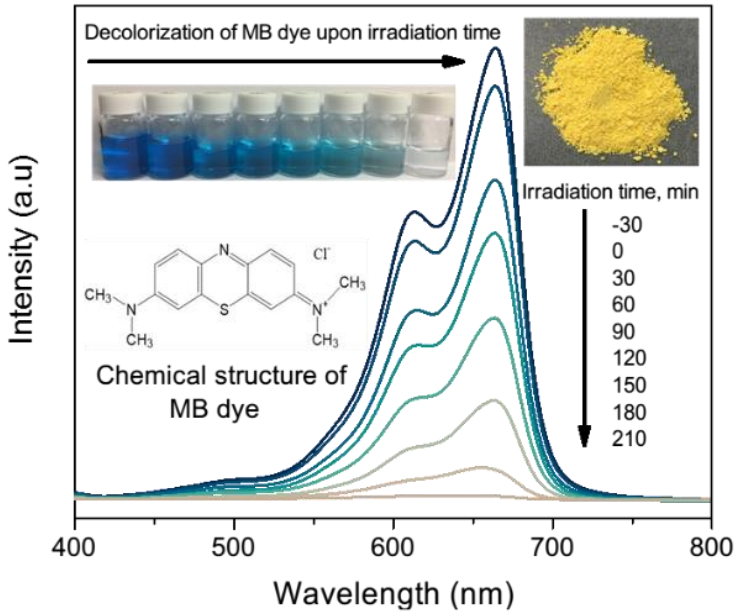

Figure 7.12 The rate of decolorization of methylene blue dye for BiVO4 microspheres calcined at 400 °C

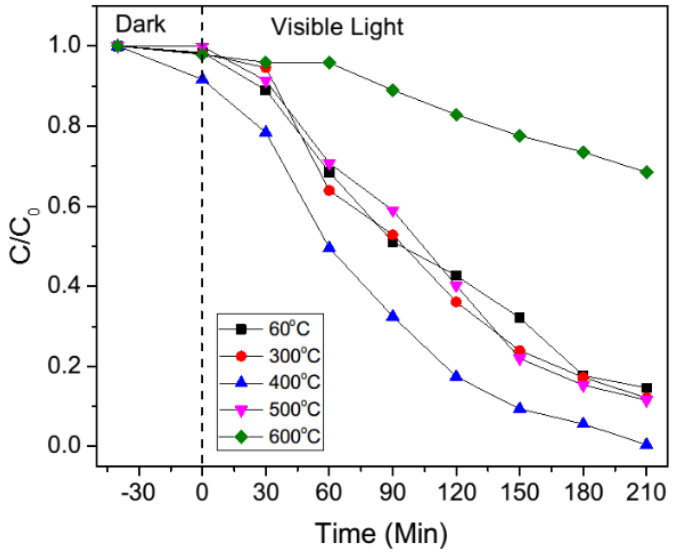

Figure 7.13 The rate of absorbance of methylene blue dye for BiVO4 microspheres under calcination temperature of 60°C, 300 °C, 400 °C, 500 °C and 600 °C

In addition, we have also conducted the TOC study on this photocatalyst, and it shows that it can degraded MB dye better than the commercialize $BiVO_4$. Thus, it has a better efficiency in decolorization and mineralization of the dye.

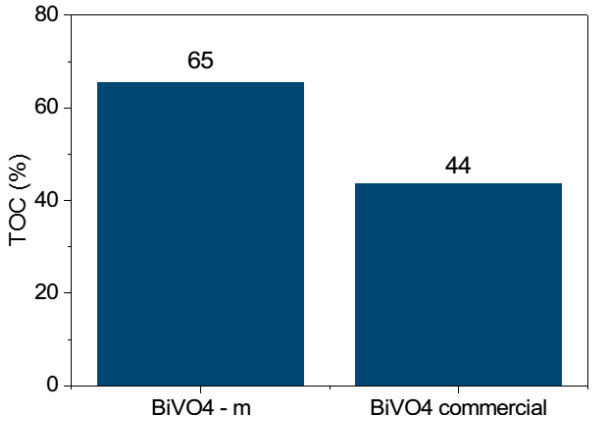

Figure 7.14 The TOC percentage of methylene blue dye for $BiVO_4$ microspheres calcined at 400 ^oC

The recyclability of this photocatalyst was also studied (Figure 7.12). It shows that this material has a good stability since it only declined from 94% to 88% after 4th cycles of the activity.

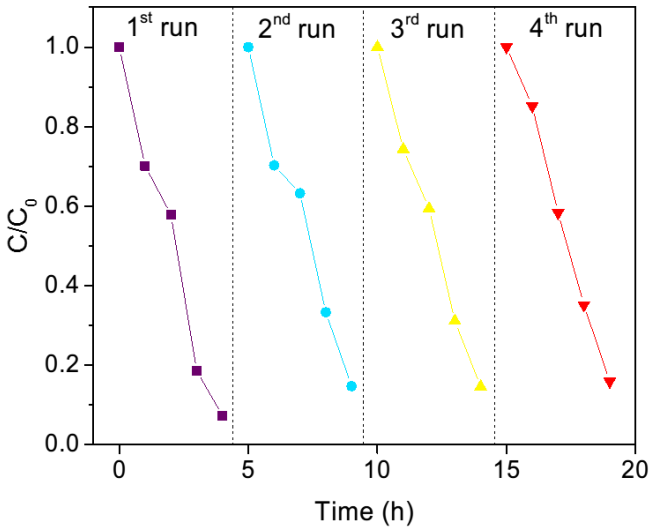

Figure 7.15 The recyclability of methylene blue dye degradation rate for BiVO4 microspheres calcined at 400 ^oC for 4 cycles

7.7 Conclusion

As a conclusion, by adding vanadium (III) acetylacetonate into the system, the flowerlike structure can be achieved at a low temperature of 60℃ for 24 hours. Although the photocatalytic performance in decolorization just slightly improved compared to the commercialize BiVO4, it can mineralize the dye better as what can be seen in the TOC analysis result. We believed that with further study, the reaction time and the photocatalytic performance can be increased. Thus, this work may open to a new and various possible ways of a low-cost self-assembly synthesizing method.

7.8 References

1. A.Fujishima et.al, Electrochemical Photolysis of Water at a Semiconductor Electrode, Nature 238, 1972, page 37-38.
2. Yin, S., Zhang, Q., et.al, Preparation of visible light-activated titania photocatalyst by mechanochemical method. Chemical Letters, 32, 2003, page 358-359.
3. G. Zhu, W. Que, J. Zhang, Synthesis and photocatalytic performance of Ag-loaded β-Bi2O3 microspheres under visible light irradiation, J. Alloys Compd., 509, 2011, page 9479–9486.
4. X.Meng, Z.Zhang, Bismuth-based photocatalytic semiconductors : Introduction, challenges and possible approaches, Journal of Molecular Catalysis A: Chemical, 423, 2016, page 533-549
5. A.Baldan, Progress in Ostwald ripening theories and their applications to nickel-base superalloys, Journal of Materials Science, 37, 2002, page 2171-2202
6. P.W.Voorhees, The theory of Ostwald Ripening, Journal of Statistical Physics, 38, 1985, page 231-253

7. L.Zhou, W.Wang et.al, Bi2O3 hierarchical nanostructures: Controllable synthesis, growth mechanism, and their application in photocatalysis, Chem. Eur. J., 2009, 15, page 1776-1782
8. Y.Shen, A.Xie et.al Self-Assembled 3D Flowerlike Hierarchical Fe3O4@Bi2O3 Core-Shell Architectures and Their Enhanced Photocatalytic Activity under Visible Light, Chem. Eur. J., 2011, 17, page 4802-4808
9. A.N. Zulkifili, A. Fujiki, S. Kimijima, Flower-like $BiVO_4$ Microspheres and Its Visible Light Driven Photocatalytic Activity, Journal of Applied Science, Vol.8, No.2, pp. 216, January 2018

CHAPTER 8

CONCLUSION AND RECOMMENDATION

This chapter discussed on the overall conclusions of the research and recommendations needed in order to improve the efficiency. Potential future work is also addressed in this chapter.

8.1 Conclusions

1. We have studied on the $NaBiO_3$ photocatalyst in different pH condition for each dye degradation. We found out that the pH plays an important role in the stability and recyclability of the photocatalyst. In this material, an improvement should be made in the future in order to increase its stability in acidic condition, since the structure of $NaBiO_3$ after one cycle under acidic condition was badly deteriorate. Thus, resulting in lower recyclability rate.
2. We have managed to synthesis alkali bismuthate of potassium and lithium by using $NaBiO_3$ in previous chapter as a starting material with lower percentage of $NaBiO_3$ presence in the product formed. The rate of degradation for both dyes increases by following reactivity $LiBiO_2$, followed by $KBiO_3$ and $NaBiO_3$.
3. We have successfully synthesis $Bi_{11}VO_{19}$-VO_2 microstructure materials which have the potential to be used as photocatalyst in the degradation of cationic dye by using a simple precipitation method at low temperature. However, modification towards this structure is needed as it cannot degrade the anionic dye, besides modification towards narrowing its band gap in order to increase its efficiency under visible light irradiation.
4. We also successfully synthesis flower-like $BiVO_4$ hierarchical structure via using the simple precipitation method at a low temperature. However, the repeatability and stability of the synthesis process was not good since we have used a complex compound in preparing the materials. A simpler compound is a key in using this

simple precipitation method. Despite that, it has a good stability in degrading the cationic dye and works better than the commercialize $BiVO_4$.

8.2 Recommendations

1. A synthesis of heterojunction between alkali bismuthate and bismuth vanadate should be made in order to increase the efficiency of decolorization and mineralization. Besides, a structure of core-shell with a higher surface shell structure should be studied.

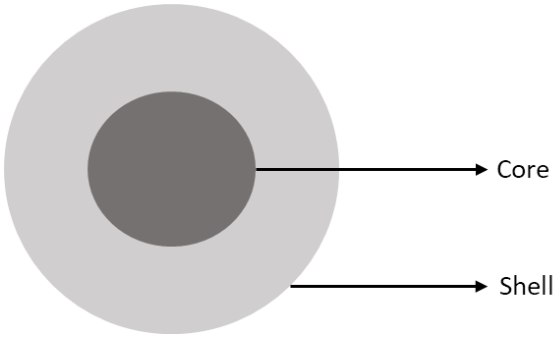

Figure 8.1 An idea on the core-shell structure of the photocatalyst

2. Besides, various test on contaminants which are not limited to dyes should be done in order to study its functionality and stability of the photocatalysts.

RESEARCH ACHIEVEMENT

International Conference・国際学会

1. Oral presentation (12th December 2015)

WSEAS International Conference on Energy and Environment 2015

A Comparison of Five Different Photocatalysts in the Degradation of Methylene Blue Dye

Arini Nuran Zulkifili, Akira Fujiki

2. Oral presentation (4th March 2016)

IIER 41st International Conference on Recent Innovations in Engineering and Technology (ICRIET)

A Basic Study on the Organic Dye Degradation by $BiNaO_3$ Photocatalyst

Arini Nuran Zulkifili, Akira Fujiki

3. Poster presentation (10th November 2016)

Applied Nanotechnology and Nanoscience International Conference (ANNIC) 2016

Self-Assembled 3D Flower-like Bi_2O_3 Microspheres and Its Visible Light Driven Photocatalytic Activity

Arini Nuran Zulkifili, Akira Fujiki

4. Poster Presentation (8th October 2017)

Applied Nanotechnology and Nanoscience International Conference (ANNIC) 2017

$Bi_{11}VO_{19}$ -VO_2 microstructure and its visible light driven photocatalytic performance in organic dye degradation

Arini Nuran Zulkifili, Shinji Kimijima, Jinhua Ye

Journal・論文

1. Arini Nuran Zulkifili, Akira Fujiki, A Comparison of Five Different Photocatalysts in the Degradation of Methylene Blue Dye, Recent Advances on Energy and Environment, pp.33-36, 2015
2. Arini Nuran Zulkifili, Akira Fujiki, A Basic Study on the Organic Dye Degradation by $BiNaO_3$ Photocatalyst, International Journal of Advances in Science Engineering and Technology 2321-9009, Volume 4, Issue 2, Special Issue 2, pp. 109-112, 2016
3. Arini Nuran Zulkifili, Akira Fujiki, Shinji Kimijima, Flower-like $BiVO_4$ Microspheres and Its Visible Light Driven Photocatalytic Activity, Journal of Applied Science, Vol.8, No.2, pp. 216, January 2018

LIST OF ABBREVIATION

Bi_2O_3 Bismuth oxide

$NaBiO_3$ Sodium bismuthate

$BiVO_4$ Bismuth vanadate

TiO_2 Titanium dioxide

$Bi(NO_3)_3{\cdot}5H_2O$ Bismuth nitrate pentahydrate

HNO_3 Nitric acid

$C_{10}H_{14}O_5V$ Vanadium(III) acetylacetonate

$NaVO_3$ Sodium metavanadate

$KBiO_3$ Potassium bismuthate

$LiBiO_2$ Lithium bismuthate

MB Methylene Blue

MO Methyl Orange

Tert-butanol Tert-butyl Alcohol

COD Chemical Oxygen Demand

TOC Total Organic Carbon

BOD Biochemical Oxygen Demand

FESEM Field Emission Scanning Electron Microscope

XRD X-ray Powder Diffraction

UV-Vis Ultraviolet–Visible Spectroscopy

FTIR Fourier Transform Infrared Spectroscopy

EDX Energy-Dispersive X-ray

SSR Solid State Reaction

LIST OF FORMULA

$$\text{Degradation rate (\%)} = \left(\frac{C_0 - C_t}{\mathrm{C_0}}\right) \times 100$$

$$\mathrm{TOC(\%)} = \left(1 - \frac{\mathrm{TOC_f}}{\mathrm{TOC_0}}\right) \times 100$$

TC (Total Carbon) – TIC (Total Inorganic Carbon) = TOC (Total Organic Carbon)

$$\text{Band gap energy, } \mathrm{E} = \frac{\mathrm{h} \times \mathrm{C}}{\gamma}$$

$$\text{Mass} = \text{Molarity} \times \text{Volume} \times \text{Molar mass}$$

Chemical structures of the model dyes in the present study

Dye	IUPAC name	Molecular Structure	Chemical Structure	M_{wt} ($gmol^{-1}$)	λ nm	pK_a	Solubility (mgL^{-1})
Cationic Dye Methylene Blue (MB)	[7-(dimethylamino) phenothiazin-3-ylidene]-dimethylazanium; chloride	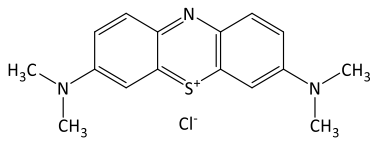	$C_{16}H_{18}ClN_3S$	319.851	664	3.8	43.6×10^3
Anionic Dye Methyl Orange (MO)	sodium;4-[[4(dimethylamino) phenyl]diazenyl] benzenesulfonate	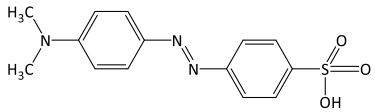	$C_{14}H_{14}N_3NaO_3S$	327.33	463	3.4	0.2×10^3